Thesis for Ph.D. Degree

entitled

ELECTRON FLOW THROUGH SPACE CHARGES IN EMISSION SYSTEMS

by B. J. Climer.

ABSTRACT.

The design of electron guns of high perveance is discussed, including a detailed survey of a Pierce-type emission system. Previous experimental work on such systems, using the pinhole projection method, is shortly described.

Pinhole camera investigations by the author on a Pierce system consisting of a concave cathode, a cathode screen and a spherical anode containing the pinhole, showed that under space charge conditions, the current density distribution and the transverse velocities of the electrons at the anode, were in approximate agreement with the ordinary electron optical expectations.

At strongly reduced cathode temperature, irregular velocity components were observed which were correlated with inhomogeneities of the cathode surface.

Similar inhomogeneities were found to be important in the performance of filamentry cathodes. With straight filaments irregular emission occurs owing to recrystallization of the tungsten, changing the surface structure and leading to multiple images in the pinhole projection.

Irregular emission phenomena observed with hairpin cathodes made from tungsten or oxide tipped platinum wire are explained in the same way.

The results demonstrate the importance of cathode irregularities in producing anomalous emission. It appears that the assumption of space charge oscillations is no longer required for an explanation of the observed phenomena.

Acknowledgement.

The author wishes to thank Dr. O. Klemperer who suggested these problems, for his advice and encouragement throughout the course of these investigations.

He also wishes to acknowledge the support of the Admiralty by a maintenance grant during the period of this research.

The large concave oxide cathodes used in the investigation of the Pierce type of emission system were presented by Electrical and Musical Industries Ltd.

The author expresses his thanks to his wife for help with the manuscript.

TABLE OF CONTENTS

		Page
	Abstract.....	2
A.	Introduction.....	10
B.	The theory of electron guns of high perveance.....	11
B1.1	The design of electron guns.....	11
B1.2	Pierce's method.....	12
B2	Performance of high perveance electron guns.....	17
B2.1	The anode aperture.....	17
B2.2	Thermal emission velocities.....	18
B2.3	Spreading of the beam due to thermal velocities.....	19
B2.4	Projection of an image by a pinhole in the anode.....	21
B2.5	Survey of the present position in the design of high perveance guns.....	22
B2.6	The experiments of Cutler and Saloom...	24
C.	Experiments by the author on a Pierce system.....	25
C1	Aim of the experiments.....	25
C2	Description of the apparatus.....	25
C2.1	Mechanical parts and the vacuum system	25

		Page
C2.2	Electrical circuits.....	32
C3	Results of measurements on an electron gun designed according to Pierce's principle.....	35
C3.1a	Current density distributions under fully space charge limited conditions..	35
C3.1b	Effect of biasing the beam-shaping screen upon the current density distribution under full space charge.....	36
C3.2	Transverse velocity distributions under full space charge.....	44
C3.2a	Anode pinhole near the axis.....	44
C3.2b	Calculation of the cathode temperature from transverse velocity distributions	44
C3.2c	Anode pinhole off axis.....	51
C3.3	Measurements with temperature limited emission.....	53
C3.3a	Current density distribution.....	53
C3.3b	Transverse velocities.....	56
C3.3c	Optical examination of a cathode.....	60
C3.3d	Comparison of irregular emission from spherical and strip oxide cathodes.....	65
C3.3e	Transverse velocities with improved resolution.....	68

		Page
C3.3f	Distance of the potential minimum from the cathode.....	69
C3.4	Perveance of the system.....	70
D.	Filamentry cathodes.....	72
D1	Introduction.....	72
D2.1a	Tungsten as a thermionic emitter.....	74
D2.1b	The performance of tungsten filaments..	77
D2.2	Experiments with tungsten filaments....	79
D2.2a	Twin hairpin cathodes with a slotted grid electrode.....	79
D2.2b	Twin hairpin cathodes with a circular grid shield.....	81
D2.2c	Interaction of emission currents from twin hairpin cathodes.....	86
D2.2d	Straight tungsten filament - Seeman's Experiment.....	87
D2.2e	Conclusions drawn from experiments with tungsten cathodes.....	88
D3	Oxide tipped hairpin cathodes.....	89
D3.1	The theory of oxide tipped cathodes....	89
D3.2a	Multiple images.....	90
D3.2b	Space charge limited emission.....	91

		Page
Appendix 1:-	Activation of the large concave oxide cathodes.....	96
Appendix 2:-	Thermal expansion and measurement of the apparatus.....	97
Appendix 3:-	Matching equipotentials at the cathode edge.....	98
Appendix 4:-	Pinhole projection and resolving power.....	100
Appendix 5:-	Pinhole position in measuring (1) Current density at the anode. (2) Transverse velocities in section C.....	101
Appendix 6:-	(1) Spurious focussing action on the pencil between pinhole and Faraday cage (1) by field penetration through the pinhole (2) by space charge and positive ions.....	105
Appendix 7:-	Influence of positive ions on the beam between cathode and anode.....	107

Page

Appendix 8:- Errors in the shapes of electrodes used in section C.... 111

Appendix 9:- Elimination of stray electric and magnetic fields affecting measurements in section C..... 111

Captions to figures..... 113

References..... 118

A. INTRODUCTION

It has been known for some time that the phenomena observed in electronic emission systems cannot always be accounted for by simple geometrical optics with a correction for space charge. The electrons are often emitted irregularly and with abnormally high velocities.

The explanations given in the literature about these irregularities are conflicting. Some authors explain them in terms of the uneven cathode surface and spherical aberration, others explain them in terms of oscillations in the space charge near the cathode.

The study of the flow of electrons from emission systems is of great interest, it can offer possibilities of obtaining fundamental information about the behaviour of electronic space charge, and it can lead to a better understanding of the emission phenomena at the cathode surface. Moreover since electron scources are used in thermionic valves, microwave tubes, electron microscopes, television image tubes etc., it is important to know every detail of their operation in order to improve them.

In the following sections experiments will be described which have been started in continuation of earlier investigations by Klemperer (1947) and by Dolder (1954). The present experiments were made mainly with large oxide coated

cathodes such as are used in klystrons, with an experimental arrangement in which both the density distribution and the transverse velocities of the electrons in the beam, could be measured with great accuracy. In this way, the electron flow has been studied both in its normal space charge limited condition and at reduced cathode temperatures.

Similar investigations carried out with filamentry cathodes are then described. The results demonstrate the importance of cathode irregularities in producing anomalous emission. It appears that the assumption of space charge oscillations is no longer required for an explanation of the observed phenomena.

B. THE THEORY OF ELECTRON GUNS OF HIGH PERVEANCE.

B1.1 The design of electron guns.

When an electron gun is designed it is relatively easy to trace trajectories, provided that the electrostatic repulsion of neighbouring electrons has a negligible effect. Empirical structures can be built in an electrolytic tank and modified to produce the desired trajectories.

When space charge interaction is considerable, it is necessary to use an iterative method involving the alternate calculation of trajectories and space charge distributions. Space charge has been simulated in the electrolytic trough

either by contouring the bottom of the trough (Musson-Genon, 1947) or by using current probes (e.g. Brewer, 1959). It is only recently that, by refining the second method Barber and Sander (1959) have developed a field plotting trough which might be simple and accurate enough for general use.

A very different approach is recommended in a method introduced by Pierce,(1940). Instead of considering the space charge to be a perturbation, he took space charge limited flow as his starting point and designed an electrode system to produce the correct variation of potential at the boundary.

The experiments performed by the author have been concerned with a gun which produces a converging cone of electrons. This type of gun is of practical importance because the maximum emission which can be drawn per unit area of a cathode is limited, thus to increase the current density in a beam, it is necessary to cause the emission from the cathode to converge to a small cross-section.

B1.2 Pierce's Method.

The converging cone of electrons is considered to be part of a rectilinear-space charge limited flow between concentric spheres, as in fig.B.1. A gun is required in which the electron flow is the same as in the arc AOB where there is rotational symmetry about OX. The electrodes of

FIG B·1

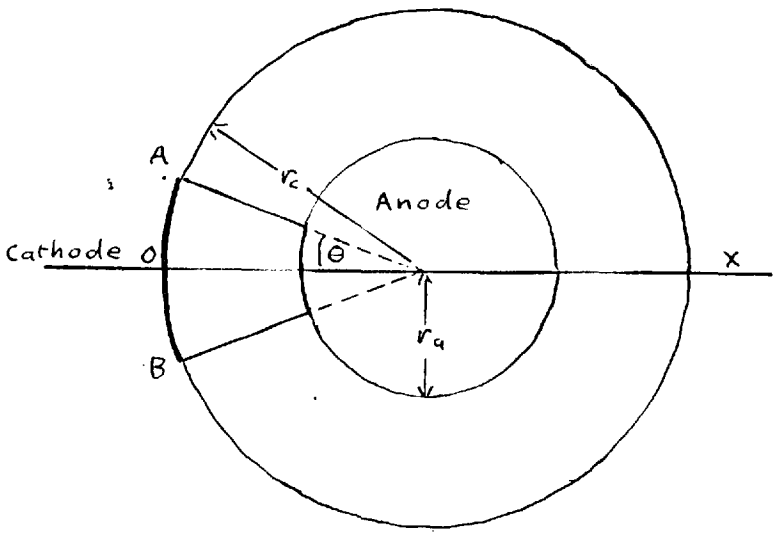
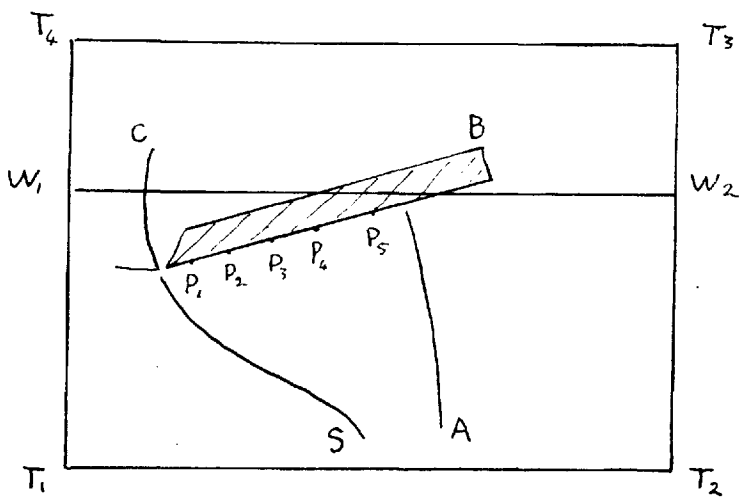


FIG B·2



the gun must be chosen to reproduce at the edges of the cone the fields due to the electrodes and space charge in the region surrounding the beam. Pierce states that this can be done by matching the radial potential distribution at the boundary of the conical beam to that inside the spherical diode.

The radial variation of potential in a space charge limited spherical diode has been calculated by I. Langmuir (1931). Let the potential as a function of radial position from the centre of curvature be $V = F(r)$.

Two electrodes are normally used to produce this field: one is the anode, the other is a "beam shaping" electrode at the same potential as the cathode. The form of the electrodes for the gun considered above is obtained using an electrolytic wedge trough as shown in fig. B.2 (see for inst. Klemperer 1953).

In this diagram W_1 W_2 is the waterline in the trough T_1 T_2 T_3 T_4. The waterline represents the axis of the gun. The strip of insulator B, with wire probes P_1 to P_5, represents the edge of the electron beam. The cathode is represented by electrode C. The beam shaping electrode S and the anode A consist of flexible conducting strips which can be adjusted until the potential along the strip, as measured by the probes, varies as F(r).

This procedure was followed by Helm et al. (1947) to produce a series of charts for various cone angles and ratios of cathode radius to anode radius. The appropriate chart was used to design the electrodes of the experimental system used. It is reproduced in fig. B.4.

Since the design is based on the spherical diode the current delivered by the gun at a given voltage can be calculated and has been tabulated by Helm et al. (1947).

According to Cutler and Hines (1955) the anode current and anode potential are related by the equation

$$I = \frac{16\,\pi\,\varepsilon_o\,\sqrt{2\,e/m}\,\sin^2\left(\frac{\theta}{2}\right)}{9\,(-a)^2}\,Va^{3/2} \quad \ldots\ldots\ldots \text{(B.1)}$$

Where,

I = beam current

ε_o = dielectric constant of free space

e/m = ratio of charge to mass of the electron

θ = semi-angle of convergence of the beam

Va = anode voltage

$-a$ = Langmuir function of the ratio of cathode radius to anode radius in the appropriate spherical diode.

The important ratio $I/Va^{3/2}$ is known as the perveance of the gun.

FIG. B·3

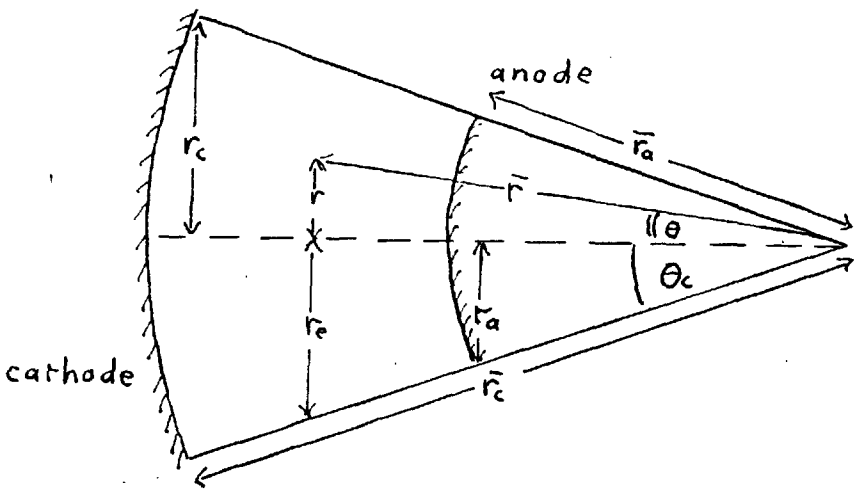
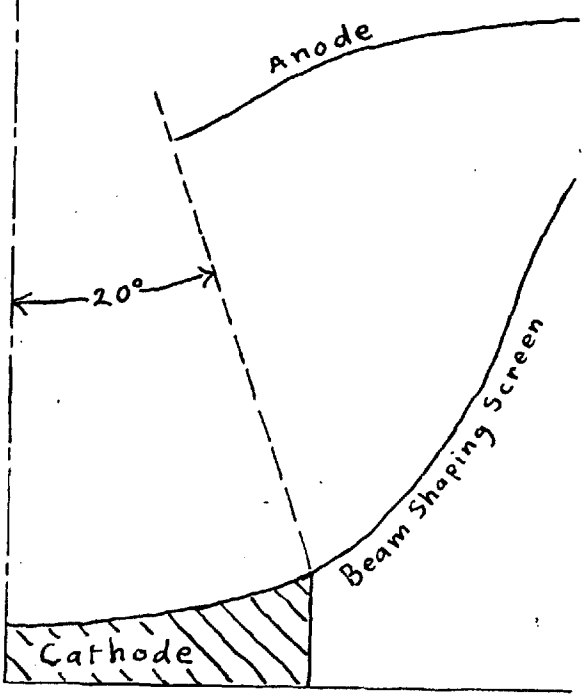

anode
r_c
$\bar{r}_a$
r
$\bar{r}$
θ
θ_c
r_e
r_a
cathode
$\bar{r}_c$

FIG. B·4


Anode
20°
Beam Shaping Screen
Cathode

B2 Performance of High Perveance Electron Guns.

B2.1 The anode aperture.

The above theory is accurate only if the equipotential of anode voltage within the beam is spherical and concentric with the cathode.

In a practical gun it is necessary to have an aperture in the anode through which the beam can emerge. This causes the anode equipotential to be distorted in such a way as to decrease the convergence of the beam and lower the perveance. These points are dealt with by Hechtel (1956) and Brewer (1957).

As a first approximation the divergence of the beam due to the anode aperture can be estimated using the Davisson and Calbick formula for the focal length of an aperture lens.

$$f = \frac{4\ Va}{E_1 - E} \qquad \ldots\ldots\ldots\ (B.2)$$

where f is the focal length of the lens and E_1 and E are the electric field strengths on either side of the aperture.

Harris (1960) has shown how formula (B.2) is modified when the aperture is cut in a curved electrode as in the Pierce gun. The diverging effect of the lens is enhanced.

B2.2 Thermal Emission Velocities.

If the gun is designed exactly according to Pierce's principle and the anode is of the correct shape, electrons leaving the cathode with zero velocity, will travel straight towards the centre of curvature of the cathode. Cutler and Hines (1955) show that if an electron is emitted from the cathode with a tangential velocity, it will not follow such a path.

Since the forces on the electrons in the beam are directed towards the centre of curvature, angular momentum about this point is conserved.

Using the nomenclature of fig.B.3, with the suffix 1 referring to a point on the cathode, we can write,

$$\bar{r}_1^2 \dot{\theta}_1 = \bar{r}^2 \dot{\theta}$$

$$d\theta = \dot{\theta} dt$$

$$\theta_1 - \theta = \dot{\theta}_1 \int_t^{t_1} \left[\frac{\bar{r}_1}{\bar{r}}\right]^2 dt \ldots\ldots\ldots \text{(B.3)}.$$

Since $\bar{r}$ is known as a function of time t from the work of Langmuir (1931), θ can be calculated as a function of $\bar{r}$.

Cutler and Hines (1955) treat the problem more generally. Using the symbols of fig. B.3, they define a quantity $\mu = \frac{r}{r_e}$. This expresses the distance of a given electron from the axis as a fraction of the beam radius. They apply Liouville's

theorem under conditions where the angles which all of the electron trajectories make with the axis are small, and obtain the equation

$$\mu - \mu_1 = \left|\frac{d\mu}{dt}\right|_1 \int_{t_1}^{t} \frac{dt}{\left[\frac{r_e}{r_{el}}\right]^2} \quad \ldots\ldots\ldots \text{(B.4)}$$

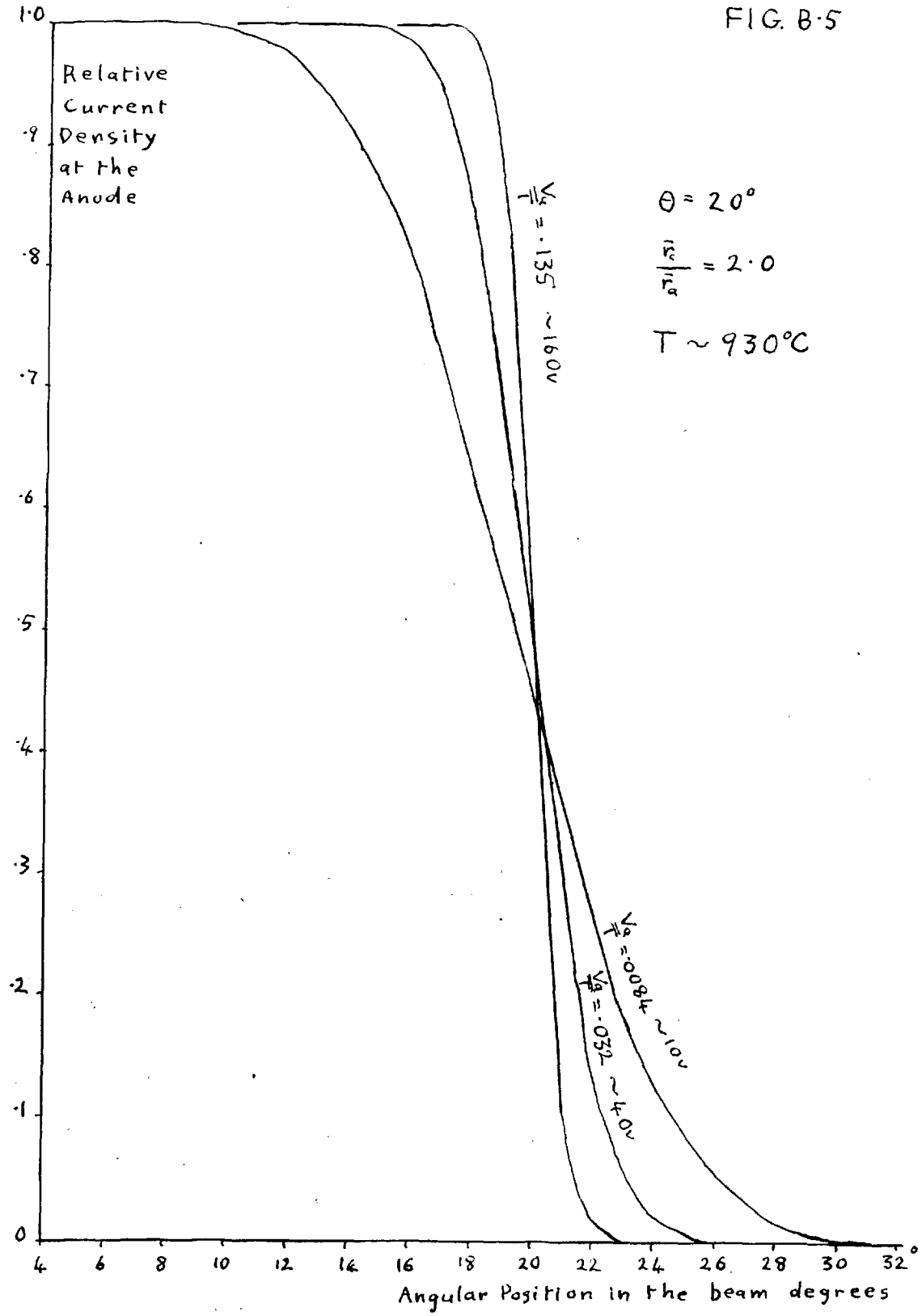
where suffix 1 again refers to a point on the cathode. Since $\frac{r_1}{r} = \frac{r_1}{r}$ between the anode and the cathode, equations (B.3) and (B.4) are identical. Cutler and Hines have integrated equn. (B.4) numerically. Their results may be expressed in terms of angles by noting that $\theta = \theta_c \mu$ where θ_c is the semi-angle subtended by the cathode.

B2.3 Spreading of the beam due to thermal velocities.

Some of the electrons with initial tangential velocities stray out of the beam. Cutler and Hines calculate the magnitude of this spreading and present their results as a series of curves with $\frac{Jr}{Jo}$ as ordinate against radial position off the gun axis. Jr is the current density at a point distant r from the axis and Jo is the current density in the absence of thermal velocities. The parameter σ, which governs the amount of thermal spreading, is defined as

$$\sigma = \left[\frac{\Delta r}{\frac{dr}{dt}}\right]_c \sqrt{\frac{kT}{m}} \quad \ldots\ldots\ldots \text{(B.5)}$$

FIG. B·5


1·0
·9
·8
·7
·6
·5
·4
·3
·2
·1
0
Relative Current Density at the Anode
$\frac{V_a}{T} = .135 \sim 160v$
$\frac{V_a}{T} = .0084 \sim 10v$
$\frac{V_a}{T} = .032 \sim 40v$
$\theta = 20°$
$\frac{r_c}{r_a} = 2·0$
$T \sim 930°C$
4 6 8 10 12 14 16 18 20 22 24 26 28 30 32°
Angular Position in the beam degrees

The value of this function at the anode is given by the authors as a function of $\bar{r}_c$, $\bar{r}_a$, Va and temperature T.

Fig.B.5 shows the current densities calculated to occur at the anode in the experimental system used by the author. The parameter σ has been expressed in terms of $Va/_T$. The approximate voltage to which each curve corresponds is also given.

B2.4 Projection of an image by a pinhole in the anode.

If r_o is the distance from the axis of an object in the plane of the cathode for instance some die marks on the cathode surface, the distance r_i from the axis of the image projected by a pinhole in the anode onto a screen distant $\bar{z}_i$ from the pinhole, is given by Cutler and Hines (1955) as,

$$r_i = r_o \cdot \frac{\bar{z}_i}{\bar{r}_a(-\alpha_a)^{2/3} A} \quad \ldots\ldots \text{(B.6)}$$

where A is a tabulated function of the geometry of the gun and the ratio $Va/_T$.

The tangential velocity of an electron arriving at the anode is increased by the ratio $r_c/r_a = I/_M$. Since the apparent temperature T of the electron beam is proportional to v_t^2, where v_t is the tangential velocity, the apparent temperature of the beam is increased by the same ratio as its area is decreased.

In the system used by the author, where equipotentials are spherical, this can be considered to be a result of the conservation of angular momentum.

An element of current arriving at the anode with tangential velocity v_t is given by Cutler and Hines (1955) as

$$dJ_a = \text{constant} \exp.[-(m/2kT)M^2 v_t^2]dv_t$$

$$\frac{r_i}{z_i} = \frac{v_t}{v_z} \quad \text{Therefore } v_t = \sqrt{\frac{2eVa}{m}} \times \frac{r_i}{z_i}$$

$$\text{and } dJ_a = \text{constant} \exp.\left[-\frac{eVa}{kT} M^2 \left(\frac{r_i}{z_i}\right)^2\right] \ldots\ldots \text{(B.7)}$$

where k is Boltzmann's constant.

This is the expected current distribution in a projected pencil as a function of r_i, the distance from the axis of the pencil.

B2.5 Survey of the Present Position in the Design of High Perveance Guns.

Above it is mentioned that the perveance and convergence of the beam of practical Pierce guns falls below the values predicted, mainly because of the anode aperture. It is also mentioned that the thin lens formula can be applied to the anode aperture, but Brewer (1957) states that this formula is incorrect by a factor of 2 or 3. The

correction applied for the curvature of the anode diaphragm by Harris (1960) amounts to only 10% with a semi beam angle of 30^{o}.

The disturbance caused by the anode aperture has led to either empirical designs e.g. by Heil (1950) or to design procedures which take account of the influence of the anode aperture e.g. Müller (1956). In the latter type of gun, the potential distribution along the beam edges, is not matched to that, which would occur at the equivalent position in a system with space charge limited flow between concentric spheres. Instead, the potential at the beam edge is matched to that which would occur at the equivalent position in a system with space charge limited flow between a perfect outer sphere and an inner sphere provided with a cylindrical hole along the axis of a diameter equal to that of the anode aperture in the final gun design.

When used in practical microwave device, guns produced in this way give a high perveance and a higher transmission through a tunnel than guns designed by Pierce's principle. However, Müller states that the spreading of the beam is still too great to be accounted for by transverse thermal velocities alone. He suggests that collisions with residual gas molecules and inaccuracies in the construction of the gun are the cause of the excess spreading of the beam.

B2.6 The experiments of Cutler and Saloom.

The performance of Pierce guns of up to 0.5 microamps/volt$^{3/2}$ perveance, has been investigated by Cutler and Saloom (1955) by putting a pinhole aperture in the beam emerging from the gun. The current passing through the aperture was proportional to the current density and the angular distribution of the projected electrons indicated their transverse velocities.

By comparing the experimental measurements with the theory developed by Cutler and Hines (1955), information could be obtained concerning the two types of defects present in the gun. The first geometrical type of defect is due to faulty electron optics and does not vary with anode voltage. The second type is dependent on anode voltage, and is due to such things as thermal velocities, contact potentials, parasitic magnetic fields or interactions between electrons leading for instance to oscillations.

The results revealed faulty positioning of the cathode relative to the beam shaping electrode, and a beam divergence greater than that obtained by applying the thin lens formula to the anode aperture. The transverse thermal velocities were in agreement with theory to within 10%. The work was continued by Danielson et al. (1956) who obtained similar results.

C. EXPERIMENTS BY THE AUTHOR ON A PIERCE SYSTEM.

C1 Aim of the experiments.

The purpose of the experiments described below was to perform investigations similar to those of Cutler and Saloom (1955) but using a system without the disturbing influence of a large anode aperture. Particular attention was devoted to measurements at low voltages, where Clarke and Jacob (1953 and 1955), observed transverse velocities which were very sensitive to the temperature of the cathode.

The apparatus was also run under temperature limited conditions, to investigate the discontinuities which Klemperer (1947), had observed in the emission from strip oxide cathodes, and to try to determine their cause.

C2 Description of the Apparatus.

C2.1 Mechanical parts and the vacuum system.

The apparatus is shown in fig. C.1.

The electrode structure was built on 3 ceramic rods, one of which is shown at A, placed symmetrically 2" from the axis of the apparatus. The various components were mounted on two brass baseplates, sealed to the two ends of the glass vacuum vessel by neoprene O-rings. The cathode is shown in greater detail in fig. C.2. The oxide coating was sprayed on to a nickel cap 3.3 cm. in diameter with a radius of curvature of 4.9 cm. subtending an angle

SCALE × ½ approx.

FIG. C·1

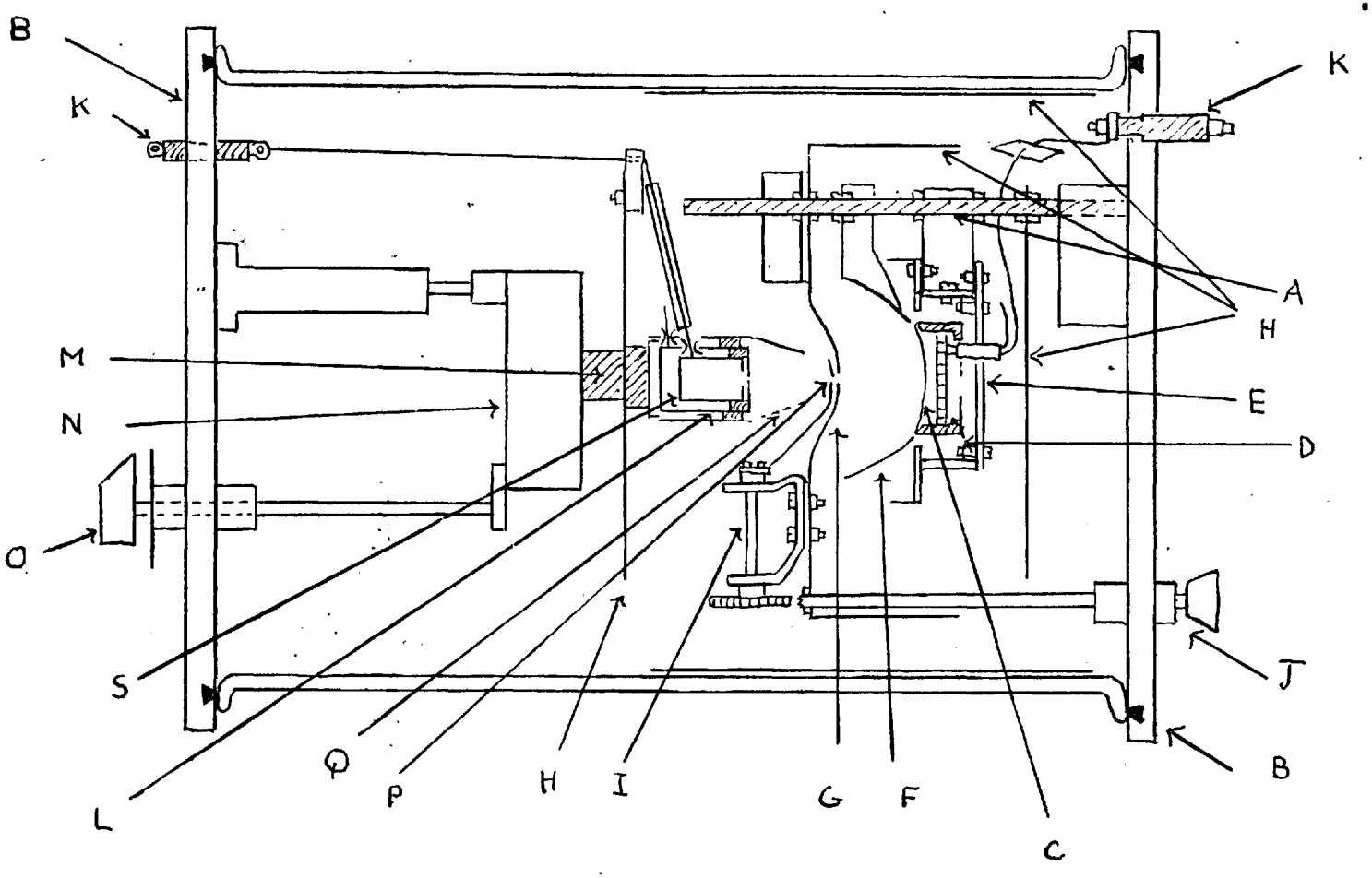
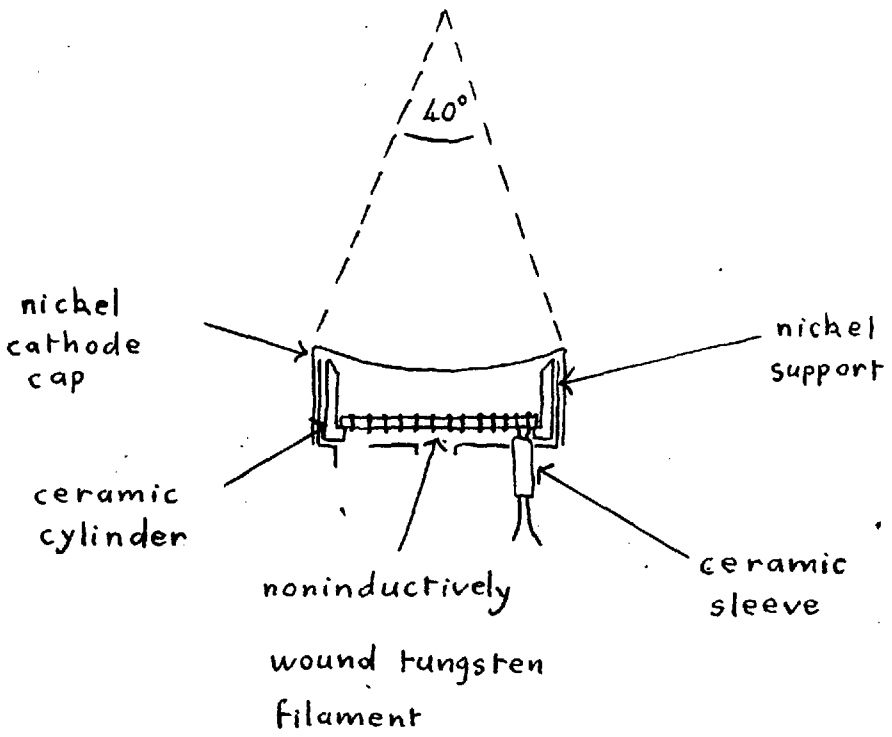


FIG. C·2



TO SCALE

of 40°. The heater consisted of a length of ½ mm. diameter tungsten wire noninductively wound on a ceramic former.

The cathode was mounted on a perforated ring of stainless steel of poor thermal conductivity D, inside a cylindrical copper box E. This type of radial mount was chosen because it is rigid and reduces axial movement due to thermal expansion (See Field 1946).

The beam shaping screen F and spherical anode G were spun in copper in accordance with the requirements of Pierce's theory. They were shaped after templates made from the curves in fig. B.4, which is taken from a paper by Helm et al. 1947. A value of 2.0 was chosen for the ratio of radius of curvature of the cathode to radius of curvature of the anode.

The gun was surrounded by 4 copper thermal reflecting screens H. Using these screens and cooling the baseplates from outside with two air blowers, the temperature of the baseplates did not exceed 40°C. when the cathode was fully heated.

The spherical anode G had a slot 1 mm. wide across its centre. The ends of the slot subtended an angle of 60° as seen from the centre of curvature of the cathode.

An inconel axle I, perpendicular to the axis of the system at the centre of curvature of the cathode, was

fitted with a steel arm and a copper strip P, beaten to a spherical form concentric with the curvature of the cathode. In the centre of the strip was a pinhole, so placed that when the axle was rotated by means of gears, the pinhole moved along the slot in the anode and the long strips blocked the remainder of the slot. The gears were turned by means of the rotating seal J.

Electrical connections were carried to terminals K, insulated by ceramic seals from the baseplates.

The current measuring arrangement consisted of a Faraday cage L, made of eureka with silica insulation between the concentric cylinders. The mycalex M, supporting the heat reflecting disc H, had a copper core, not shown in the diagram, to provide a thermal shunt between the Faraday cage and the heavy brass components behind the shield H.

The Faraday cage and thermal shield were mounted on a small carriage which could be moved in two perpendicular directions at right angles to the axis of the system, by means of a rack and pinion device N, operated through two rotating seals, one of which is shown at O.

The cage could initially be moved to an accuracy of $\pm$ 0.05 mm. over a range of 2 cm. Subsequently the accuracy was improved so that when the movement was checked

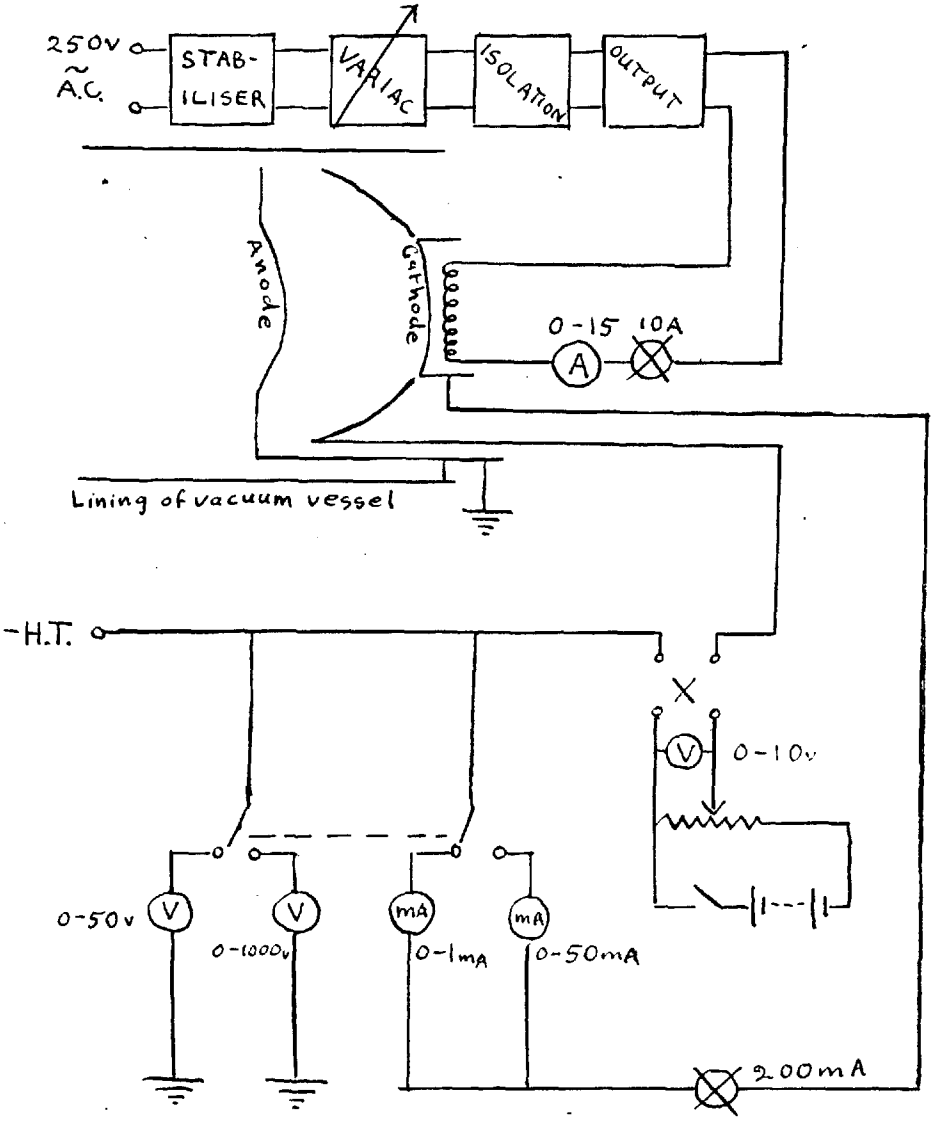
with a travelling microscope, a plot of the position of the Faraday cage against rotation of the seal, gave a straight line with deviations of only $\pm$ .005 mm. The front surface of the Faraday cage L was used to measure the total current projected by the pinhole in the anode. Secondary electrons released at the aperture in the anode P, were prevented from reaching the Faraday cage by a saddle field, set up by a conical electrode Q, at the front of the Faraday shield.

A coating of Willemite on the front surface of the Faraday cage L, which could be viewed through a small gauze window in the side of the shield, indicated the position of the beam when the anode voltage was sufficiently high.

The inner collector S, received electrons passing through the aperture in the front of the Faraday cage and was used to measure the transverse velocity distribution of electrons passing through the pinhole in the anode. The leads from the Faraday cage were very carefully screened by shields not shown in fig.C.1.

The glass vacuum vessel was pumped by a single stage mercury diffusion pump. The pump and its associated liquid oxygen trap were of glass. The ultimate vacuum as read on a cold cathode ionization gauge, was 10^{-5} mm.Hg.

FIG. C·3


250V
~
A.C.
STAB-
ILISER
VARIAC
ISOLATION
OUTPUT
Anode
Cathode
0-15 10A
A
Lining of vacuum vessel
-H.T.
X
V
0-10v
0-50v
V
0-1000v
mA
0-1mA
mA
0-50mA
200mA

The temperature of the cathode was measured with a nickel nichrome thermocouple. The two $\frac{1}{2}$ mm. diameter wires were spot welded to the cathode cap about 1 mm. apart and taken to the terminals in the baseplate. Since the baseplate was warm, the wires were extended for about 9" to a cold junction at room temperature. The voltage of the thermocouple was of the order of 25 mV. Various methods of measuring the temperature of thermionic cathodes have been discussed by Coppola (1960).

C2.2 Electrical Circuits.

The circuits associated with the electron gun are shown in fig.C.3. At the top of the diagram is a chain of transformers. This consisted of a 250 watt "Advance" stabilizing transformer followed by a variable autotransformer, isolation transformer and finally the output transformer. This supplied a current of about 10 amps at a stabilized potential of about 15 volts to the cathode heater.

The anode and the lining of the vacuum vessel were at earth potential, while a negative voltage was applied to the cathode. The cathode current and voltage could be read on two pairs of meters covering the high and low voltage ranges. A negative or positive bias could be applied to the beam shaping screen.

FIG. C·4

MEASUREMENT OF CURRENT DENSITY

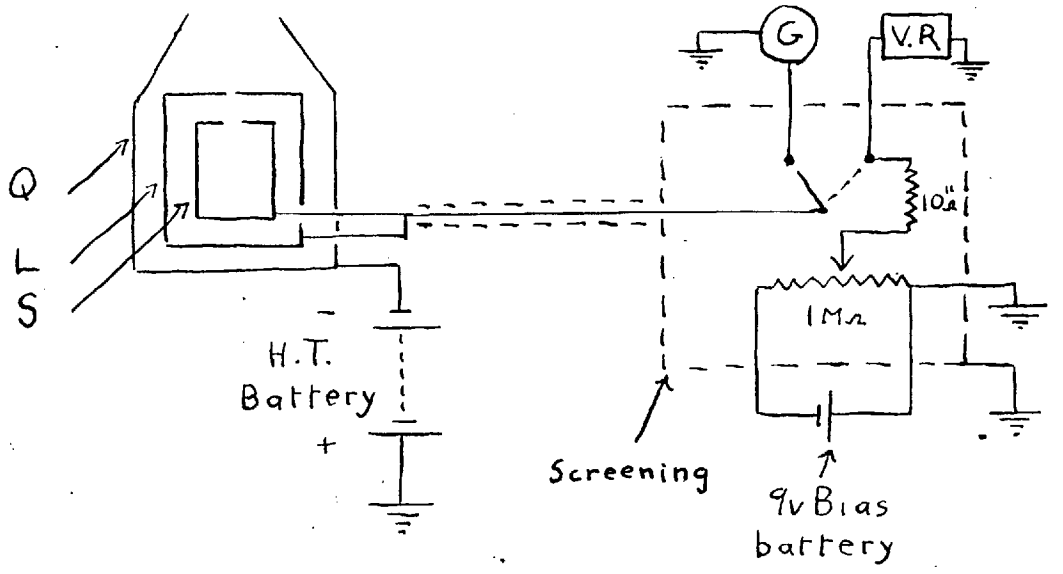
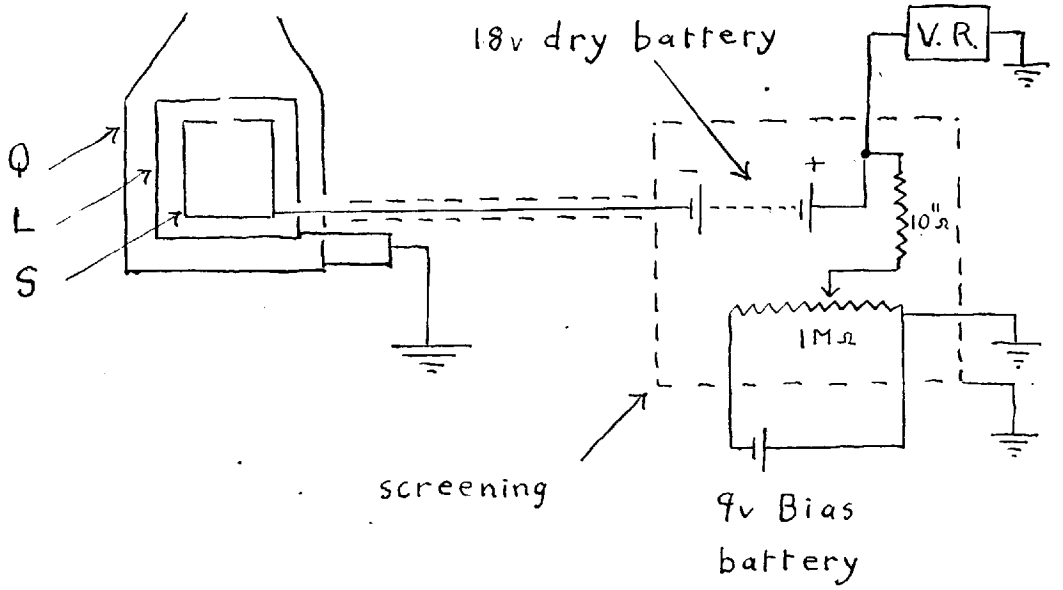


FIG. C·5

MEASUREMENT OF TRANSVERSE VELOCITIES



The screened leads of the Faraday cage were taken to coaxial sockets in a metal box. Other sockets in the box were connected to a mirror galvanometer and on "Ecko" vibrating reed electrometer. By means of short loops of coaxial cable, the various sockets could be interconnected to give either of the circuits in figs. C.4 and C.5.

To measure current density across the beam at the anode, the circuit in fig. C.4 was used. The front of the Faraday cage L was joined electrically to the inner collector S and both were connected to either the vibrating reed electrometer or the mirror galvanometer. When the electrometer was in use, any residual current flowing to its input via the insulation, was compensated by a current passed through a resistance of $10^{11}\Omega$ within the screened box. The highest input resistance of the electrometer used was $10^{10}\Omega$, so the sensitivity was not seriously impaired.

A dry cell battery of 120 volts was used to bias the outer shield Q to a negative potential with respect to the anode. This prevented slow secondary electrons from the anode aperture from reaching the front of L.

When transverse velocity distributions were to be measured the circuit in fig. C.5 was made up. The outer shield Q and cylinder L were both earthed while the innermost cylinder S was connected to the input of the

electrometer via an 1.8 volt dry battery within the screening box. The battery was very carefully insulated with polythene and a small canister of drying agent was included.

C3 Results of Measurements on an Electron Gun Designed According to Pierce's Principle.

C3.1a Current density distributions under fully space charge limited conditions.

In order to measure the current density distribution across the beam, the Faraday cage was kept at a fixed position on the axis of the apparatus and the pinhole P, in fig.C.1, was moved across the beam. The current arriving at the front of the Faraday cage L, was measured using a mirror galvanometer or the vibrating reed electrometer.

A voltage of up to 120 v. was applied to the shield electrode Q, to suppress secondaries. When the anode voltage was less than 120 v., about 90% of the anode voltage was applied to Q.

The Faraday cage was adjusted to the axis of the apparatus by putting the anode pinhole roughly in the centre of the anode slot and moving the Faraday cage until the spot on the fluorescent front was central. The anode pinhole which was 150 μ in diameter, was moved across the beam in steps of about 3°. The exact relationship between rotation

of the seal and movement of the anode pinhole is dealt with in appendix 5.

Figs. C.6 to C.9 show the results obtained compared with theoretical curves. The parameters are marked on the curves, Va is the anode voltage, Ia anode current and T is the temperature of the cathode.

Discussion.

The agreement with theory was not close. The deviations are believed to be due to faulty positioning of the cathode. This created tangential velocity components which caused the irregularity of the 640 v. distribution. When the anode potential was 10 v., the thermal transverse velocities were 8 times more important and overbalanced the geometrical imperfections. Hence the curve taken at 10 v. was in closer agreement with theory. The beam diameter, as measured between points where the intensity has fallen to half the axial intensity, is consistently about 10% greater than the theoretical value.

C3.1b Effect of biasing the beam-shaping screen upon the current density distribution under full space charge.

Since it was inconvenient to move the cathode during an experiment, the potential of the beam shaping screen was varied, to see if it made the current density distribution

FIG. C·6

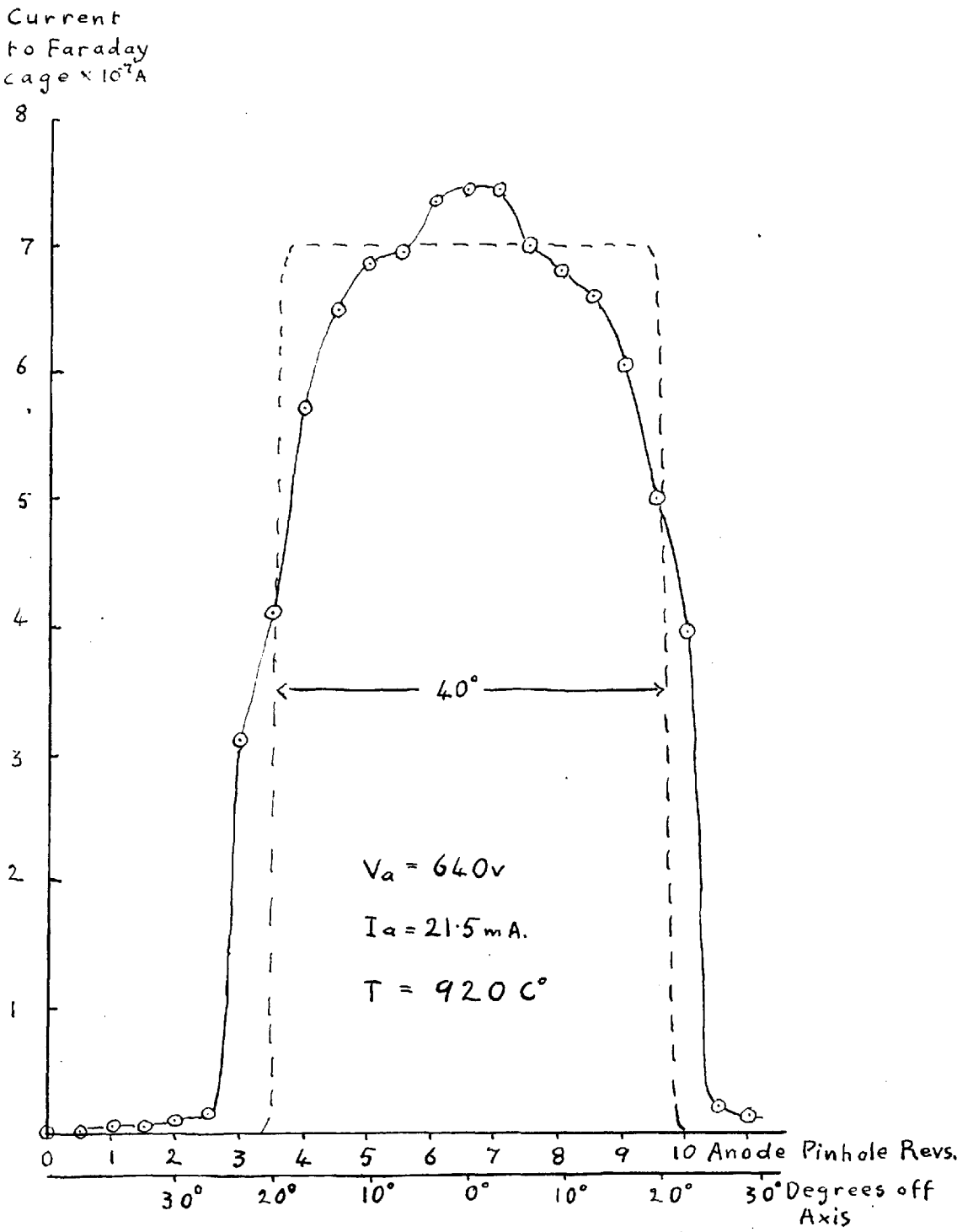

Current to Faraday cage × 10⁻⁷A
8
7
6
5
4
3
2
1
40°
Va = 640v
Ia = 21·5 mA.
T = 920 C°
0 1 2 3 4 5 6 7 8 9 10 Anode Pinhole Revs.
30° 20° 10° 0° 10° 20° 30° Degrees off Axis

FIG. C·7

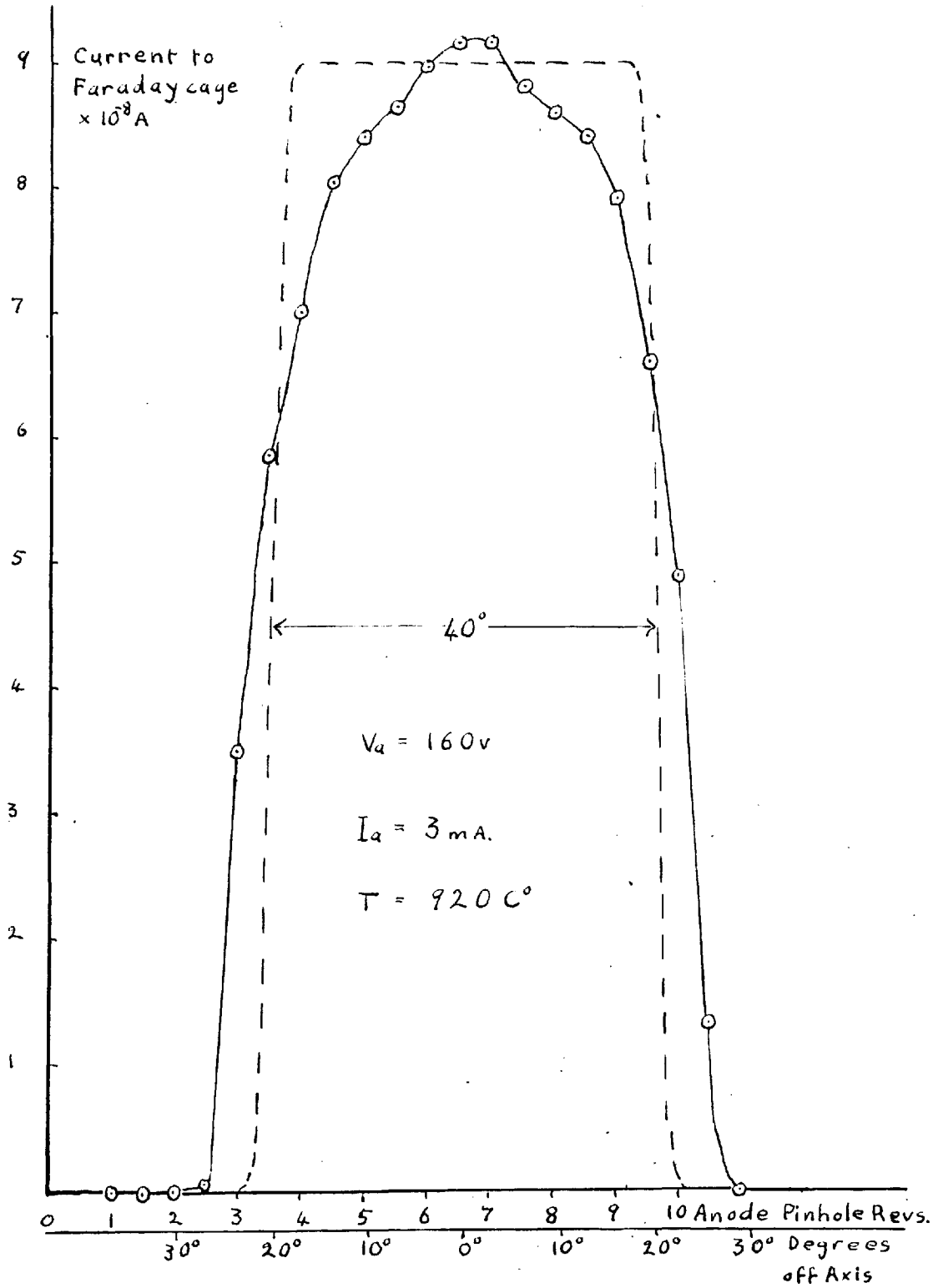

Current to Faraday cage
× 10⁻⁸ A
9
8
7
6
5
4
3
2
1
40°
Va = 160v
Ia = 3 mA.
T = 920 C°
0 1 2 3 4 5 6 7 8 9 10 Anode Pinhole Revs.
30° 20° 10° 0° 10° 20° 30° Degrees off Axis

FIG. C·8

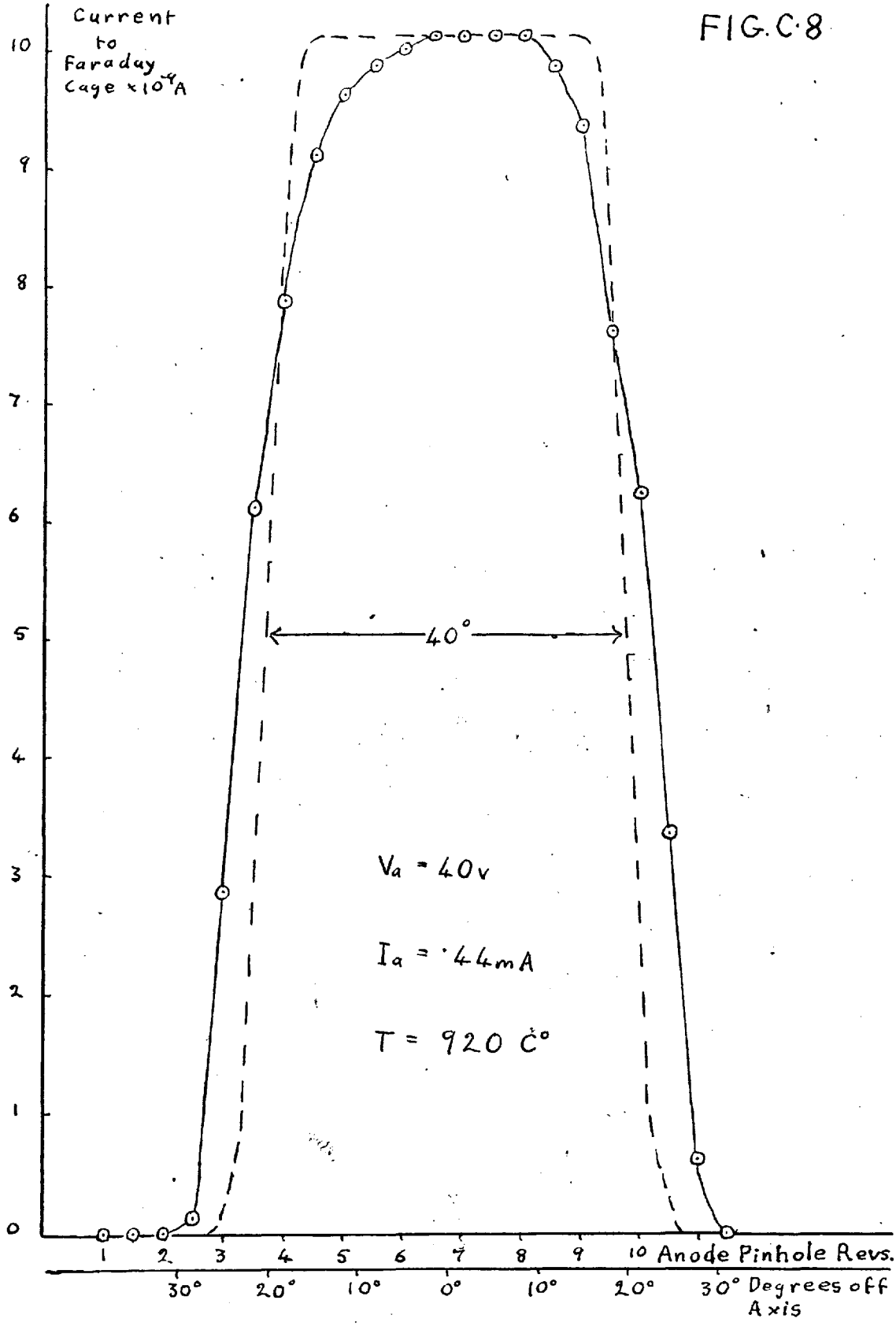
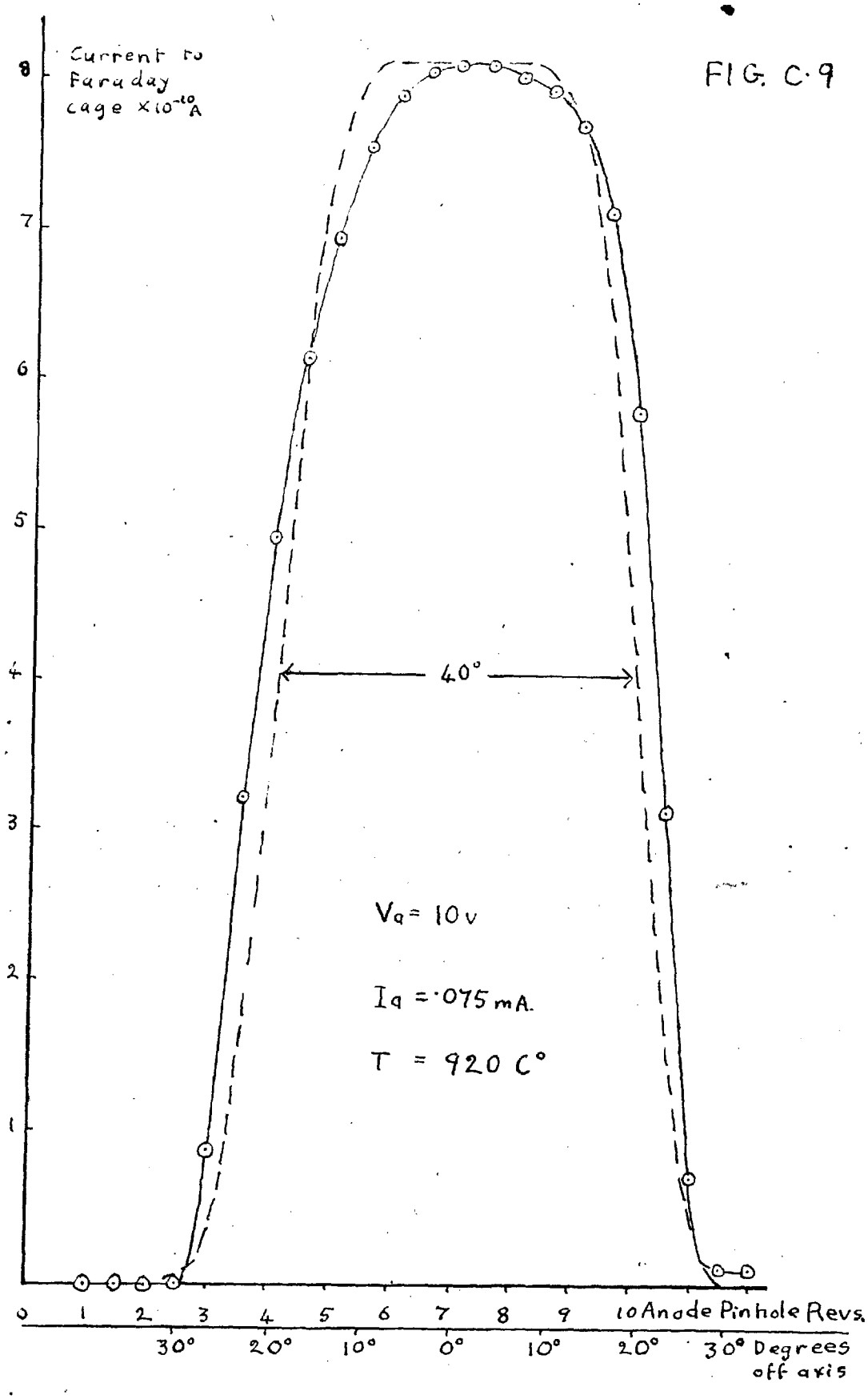

Current to Faraday Cage ×10⁻⁴A
10
9
8
7
6
5
4
3
2
1
0
40°
Va = 40v
Ia = ·44mA
T = 920 C°
1 2 3 4 5 6 7 8 9 10 Anode Pinhole Revs.
30° 20° 10° 0° 10° 20° 30° Degrees off Axis

FIG. C·9


Current to Faraday cage $\times 10^{-10}$ A
8
7
6
5
4
3
2
1
40°
V_a = 10 v
I_a = ·075 mA.
T = 920 C°
0 1 2 3 4 5 6 7 8 9 10 Anode Pinhole Revs.
30° 20° 10° 0° 10° 20° 30° Degrees off axis

in the beam, agree more closely with theory.

Fig.C.3 shows the circuit used to bias the beam shaping screen. Fig.C.10 shows points obtained with 3 different values of bias compared with the theoretical curve for an anode potential of 640 v. Fig.C.11 shows similar curves measured with an anode voltage of 10 v. and values of bias approximately the same as in fig.C.10 if expressed as a percentage of the anode potential.

Discussion.

At an anode potential of 640 v., application of a bias of 10 v. had a very striking effect on the current density distribution. The marginal current density was increased so that the observed distribution was in closer agreement with theory, both in respect to uniformity of current density, and in the width of the beam. At an anode potential of 10 v., the application of a similar percentage bias had a much less marked effect, probably due to the greater importance of transverse thermal velocities.

Since a negative bias had to be applied to improve the distribution, the cathode must have been too close to the beam shaping electrode in the above experiment.

FIG. C10

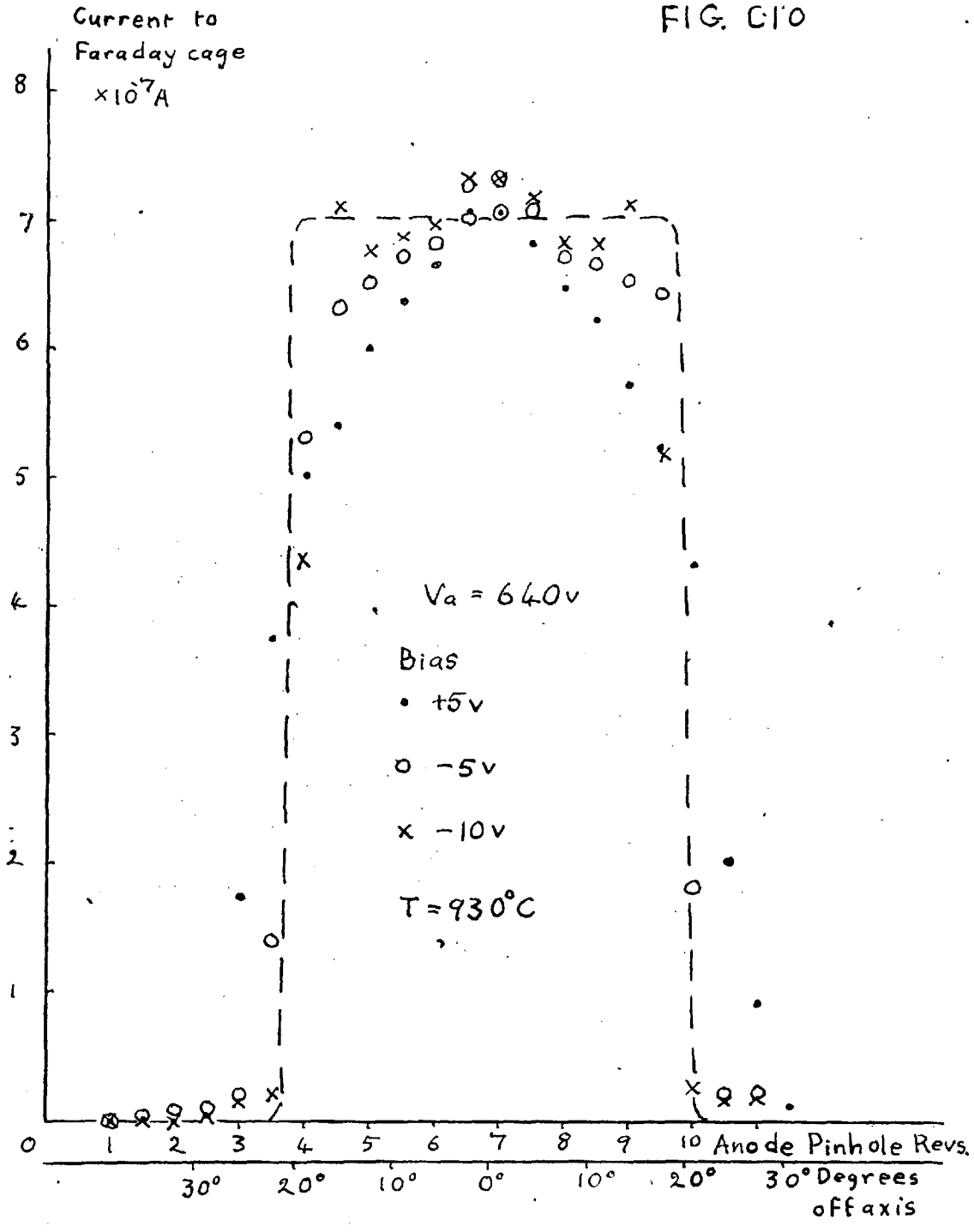
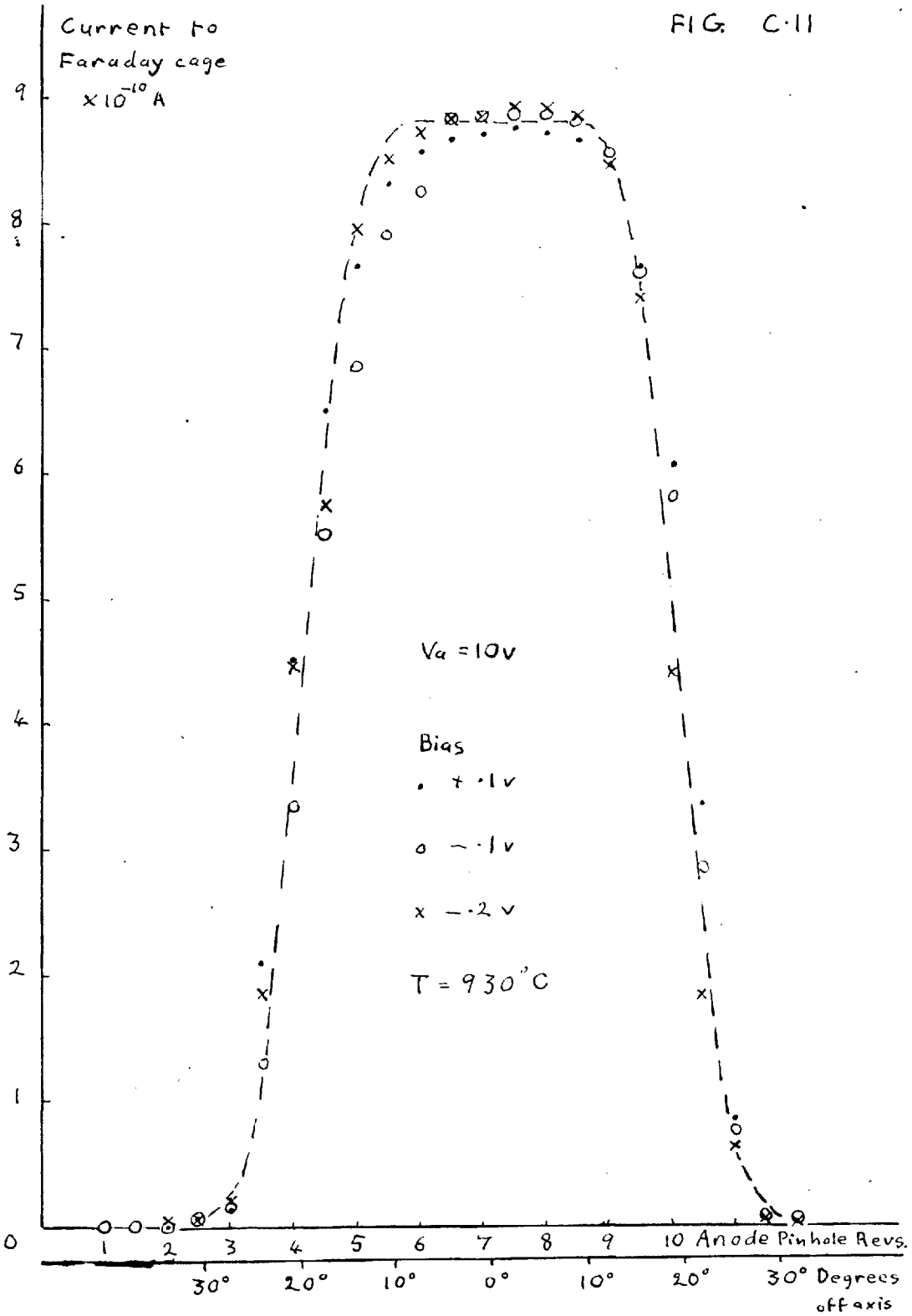

Current to Faraday cage
×10⁻⁷A
8
7
6
5
4
3
2
1
0
Va = 640v
Bias
• +5v
o −5v
x −10v
T = 930°C
1 2 3 4 5 6 7 8 9 10 Anode Pinhole Revs.
30° 20° 10° 0° 10° 20° 30° Degrees off axis

FIG. C·11


Current to
Faraday cage
×10⁻¹⁰ A
9
8
7
6
5
4
3
2
1
0
Va = 10v
Bias
• + ·1 v
o — ·1 v
x — ·2 v
T = 930°C
1 2 3 4 5 6 7 8 9 10 Anode Pinhole Revs.
30° 20° 10° 0° 10° 20° 30° Degrees off axis

C3.2 Transverse Velocity Distributions Under Full Space Charge.

C3.2a Anode pinhole near the axis.

To make this type of measurement, the anode pinhole was placed at a given position and the Faraday cage was moved to measure the current distribution in the projected pencil.

Fig.C.5, shows how the current reaching the innermost cylinder of the Faraday cage was measured. The innermost collector was biased to -18 v., to prevent the access of slow secondary electrons.

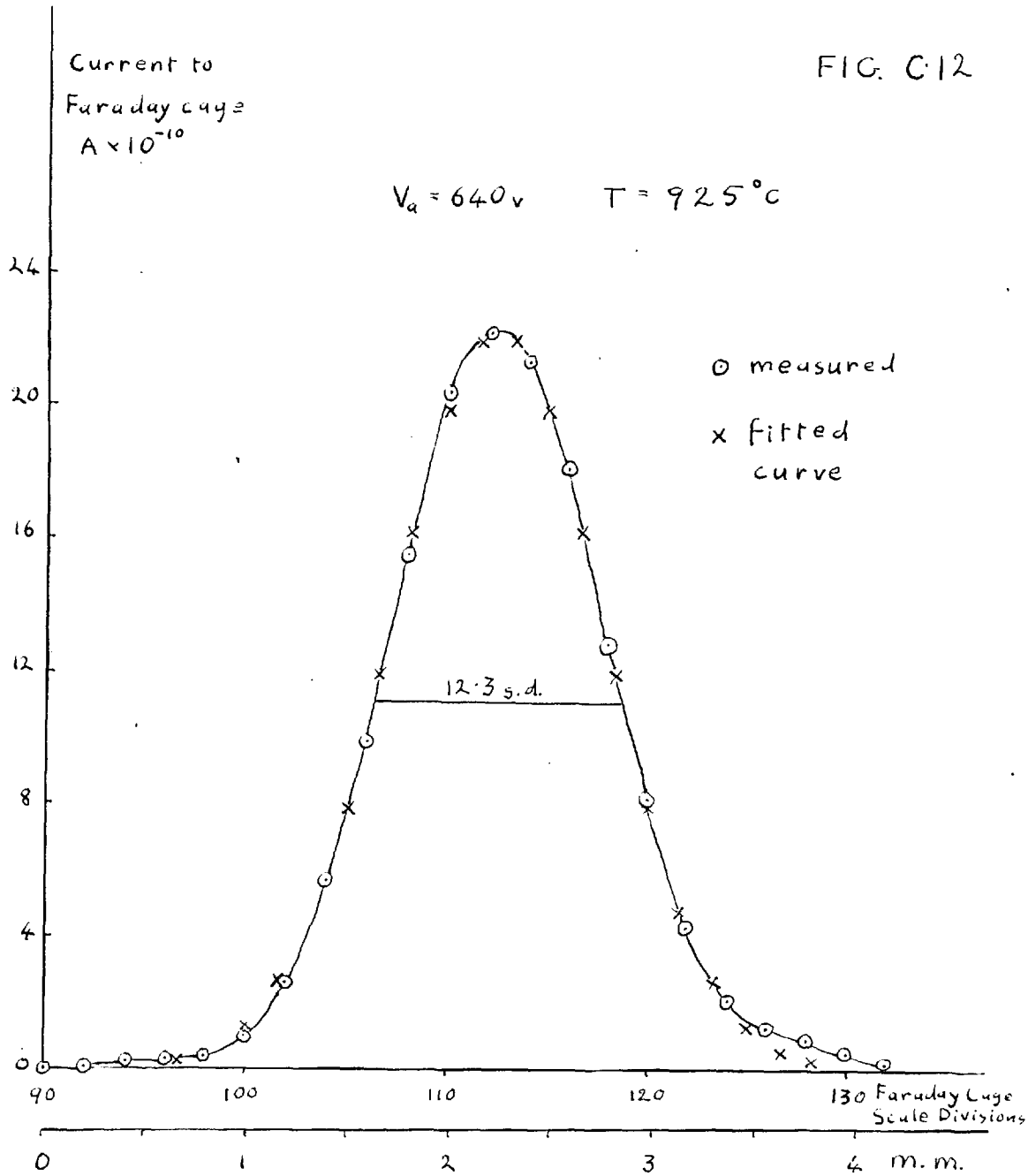
Figs.C.12 to C.14 show the transverse velocity distributions measured at anode potentials of 640 v., 160 v. and 40 v. respectively. The half widths of the curves are plotted in fig.C.15 against $Va^{-\frac{1}{2}}$. It will be explained below why this is expected to give a straight line graph passing through the origin. The anode pinhole position was 5.0 (c.f. figs.C.6 to C.8), i.e. about 10^{o} from the axis.

C3.2b Calculation of the cathode temperature from transverse velocity distributions.

Equation B.7 of section B2.4 gives the expected current density distribution in a pencil projected by the anode pinhole as

$$dJa = \text{const.} \exp.\left[-\frac{eVa}{kT} M^2 \left[\frac{r_i}{z_i}\right]^2\right] \quad \ldots\ldots\ldots (B.7)$$

FIG. C·12


Current to
Faraday cage
A × 10⁻¹⁰
V_a = 640 v
T = 925 °C
o measured
x fitted
curve
12·3 s.d.
24
20
16
12
8
4
0
90
100
110
120
130 Faraday Cage
Scale Divisions
0
1
2
3
4 m.m.

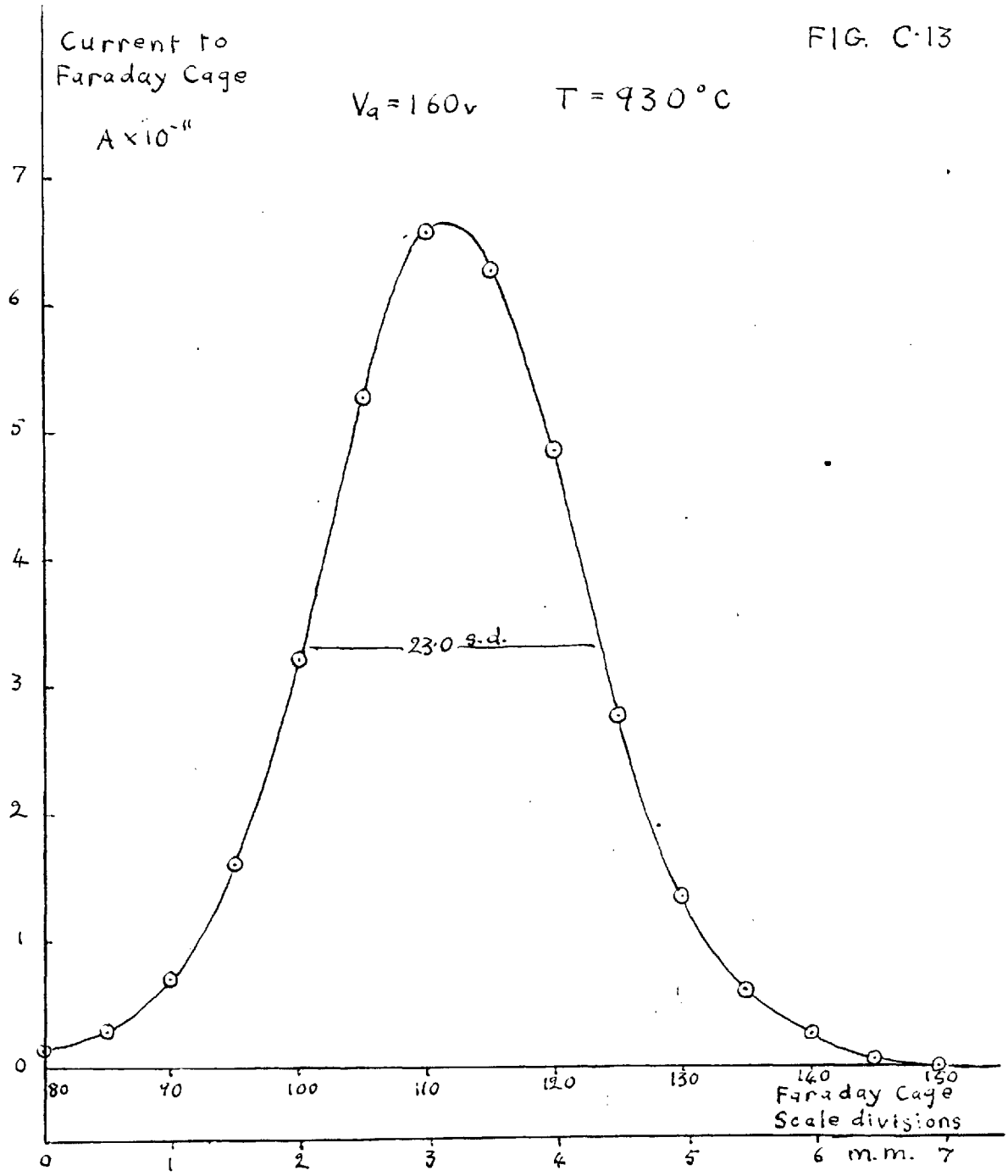

Current to Faraday Cage
A x 10⁻¹¹
V_a = 160v
T = 930°C
7
6
5
4
3
2
1
0
23·0 s.d.
80
90
100
110
120
130
140
150
Faraday Cage Scale divisions
0
1
2
3
4
5
6 m.m. 7

FIG. C·13

FIG. C·14

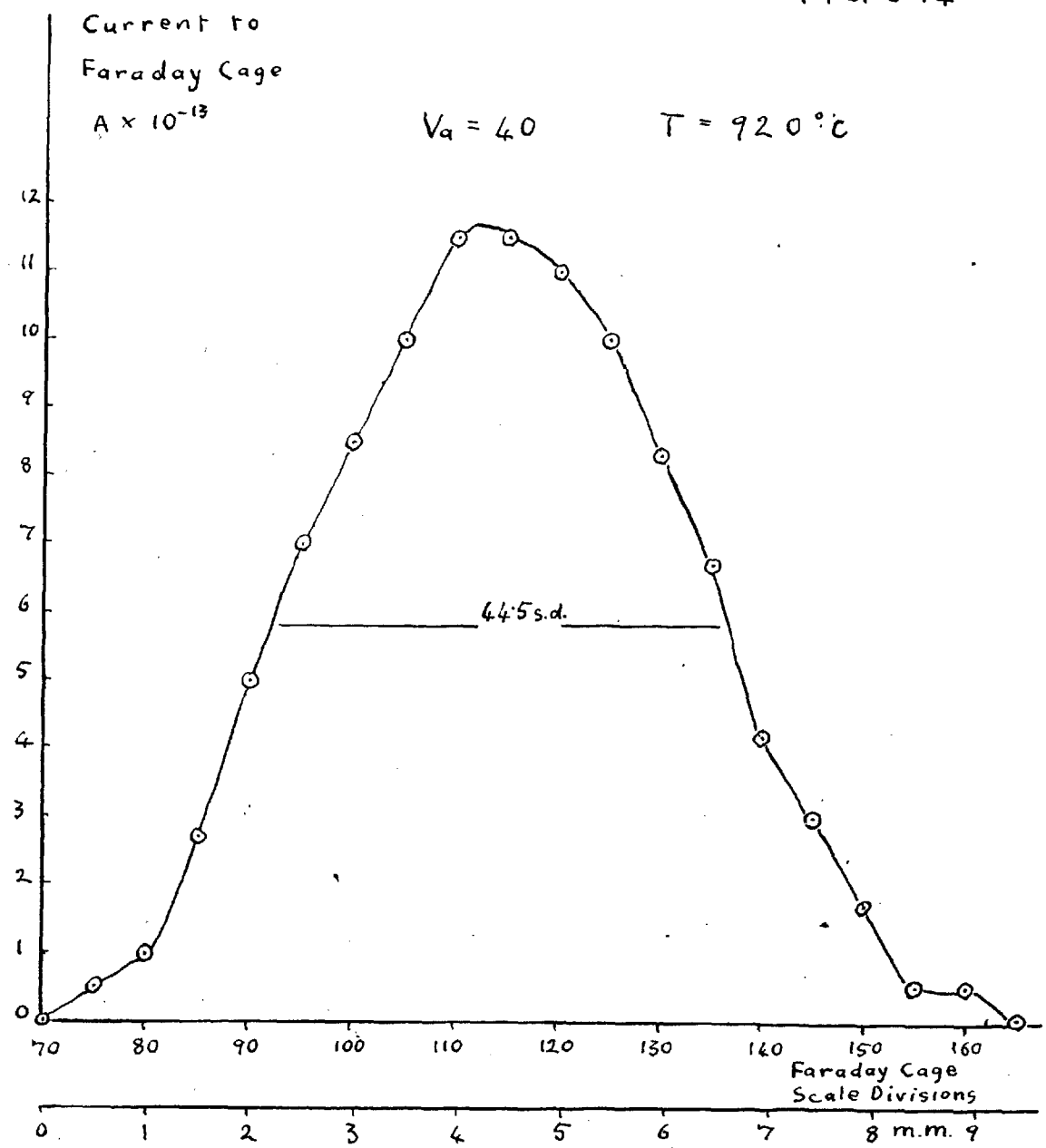
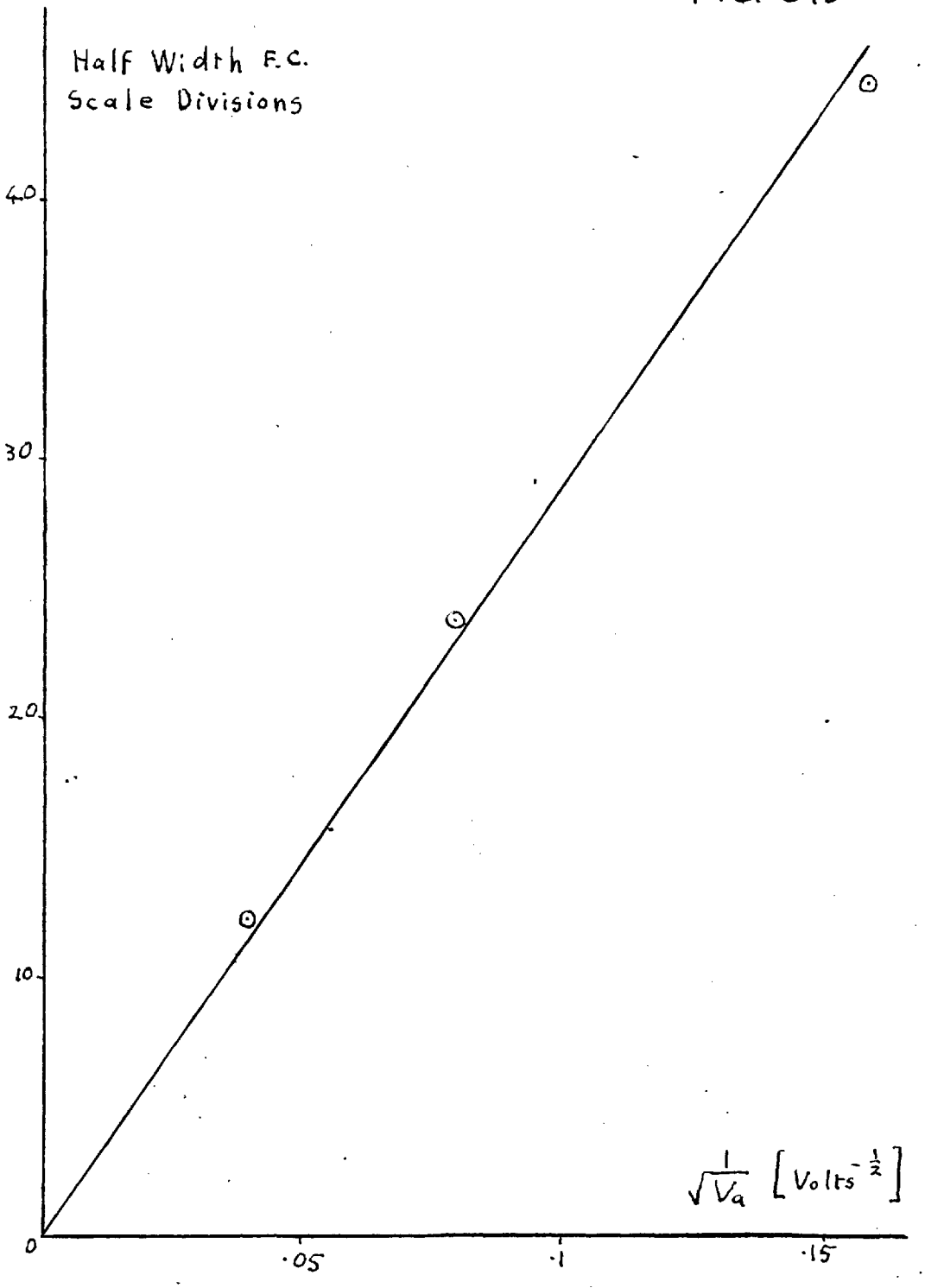

Current to
Faraday Cage
A × 10⁻¹³
Va = 40
T = 920 °C
12
11
10
9
8
7
6
5
4
3
2
1
0
44·5 s.d.
70
80
90
100
110
120
130
140
150
160
Faraday Cage
Scale Divisions
0
1
2
3
4
5
6
7
8 m.m. 9

FIG. C·15


Half Width F.C.
Scale Divisions
40
30
20
10
0
·05
·1
·15
$\frac{1}{\sqrt{V_a}}$ [Volts$^{-\frac{1}{2}}$]

where M is the compression of the beam at the anode, r_i is the radial position in the plane of the front of the Faraday cage, which is distant $\bar{z}_i$ from the anode pinhole.

The width of the experimental distributions was measured at the point where dJa had fallen to half the value measured on the axis, i.e. when

$$\log_e \tfrac{1}{2} = -.693 = \left[-\frac{eVa}{kT} M^2 \left(\frac{r_i}{\bar{z}_i}\right)^2\right]$$

Thus

$$(.693)^{\frac{1}{2}} = \left(\frac{eVa}{kT}\right)^{\frac{1}{2}} M \frac{r_H}{\bar{z}_i} \quad \ldots\ldots\ldots \text{(C.1) where } r_H$$

is the value of r_i at half height.

For a given temperature and geometry, r_H is a linear function of $Va^{-\frac{1}{2}}$.

The temperature of the cathode is connected with the radius of the projected pencil by the relation

$$T = 4{,}190 \frac{1}{\bar{z}_i^{\,2}} \left[\frac{r_H}{Va^{-\frac{1}{2}}}\right]^2$$

This follows from equation C.1 by squaring both sides and inserting numerical values for e, k and M.

The term in brackets is equal to the slope of the graph in fig. C.15 while $\bar{z}_i$ had the value $3.2 \pm .1$ cm.

The corrections applied leading to this value of $\bar{z}_i$ are discussed in Appendices 2 and 5.

Each Faraday cage scale division moved the carriage .099 ± .001 mm. so that

$$T = \frac{4,190}{3.2^2}\left(\frac{2.94 \times .99}{2}\right)^2 = \underline{870^\circ \pm 50^\circ K}$$

The quoted error is a maximum probable error due to inaccuracy of $\bar{z}_1$.

The mean temperature of the cathode as measured by the thermocouple was $1200^\circ \pm 10^\circ K$.

Discussion.

The velocity distributions measured were all of a Gaussian form with no striking irregularities. A theoretical Gaussian curve was fitted to the results obtained at 640 v. anode potential. Points on this theoretical curve are plotted in fig. C.12. The agreement with observations was good except on the fringes. The departures are probably due to drifting of the zero of the measuring circuit.

The comparative irregularity of the curve taken at an anode potential of 40 v. (fig.C.14), was probably also due to the same cause rather than a systematic departure from a Gaussian distribution.

The temperature measured was 27% low. This was probably due to the beam shaping screen being wrongly placed. If the beam diameter at the anode is greater than it should

be by 14%, this would make the measured temperature 27% low. The beam was in fact 10% too broad, so that the emission velocities must have been anomalously low. This is unusual since if the observed velocities depart from theory, they are usually found to be too high e.g. Meltzer and Holmes (1958) also Dietrich (1958). Perhaps the relatively poor vacuum conditions are relevant in this connection. Another possible contributary cause in the drop of some tens of degrees which sometimes occurs across the thickness of the cathode coating (Coppola 1960). It will be shown in Appendix 6 that the effects of focussing by the anode pinhole of space charge and of positive ions are negligible.

C3.2c Anode Pinhole off Axis.

If the anode pinhole is placed exactly at the edge of the beam, the pencil should theoretically be half missing, since no electrons could originate from points farther from the axis than the edge of the cathode. Figs.C.16 and C.17 show transverse velocity distributions obtained under these conditions. The anode pinhole positions can be compared with figs.C.6 and C.8 respectively. To obtain these results the Faraday cage was moved in the direction perpendicular to that previously employed. One 5° scale division on the rotating seal moved the Faraday cage $.274 \pm .003$ mm.

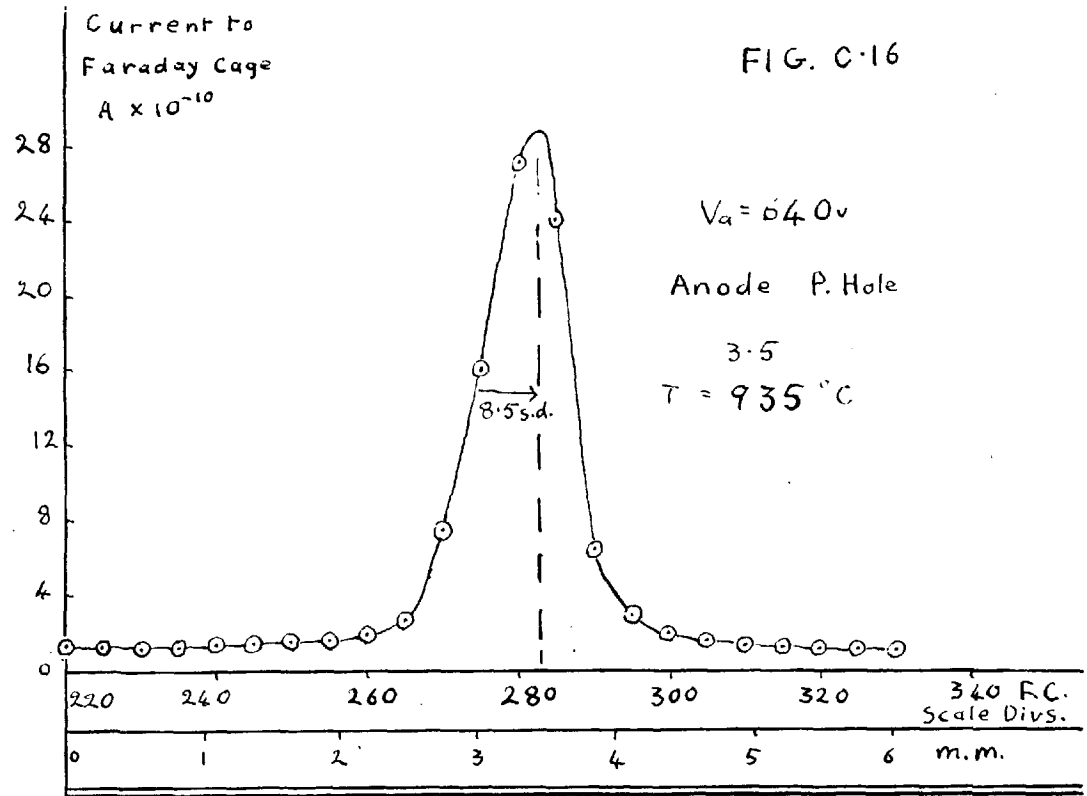


FIG. C·16

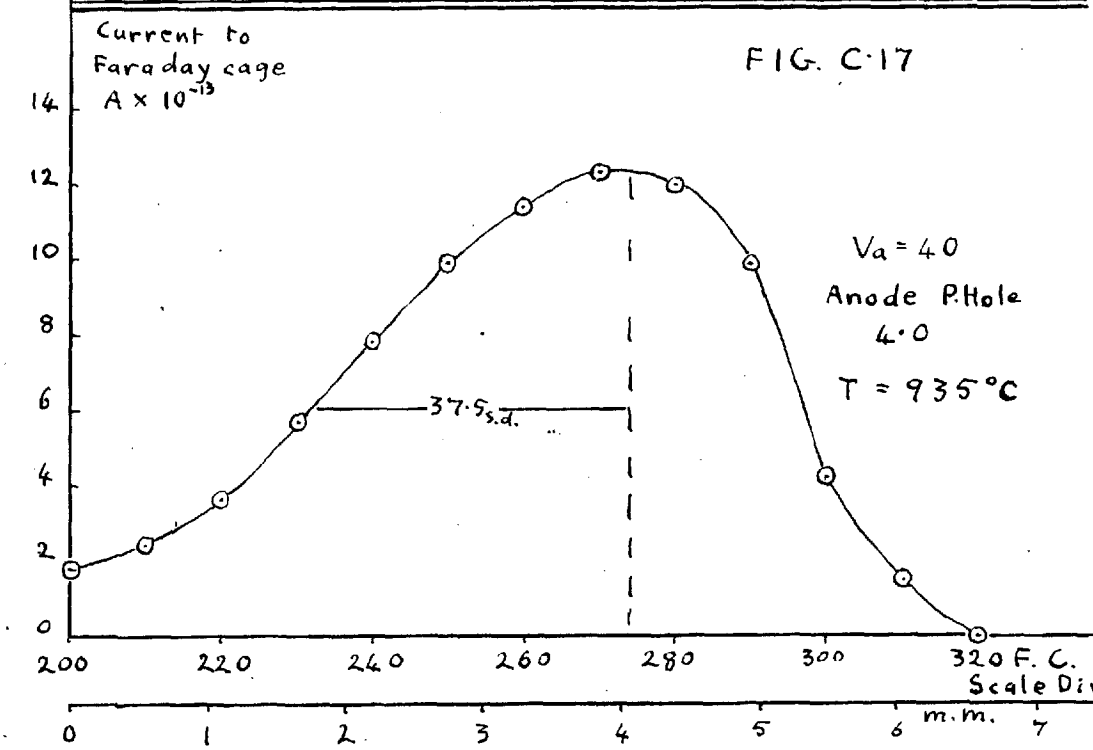


FIG. C·17

Discussion.

At anode potentials of both 640 v. and 40 v. the observed transverse velocity distributions were qualitatively correct. The current fell off twice as quickly as the Faraday cage was moved towards the axis of the apparatus as when it was moved away from the axis. When the Gaussian portion to the left of the maxima in figs. C.16 and C.17 are compared with figs. C.12 and C.14 respectively, the half widths measured at the edges of the beam are found to be 25% narrower. This is probably due to the convergence of the beam being lower at the edge of the beam than on the axis, since the equipotentials are not exactly spherical at the edge. The effect could not be accounted for by the cosine error (see Appendix 4).

C3.3 Measurements with Temperature Limited Emission.

C3.3a Current Density distribution.

Fig. C.18 shows the current density distribution across the beam measured at an anode voltage of 640 v. and a cathode temperature of 830°C. Under these conditions the emission current was .5 mA., about $\frac{1}{40}$th of the space charge limited value. Under these conditions the half width of the beam approaches $\frac{1}{4}$ its previous value and the current density distribution approaches a Gaussian shape. Fig. C.18 may be compared directly with Fig. C.6.

FIG. C·18

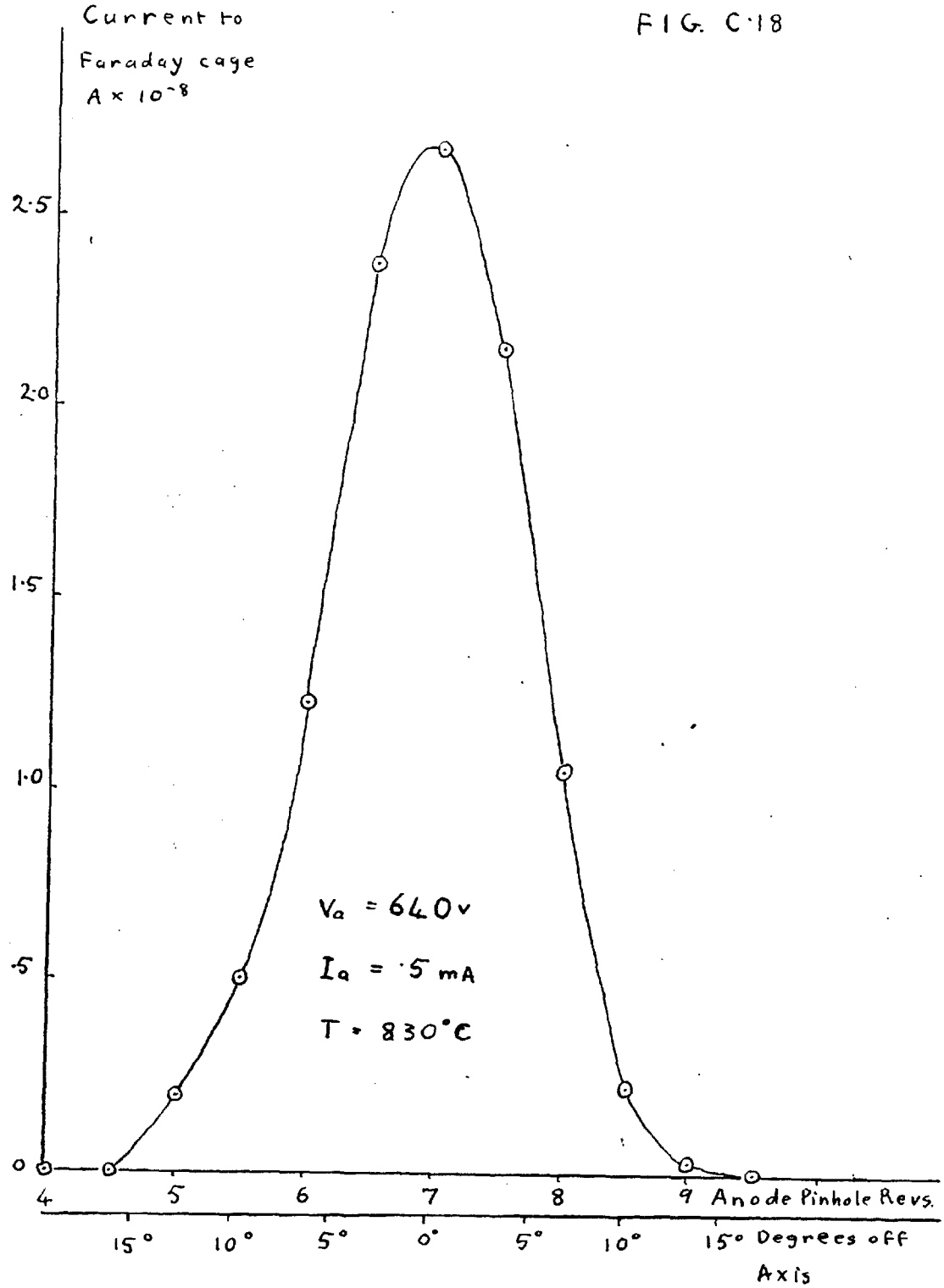
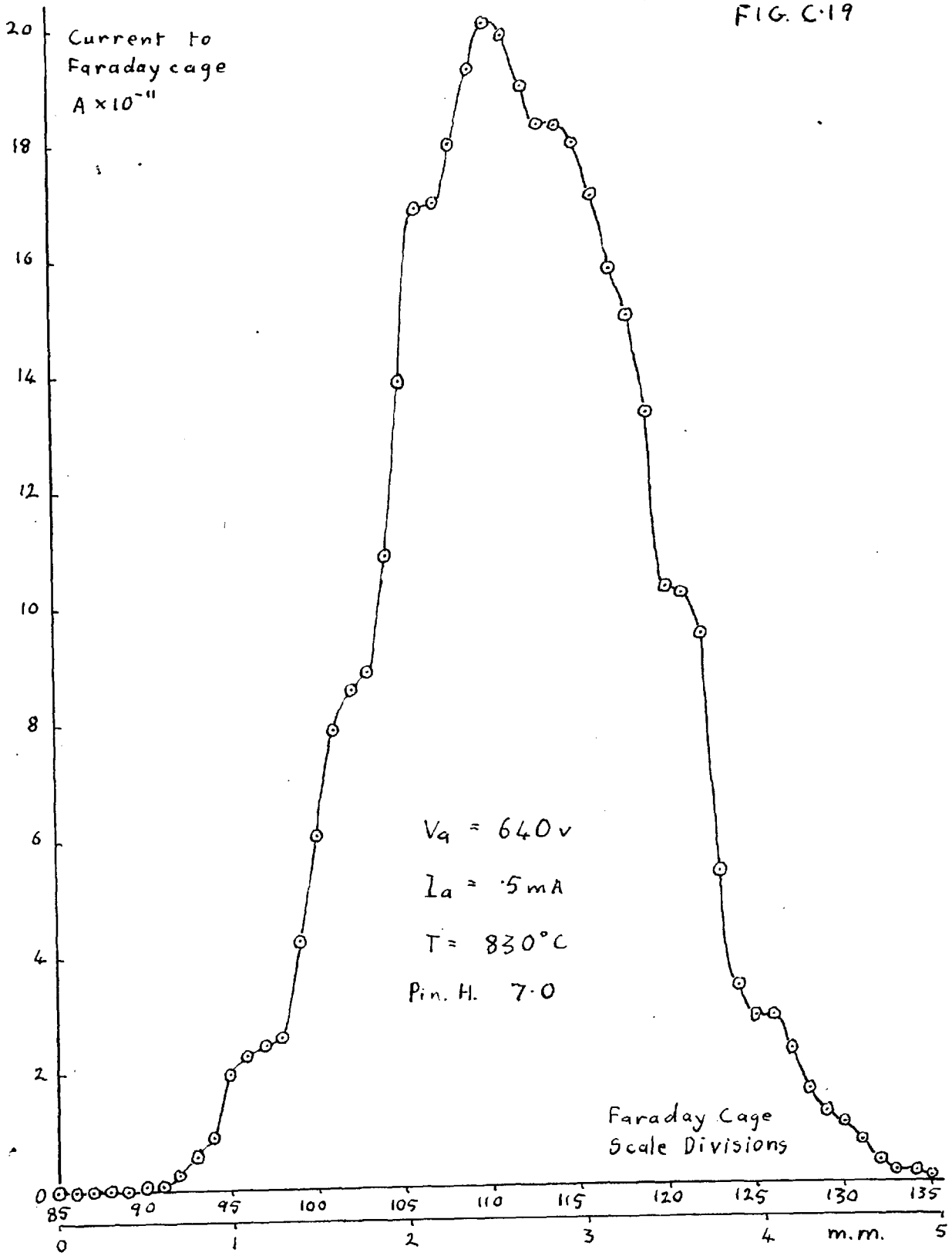

Current to
Faraday cage
A x 10⁻⁸
2·5
2·0
1·5
1·0
·5
0
V_a = 640v
I_a = ·5 mA
T = 830°C
4
5
6
7
8
9
Anode Pinhole Revs.
15°
10°
5°
0°
5°
10°
15° Degrees off
Axis

FIG. C·19


Current to Faraday cage
A x 10⁻¹¹
20
18
16
14
12
10
8
6
4
2
0
V_a = 640 v
I_a = ·5 mA
T = 830°C
Pin. H. 7·0
Faraday Cage Scale Divisions
85
90
95
100
105
110
115
120
125
130
135
0
1
2
3
4
m.m.
5

The contraction of the beam is due to the reduction of space charge.

C3.3b Transverse Velocities.

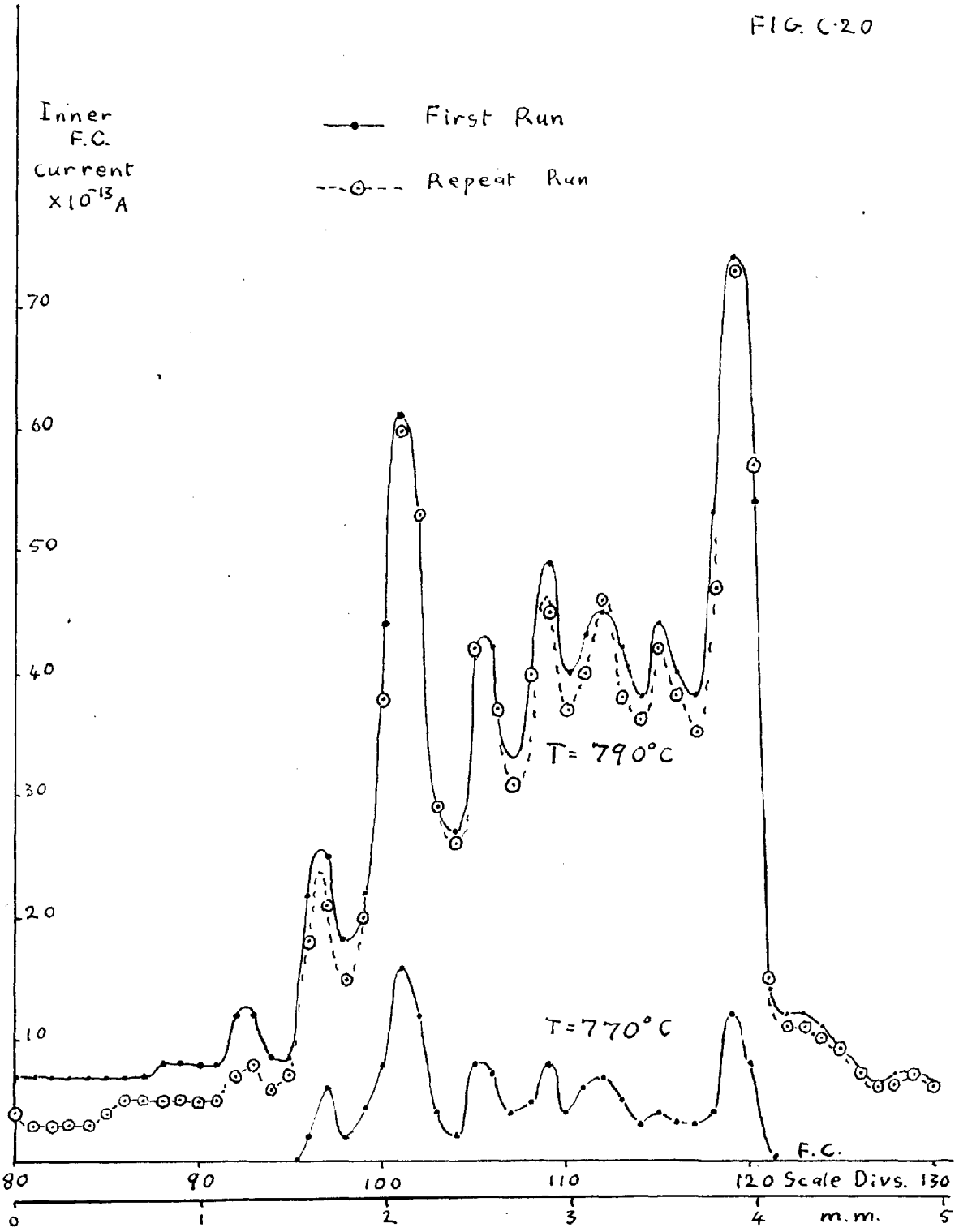
Fig.C.19 shows the thermal velocity distribution obtained with the anode pinhole on the axis and the cathode conditions the same as for fig.C.18. The same cathode was also used.

The striking appearance of this curve suggested a series of measurements of transverse velocity as a function of temperature. These results are shown in figs. C.20 to 22. The results were all taken over a period of about 4 hours with an anode potential of 640 volts. The temperature was varied from 770°C. to 880°C., which changed the emission current by a factor of about 1000.

Discussion.

At the lowest temperature used, the curve consisted of a series of maxima, the current falling to almost zero between them. As the temperature was increased, the maxima became superimposed on a distribution curve of Gaussian type, which became more and more regular, with the maxima indicated only by slight inflections.

FIG. C·20


Inner F.C. current $\times 10^{-13}$ A
First Run
Repeat Run
70
60
50
40
30
20
10
T= 790°C
T=770°C
F.C.
80
90
100
110
120 Scale Divs. 130
0
1
2
3
4
m.m.
5

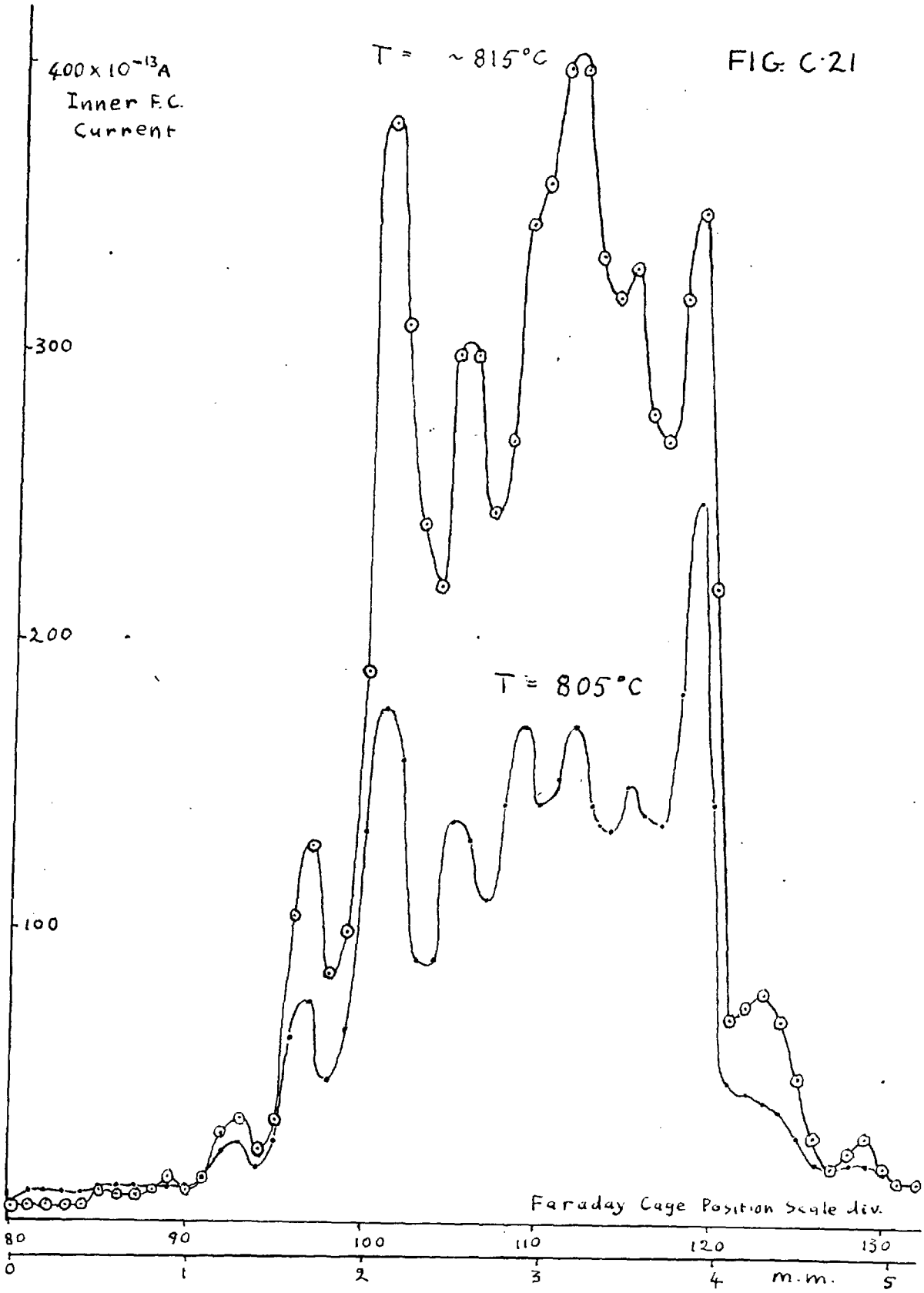
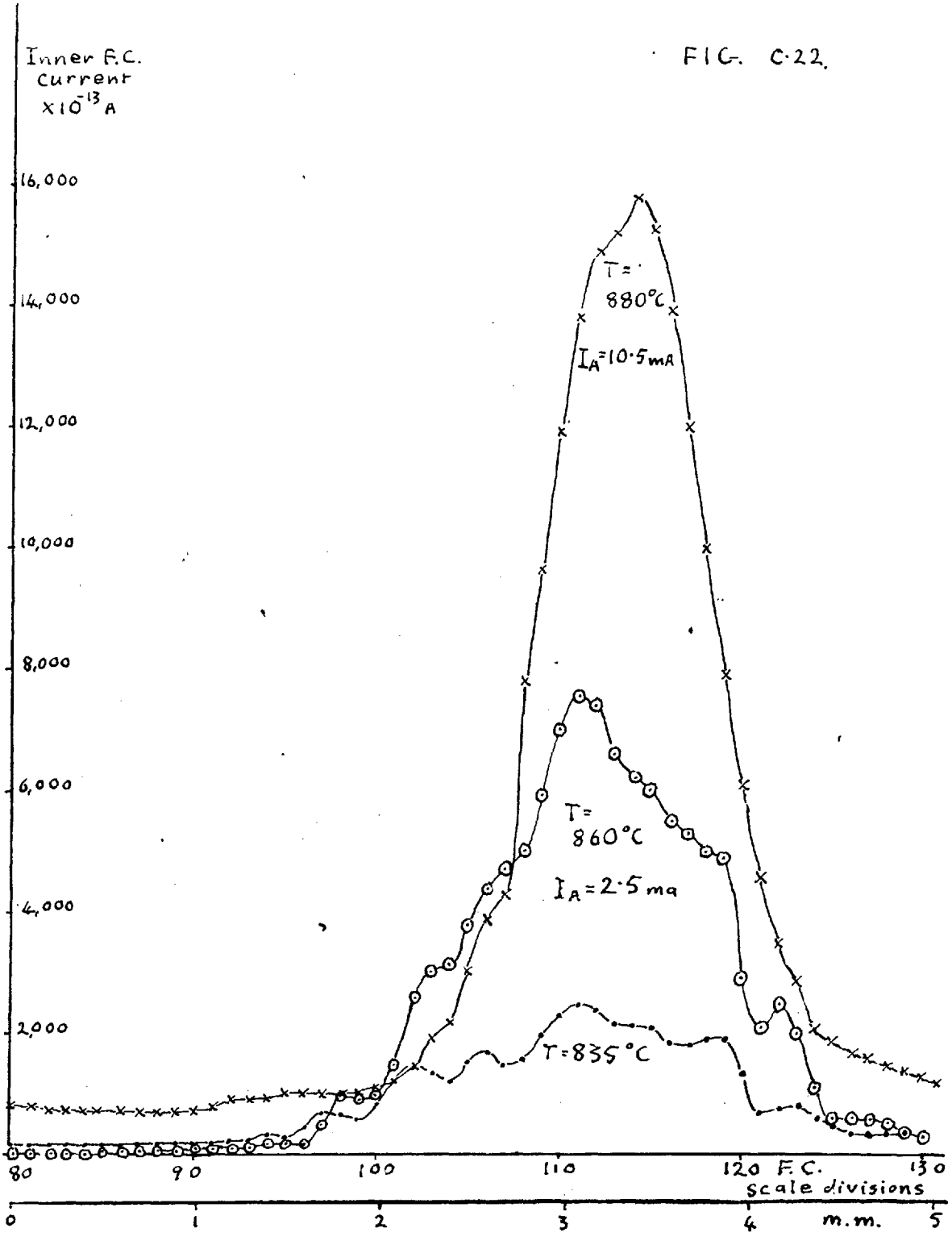

400 x 10⁻¹³A
Inner F.C.
Current
T = ~815°C
T = 805°C
300
200
100
Faraday Cage Position Scale div.
80
90
100
110
120
130
0
1
2
3
4
m.m.
5

FIG. C·21

FIG. C·22.


Inner F.C. current ×10⁻¹³ A
16,000
14,000
12,000
10,000
8,000
6,000
4,000
2,000
T = 880°C
I_A = 10·5 mA
T = 860°C
I_A = 2·5 ma
T = 835°C
80
90
100
110
120 F.C.
130
scale divisions
0
1
2
3
4
m.m.
5

The positions of all the peaks and inflections in figs. C.20 to C.22, are plotted as a function of temperature in fig.C.23. There is seen to be little uncertainty about the identity of each peak. When the total current to the anode exceeds about 10% of the saturation value, the pattern contracts. This is because space charge dilates the beam reducing the transverse velocities. (See sect.B2.4).

It was difficult to measure the height of the maxima above the background, but in fig.C.24, an attempt has been made to plot peak height against temperature for 7 representative maxima. The height of each maximum always rose monotonically up to the reading at 835°C., but it apparently saturated as the temperature rose above this value. In some cases neighbouring sources reduced the local field at the cathode, causing the height of a maximum to fall.

C3.3c Optical Examination of the Cathode.

Fig.C.25 is a drawing of a typical area of the surface of the cathodes used in all the investigations. This was as seen under a light optical microscope at a magnification of X150. There was a uniform coating of crystals about 5-10 microns in diameter, with a series of heaps of similar crystals superimposed. Only the latter are shown in the sketch. The heaps were typically about 150 μ in diameter. Using the calibrated focus adjusting micrometer of the microscope, they were found to project about 100 μ from the rest

FIG. C·23

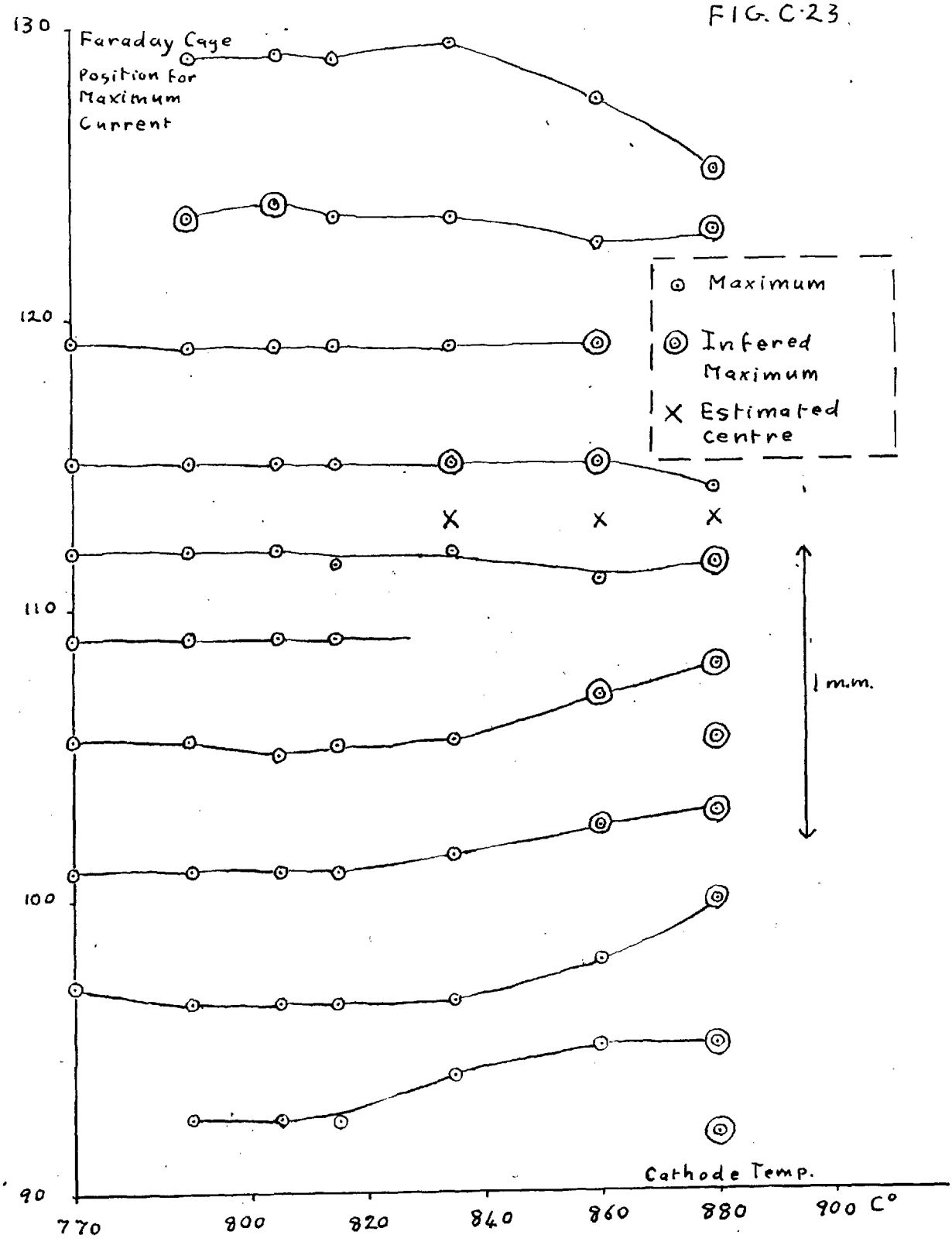

130
120
110
100
90
Faraday Cage
Position for
Maximum
Current
Maximum
Infered
Maximum
Estimated
centre
1 m.m.
Cathode Temp.
770
800
820
840
860
880
900 C°

FIG. C·24

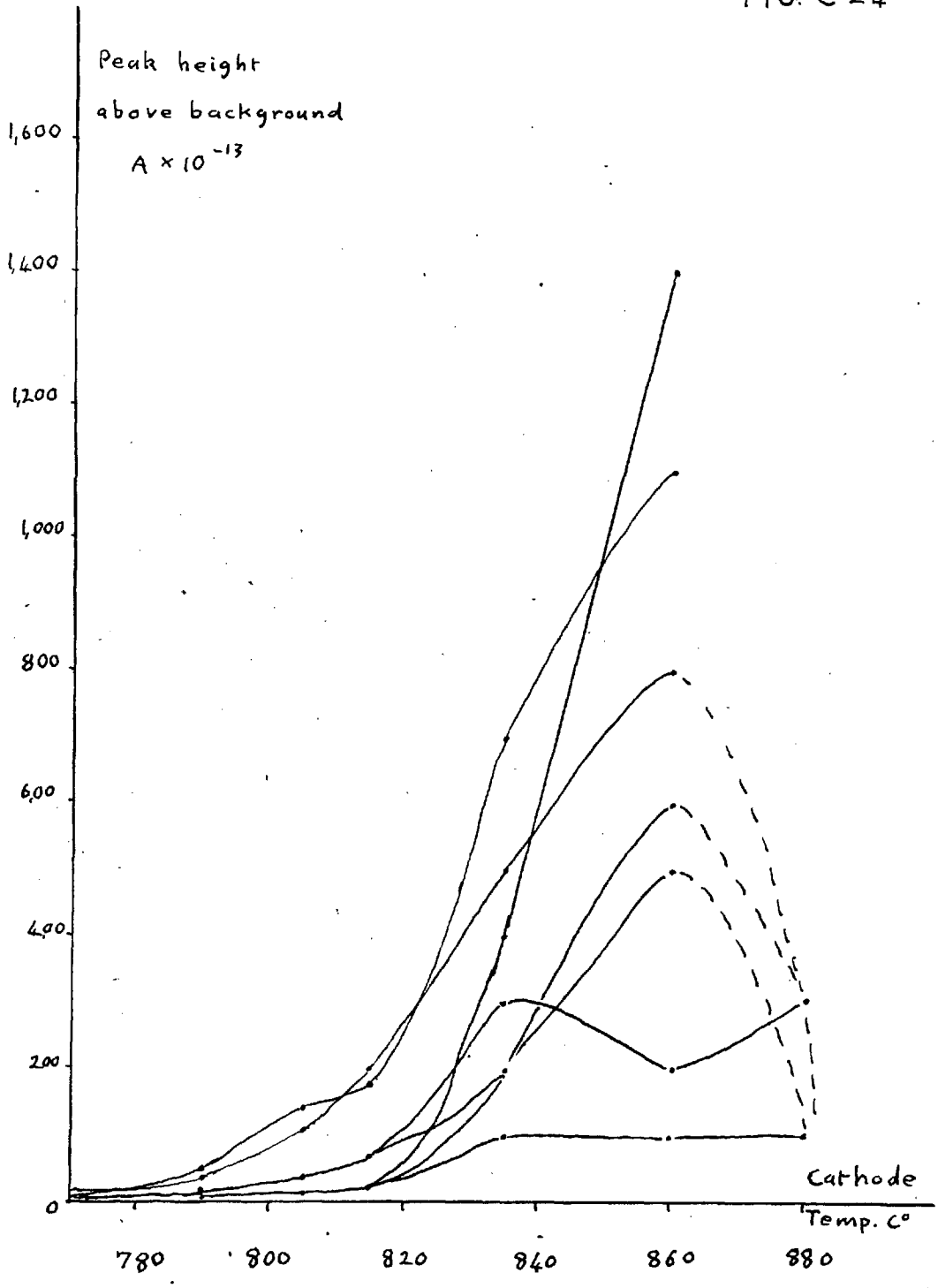

Peak height
above background
A × 10⁻¹³
1,600
1,400
1,200
1,000
800
600
400
200
0
Cathode
Temp. C°
780
800
820
840
860
880

FIG. C.25

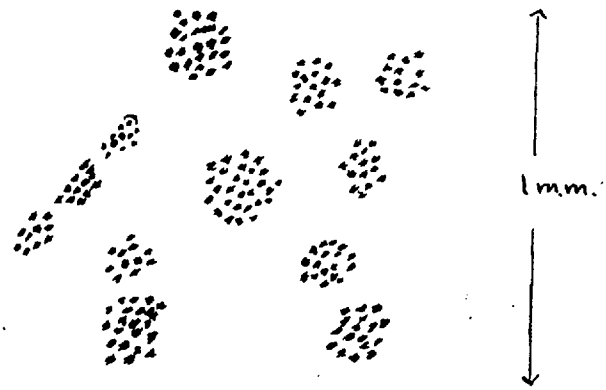
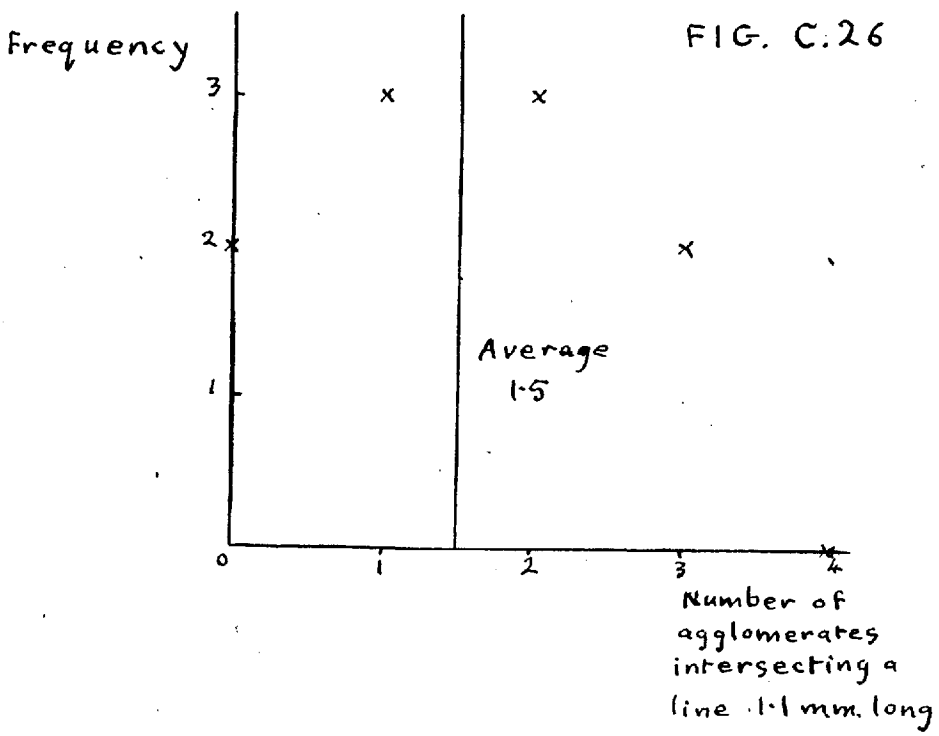


FIG. C.26



of the coating.

When transverse velocities are being measured, the electrometer registers electrons from a small patch of the cathode. As the Faraday cage is moved, the patch moves in a straight line across the cathode. Thus it is of interest to know the average number of agglomerates intersected by a line across the cathode.

A straight line in the microscope eyepiece, equivalent to 1.1 mm. length at the object, was superimposed at random points of the cathode surface. Fig. C.26 is a frequency chart showing the frequency with which a given number of agglomerates fell on the line.

The mean number of intersections was 1.5, so that the mean spacing of agglomerates was .7 mm.

The mean separation of the maxima observed at the Faraday cage in section C3.3b was about .5 m.m., while the electron optical magnification in the absence of space charge was about 1.

Thus the maxima observed in section 3.3b, were probably associated with the agglomerates.

Uneven withdrawal of emission from oxide cathodes has already been apparent in emission microscope studies, e.g. Johannson (1933).

C3.3d Comparison of Irregular Emission from Spherical and Strip Oxide Cathodes.

It is of interest to compare the results of section C3.3b, with similar results obtained by Klemperer (1947) using a strip oxide cathode.

The transverse emission energy and source position relative to the approximate centre of the distribution, were calculated using the theory given in Klemperer's paper and that in sect. B2.4.

Strip System (data from figs.12 and 14 of the paper by Klemperer.)

Temperature of cathode $\sim 700^{\circ}C$

Anode voltage 2500 v.

Anode current 900 μA

Anode current as a fraction of space charge limited value 0.033

Position	-1.1	-.4	+ .3	+ .6	+ 2.0 mm.
Transverse energy	.55	.07	.04	.16	1.8 eV.

Spherical System.

From fig. C.22

Temperature of the cathode $835^{\circ}C$

Anode voltage 640 v.

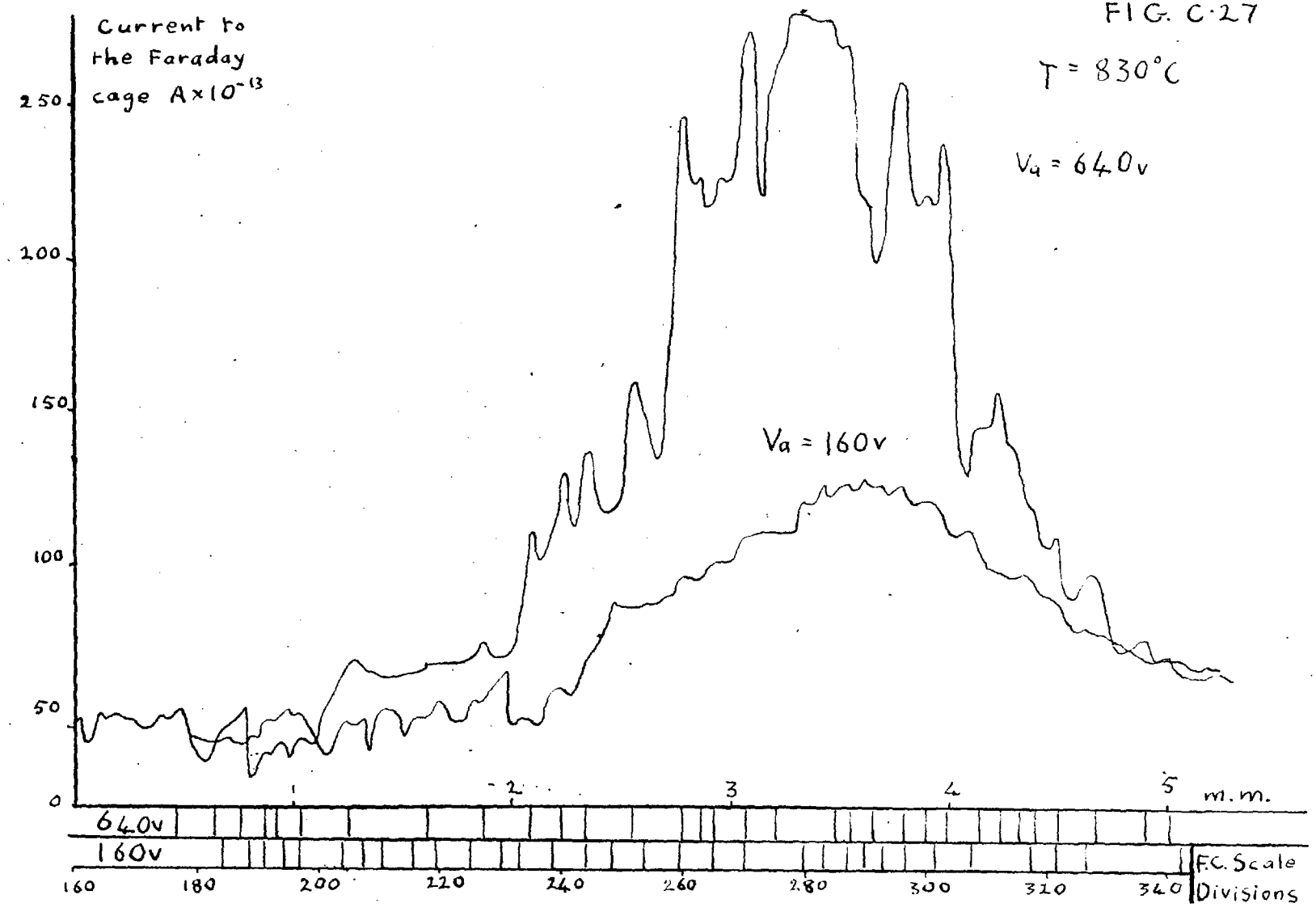
Anode current 800 μA

Anode current as a fraction of space charge limited value 0.1

Position	-3.2	-2.0	-1.2	-.4	+.2	+ 1.4	+2.2	+3.2	+3.8 mm.
Transverse Energy	1.8	.72	.26	.029	.0072	.35	.87	1.8	2.6 eV.

Klemperer (1947, p.389) tentatively put forward the theory that transverse oscillations of the space charge might be initiated by the unequal withdrawal of current from the cathode surface, and that the resulting standing waves in the space charge would be responsible for the large increase of transverse velocity components. However, if space charge oscillations were causing the maxima in the transverse velocity distribution, the position of these maxima would be unlikely to remain stable while the total emission changed by a factor of 1000.

If the emission from the cathode was irregular, the image projected by the anode pinhole would also be irregular. When numerical values were inserted in equn. B.6 the magnification under space charge limited conditions was found to be 0.8, In the absence of space charge the convergence of the beam was greater, leading to a higher magnification, estimated to be about 1. In section C3.3d, it is shown that the average spacing of maxima in the image is in agreement with the average separation of small heaps of oxide material on the surface of the cathode.


FIG. C·27
T = 830°C
V_a = 640v
V_a = 160v
Current to the Faraday cage A×10⁻¹³
250
200
150
100
50
0
1
2
3
4
5
m.m.
640v
160v
160
180
200
220
240
260
280
300
320
340
F.C. Scale Divisions

C3.3e Transverse velocities with improved resolution.

Fig. C.27 shows two transverse velocity distributions measured at different voltages and the same temperature with improved resolution and a more sensitive movement for the Faraday cage. The anode pinhole was now 40 μ in diameter and the Faraday cage aperture 60 μ in diameter. It is shown in Appendix 4, that this system should resolve points about 0.3 m.m. apart at the cathode.

The curve taken at an anode potential of 160 v. is more regular than that at 640 v., because the total emission is greater than $\frac{1}{2}$ of the full space charge value in the former case.

At the bottom of fig. C.27, all of the maxima and inflections are plotted. There is no correlation between the positions of maxima at the two different anode voltages. This is probably due to the Faraday cage receiving emission from an entirely different strip of cathode after the anode voltage had been changed. This could be a result of either a slight mechanical movement of the various components or a stray magnetic field. To produce a shift of 0.3 m.m. in the 5 cm. long trajectory of a 160 v. electron, a magnetic flux density of 10^{-5} wm^{-2} perpendicular to the trajectory would be required. Since this amounts to half of the residual magnetic field along the axis of the apparatus, it is difficult to see how such a large magnetic field could occur.

C3.3f Distance of the potential minimum from the cathode.

Due to the emission velocities of electrons perpendicular to the surface, a potential minimum is formed in front of the cathode. This minimum is well known as an agent for reducing noise in thermionic valves. Here, where it is playing a similar role in making velocity distribution curves more regular, it is of interest to compare the distance of the minimum from the cathode surface, with the height of the surface irregularities.

Using a formula given by Klemperer (1959, p.74), it is found that when the specific emission from the cathode is 5 times the current per unit area actually drawn, the minimum is about 60 μ from the cathode. Thus it will, to some extent, mask the surface irregularities of the cathode. However, if the specific emission is very high, say 500 times the current withdrawn per unit area, the minimum moves to within 20 μ of the cathode surface. It is at present a matter of speculation whether under such conditions the irregularities would reappear.

Conclusions.

In view of the stability of the irregularities of transverse velocity distributions observed, they are believed to be due to surface irregularity of the cathode. The

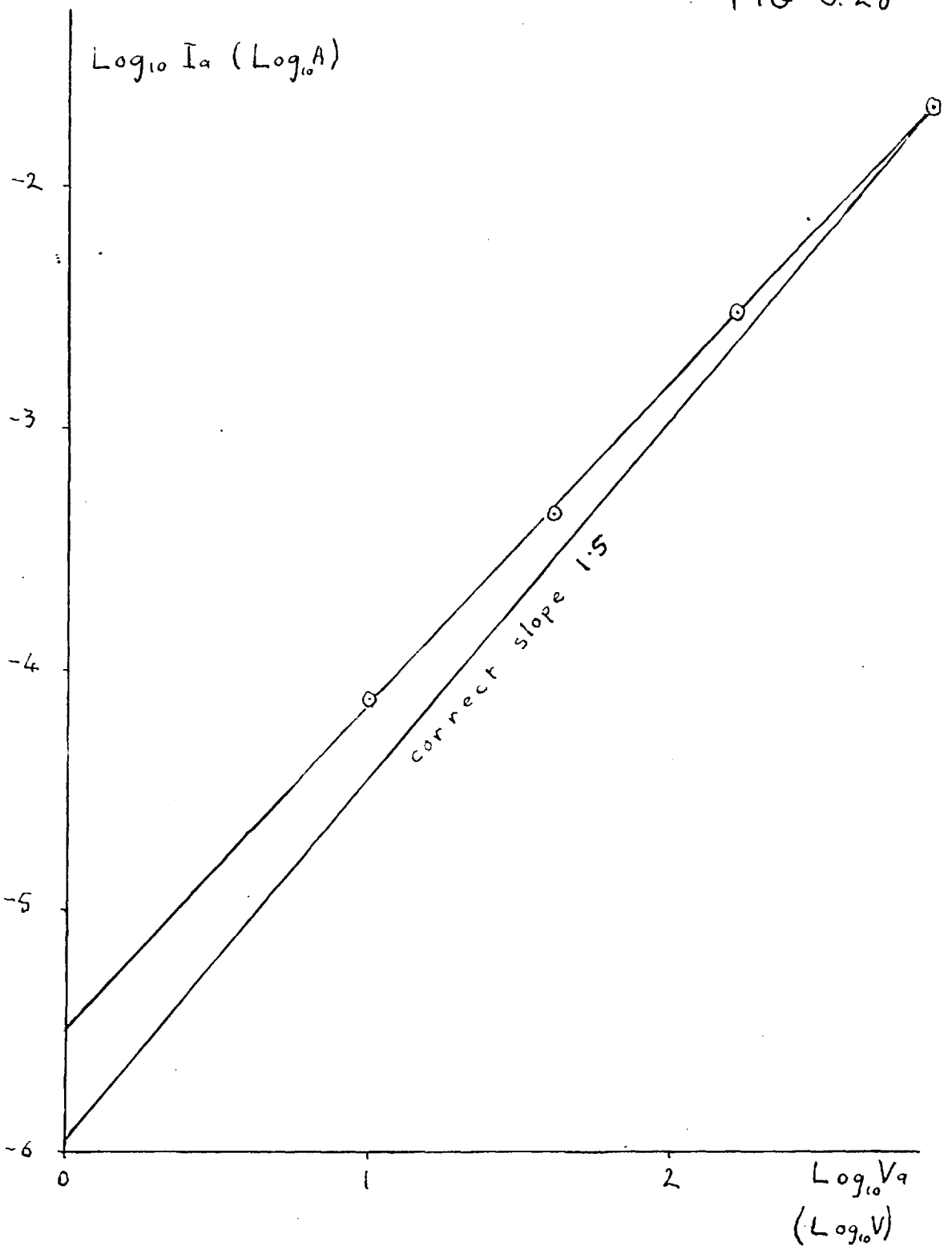
separation of the sources at the cathode is about equal to the size of the coarser surface irregularities.

Space charge limitation renders the irregularities ineffective under normal experimental conditions. If the temperature of the cathode is very high, the virtual cathode moves so close to the surface of the cathode that it may faithfully follow the surface irregularities. Under such conditions careful measurements at a high resolution might reveal that irregular transverse velocities are again present.

C3.4 Perveance of the system.

In fig.C.28 the anode current has been plotted against the anode voltage on a logarithmic scale. The linearity is satisfactory, but the slope is 1.34 instead of 1.5. This is due to the effect of emission velocities and the potential minimum, which cause departures from the three-halves power law at low anode potentials. The intercept of the line gives a perveance of 3.0×10^{-6} $AV^{-3/2}$. The data for an anode potential of 640 v. gave a value of 1.12×10^{-6} $AV^{-3/2}$, in better agreement with the theoretical value.

FIG C.28



D. FILAMENTRY CATHODES.

D1 Introduction.

Heated tungsten wire has long been used as a source of electrons. In X-ray tubes it is used in the form of a spiral or as a straight wire: in electron microscopes it is used in the form of a sharply bent, hairpin shaped loop. The tip of the hairpin is the hottest part, so that it forms something approaching a point source.

Hairpin cathodes are usually made from tungsten wire, but sometimes they have been made from platinum wire with an oxide coated tip. This type of cathode has been used for instance by Sakaki and Möllenstedt (1956), by Dietrich (1958) and in some commercial electron microscopes.

Under some conditions the distribution of emission from electron guns with hairpin cathodes is not what one would expect. Sometimes the beam is hollow with almost no electrons emitted along the axis, or the beam may consist of a number of discrete pencils.

These effects have often been attributed to a combination of irregularities in the cathode surface and electron optical aberrations. It has also been suspected that space charge oscillations may be the cause of the irregular emission distributions and there has been so far no general agreement about the explanation of the anomalous emission.

FIG. D:1

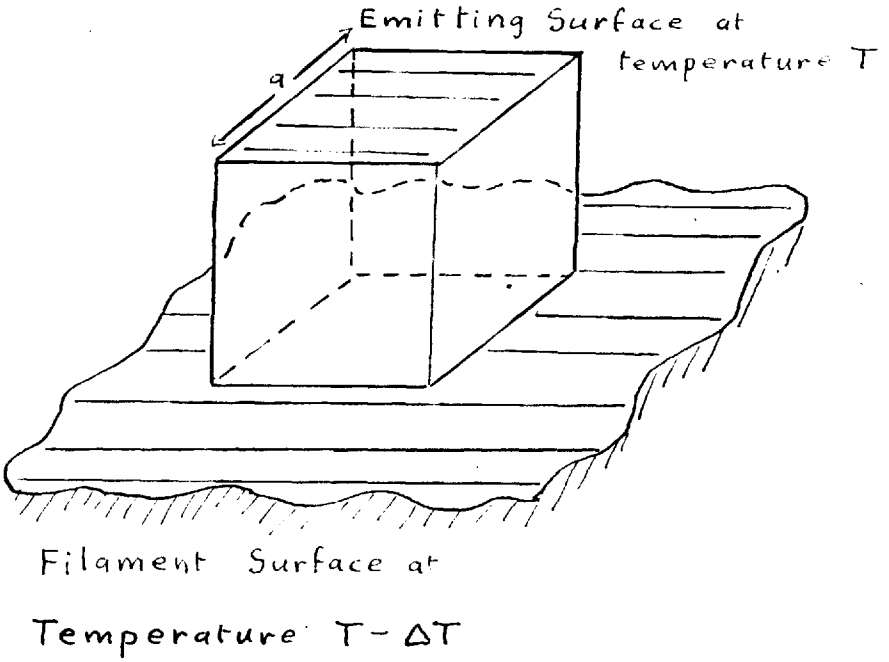
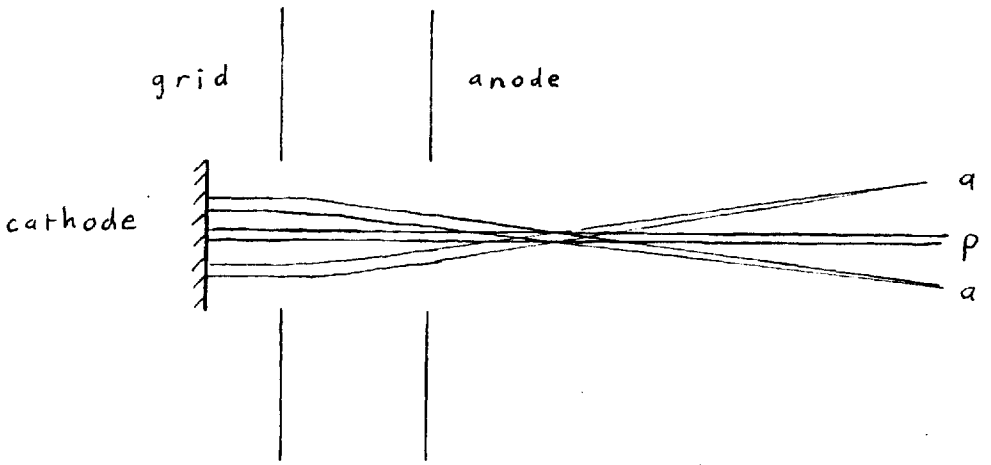

Emitting Surface at
temperature T
a
Filament Surface at
Temperature T – ΔT

FIG D·2


grid
anode
cathode
a
p
a

D2.1a Theory of Tungsten as a Thermionic Emitter.

A survey of the properties of tungsten as a thermionic emitter has been given by Nottingham (1956). After a tungsten filament has operated at its normal working temperature of about 2500°C for about an hour, the filament recrystallises, giving a rough polycrystalline surface as described by Seeman (1932). Under these conditions, the field at the surface, varies due to the geometrical imperfections and the crystal faces have different work functions, which cause contact potentials and thermionic emission of different intensities. These three factors all produce irregular emission.

Seeman (1932), also states that crystal spikes projecting from the surface of the tungsten, are cooler than the remainder of the filament.

Consider such a projection to be a cube of side a, joined to the filament as shown in fig.D.1. In order to obtain an estimate of the temperature difference across this cube, let the simplifying assumption be made that only the surface farthest from the filament is considered to radiate at temperature T, with emissivity ε.

Since the whole of the tungsten filament is small compared with the grid structure which encloses it, the Stefan-Boltzmann law may be written as $W = \sigma \varepsilon (T^4 - To^4)$, where W is the energy radiated in $cal.m^{-2}sec.^{-1}$ (see, for instance,

Sears 1949 p.317).

To, the temperature of the grid, is low enough to be neglected.

Thus the heat energy radiated from the outer surface of the projecting cube may be equated to the heat conducted across the cube owing to a temperature difference ΔT.

$$aC\Delta T = \varepsilon T^4 \sigma a^2$$

$$\Delta T = \frac{\varepsilon a \sigma}{C} T^4$$

Where C is the thermal conductivity at temp.T.

If $a = 10^{-5}$m. $c = 21$ joules m^{-1} deg^{-1} $T = 3000^{\circ}K$ $\sigma = 5.67 \times 10^{-8}$ joules m^{-2} deg^{-4} sec^{-1} and $\varepsilon = .3$, then

$$\Delta T \sim .7^{\circ}C$$

Consider now the percentage difference in thermionic emission corresponding to temperature difference ΔT.

The Langmuir-Richardson equation for the thermionic emission per unit area may be written:

$$I = AT^2 \exp.- \frac{e\phi}{kT}$$

where e is the electronic charge, k Baltzmann's constant, ϕ the work function of tungsten, and A is a constant.

Differentiating, and dividing both sides by I we obtain:

$$\frac{\Delta I}{I} = \left(\frac{2}{T} + \frac{e\phi}{kT^2}\right) \Delta T$$

Inserting numerical values $T = 3000^{\circ}K$ $e/k = 11{,}600$ deg./electron volt $\phi = 4.5$ volts $\Delta T = .7^{\circ}C.$, it is found that $\frac{\Delta I}{I} \sim .0046$.

Thus the projecting surface will emit .5 per cent less electrons per unit area than the rest of the surface. This variation is negligible in comparison with the effect of the work function varying from surface to surface.

A current per unit area of about 10^3 Am^{-2}, is commonly drawn from tungsten. If the anode potential is not sufficiently high to cause temperature limitation, a potential minimum is formed close to the cathode surface.

The depth and position of the minimum may be calculated (see for instance Klemperer, 1959), from the formulae

$$i = io \exp - \frac{eVm}{kT} \quad \text{and}$$

$$io = 2.3 \times 10^{-6} \, Vm^{3/2}/x_m^2$$

where i is the current per unit area passing from cathode to anode, io is the total current density adjacent to the cathode, Vm is the depth of the potential minimum and xm is its distance from the cathode. e, k and T have their usual meanings. If the specific emission is, for example, 10^3 Am^{-2} and 500 Am^{-2} current is drawn at a temperature of about 3000°K, the potential minimum will amount to -0.2 eV and is at a distance of approximately 10 μ from the surface of the cathode.

Wire of about 100 μ diameter is used to make hairpin filaments, so that when the applied anode voltage is not too high, the filament can be surrounded by a virtual

cathode. Its distance from the surface of the cathode is similar to the size of the surface irregularities, so that the virtual cathode is likely to follow surface irregularities to some extent.

D2.Jb The performance of tungsten filaments.

When tungsten wire is used as a hairpin cathode, the tip of the hairpin filament is the hottest part, due to conduction of heat to the supports and mutual heating of the closely adjacent sides of the loop. Some electrons are still emitted from the "legs" of the hairpin, but these can be suppressed by application of negative grid bias. Wittry (1957), describes a method for etching tungsten wire to reduce its cross section at the filament tip producing a locally higher temperature, which reduces emission from the filament legs. It has the further advantage of reducing the size of the source.

Experiments by Dolder and Klemperer (1956, 1957) indicated that oscillations may occur in the space charge near hairpin cathodes. The wavelengths due to such oscillations as calculated from Langmuir's plasma frequency formula appeared to be in approximate agreement with the separation of intensity maxima measured by pinhole camera observations. Other authors, however, ascribed the intensity maxima of emission to a roughness of the filament

surface, see for instance Hillier and Baker (1945). Moreover, Haine and Einstein (1952) have shown that hollow beams can be formed due to spherical aberration in the emission system. The way in which hollow beams can be formed in systems with spherical aberration, has originally been pointed out in the description of a pinhole camera test for spherical aberration by Klemperer (1951). There it is shown that electrons of an initially uniform current distribution over the cross section of the beam, can converge into distinct zones.

Another interesting phenomenon observed with electron guns with hairpin cathodes is the anomalously high thermal velocities of the emitted electrons, (Dietrich 1958) and the variation of the apparent electron temperature with beam current.

Fack (1955) decided that it is impossible for ordered translational energy to be converted into disordered thermal energy. He stated that the anomalous temperatures are caused by mutual interaction of local space charges caused by the shot effect. He finds that the anomalous temperature depends on the square root of the current density in the beam.

Another phenomenon which might increase the beam temperature under the appropriate conditions is the beam compression effect mentioned in section B2.4. As a

consequence of the conservation of energy, the range of thermal energies along the axis is also increased. Translational energy is converted to thermal energy in this process.

It has been found (e.g. Meltzer and Holmes, 1958) that when the beam from an electron gun is allowed to fall on a collector, negative with respect to the cathode, a plot of current to the collector against its negative potential shows two regions. In both regions the current falls exponentially with the collector voltage but in one, falls more slowly, corresponding to a higher apparent cathode temperature.

This is possibly due to beam compression combined with complicated spherical aberration.

Fig.D.2 shows the type of situation which might occur. Spherical aberration has divided the beam into two regions, a paraxial pencil p, and an annular region a. If the beam compression is different in the two regions, a double beam temperature will be observed.

D2.2 Experiments with Tungsten Filaments.

D2.2a Twin hairpin cathodes with a slotted grid electrode.

Dolder (1954) reported an experiment with two tungsten hairpin filaments arranged at either end of a rectangular slot in the grid electrode (see fig.D.3).

FIG. D·3

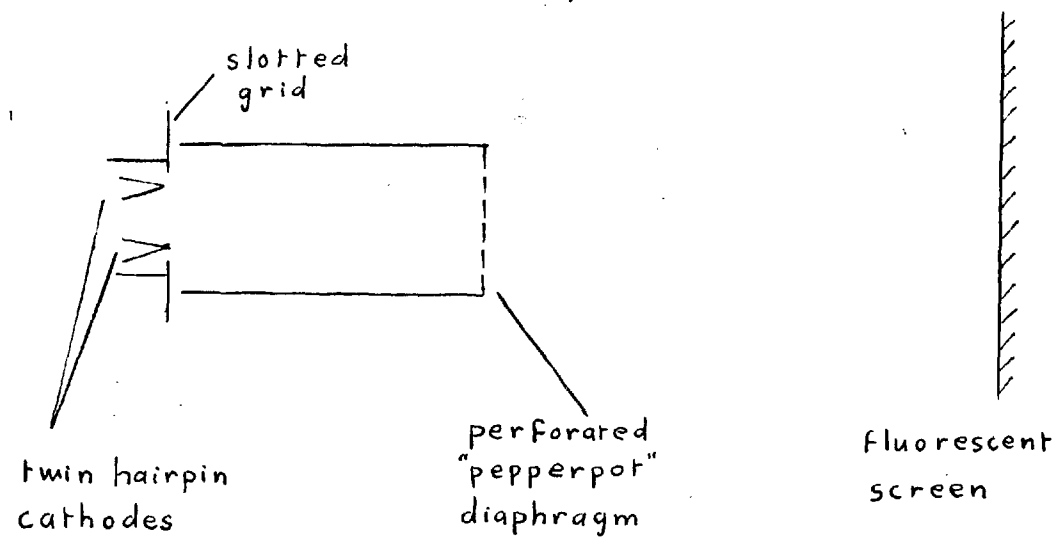
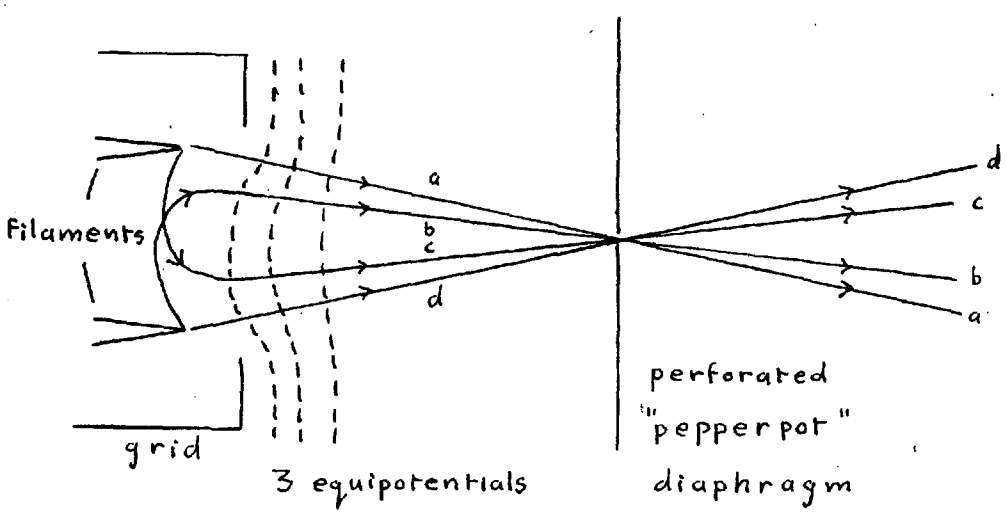

slotted grid
twin hairpin cathodes
perforated "pepperpot" diaphragm
Fluorescent screen

FIG. D·4


Filaments
a
b
c
d
grid
3 equipotentials
perforated "pepperpot" diaphragm
d
c
b
a

Some of the electrons emitted by the filaments, passed through the pinholes in the anode forming an image on the fluorescent screen.

As in Dolder's experiments, the image projected usually consisted of a number of spots often arranged in a straight line, but in addition, it was found that the pattern can sometimes consist of two overlapping patterns, each fed by one filament. This suggested that the spots are the result of geometric effects.

In fig.D.4 a possible explanation of the overlapping patterns is shown. The dimensions are distorted for clarity.

The electrons following trajectories b and c, have a high thermal velocity and pass through a region where the equipotentials are so shaped as to concentrate a number of similar trajectories towards the pinhole (cf. Klemperer's test for spherical aberration (1951)). Thus pencils b and c cause the projected patterns to overlap. The quantitative agreement of Dolder's results with theory based on space charge oscillations was probably fortuitous.

D2.2b Twin hairpin cathodes with a circular grid shield.

This experiment was a repetition of work reported by Dolder (1954). The apparatus used was similar to that

shown in fig.D.3, with the difference that the filament tips were placed about 1mm. apart, behind a grid electrode with a circular aperture 2 mm. in diameter.

According to Dolder's observations the multiple images projected by each pinhole suddenly fused together when the filaments were gradually withdrawn from the grid aperture. A simultaneous observation of the angular distribution of the electrons emitted from the system, showed the transition from a complicated distribution into a simple Gaussian distribution when fusion had taken place. The pinhole camera observations were repeated here with finer camera holes and it was seen that sudden complete fusion of the images never took place. It might therefore be assumed that with distances of the order 1 mm. between the cathode tips, a superposition rather than coalescence of images takes place, and that the scource is formed by a cross-over rather than by a virtual cathode.

In the case of a cross-over of rays, however, it should be possible to see distinctly separate images of the two filament tips.

The apparent fusion of images was observed by Dolder to occur at a well defined grid bias, which could be plotted as a linear function of applied anode voltage. No well defined grid voltage for the fusion could be found here although several experimental variations were tried in order

to reproduce exactly Dolder's experimental conditions.

These variations were concerned with:-

1. The potential of the glass bead supporting the filaments. This was varied by means of an evaporated aluminium coating with a suitable contact. (This did change the projected images but not in accordance with Dolder's results.)
2. Accuracy of construction. Due to distortion of the tungsten filaments when they were heated, the accuracy of construction was limited, but of the 15 different pairs of filaments used, at least some should have been similar to Dolder's. In the later experiments shorter filaments were used to reduce distortion.
3. Relative potential of the filament tips. This was varied in steps of 0.05 volts between $\pm$ 1 volt.
4. Shape of the filament tips. The sharpness of the bend was varied.
5. Spacing between the filaments. A few experiments were made with exactly controlled spacings between the tips of the filaments. Some difficulties were, however, experienced owing to changes of these spacings occurring when the filaments were heated.
6. Fields produced by the filament legs. The D.C. heating current through one of the filaments was reversed to see whether this produced any important effect due to

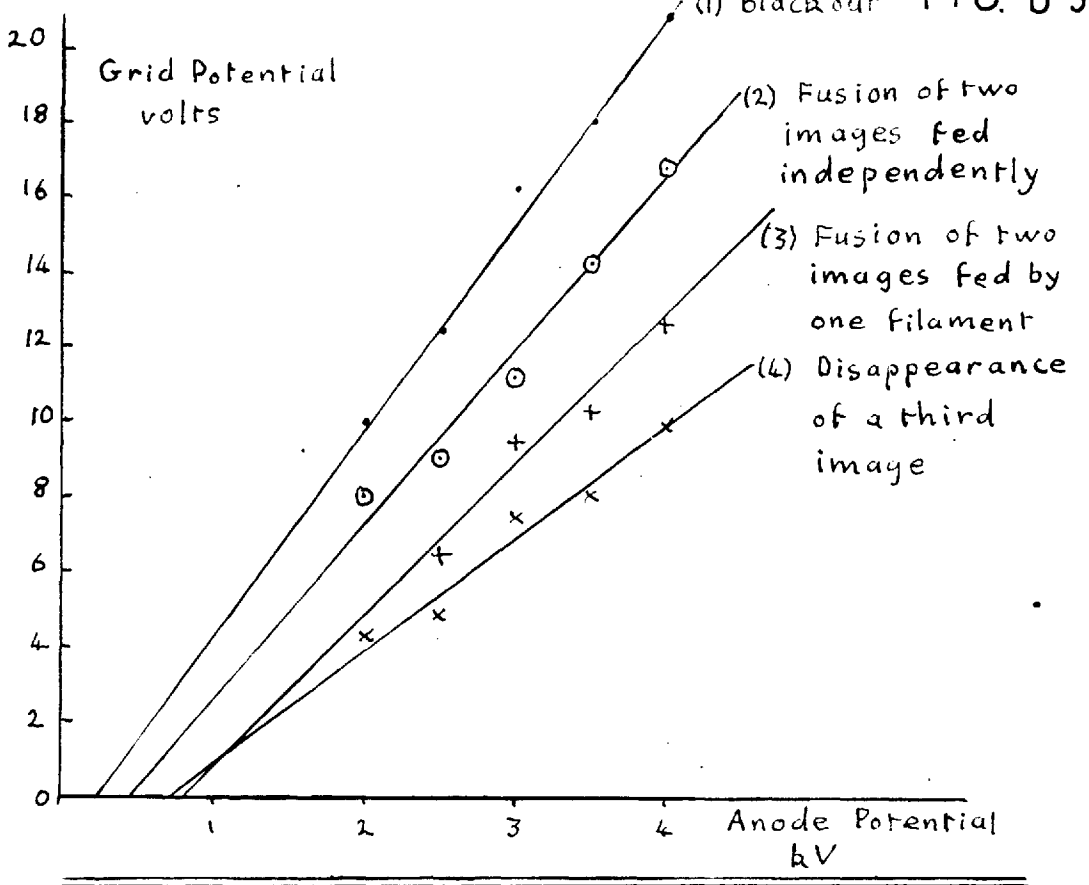

(1) Blackout
(2) Fusion of two images fed independently
(3) Fusion of two images fed by one filament
(4) Disappearance of a third image
Grid Potential volts
20
18
16
14
12
10
8
6
4
2
0
1
2
3
4
Anode Potential kV

FIG. D·5

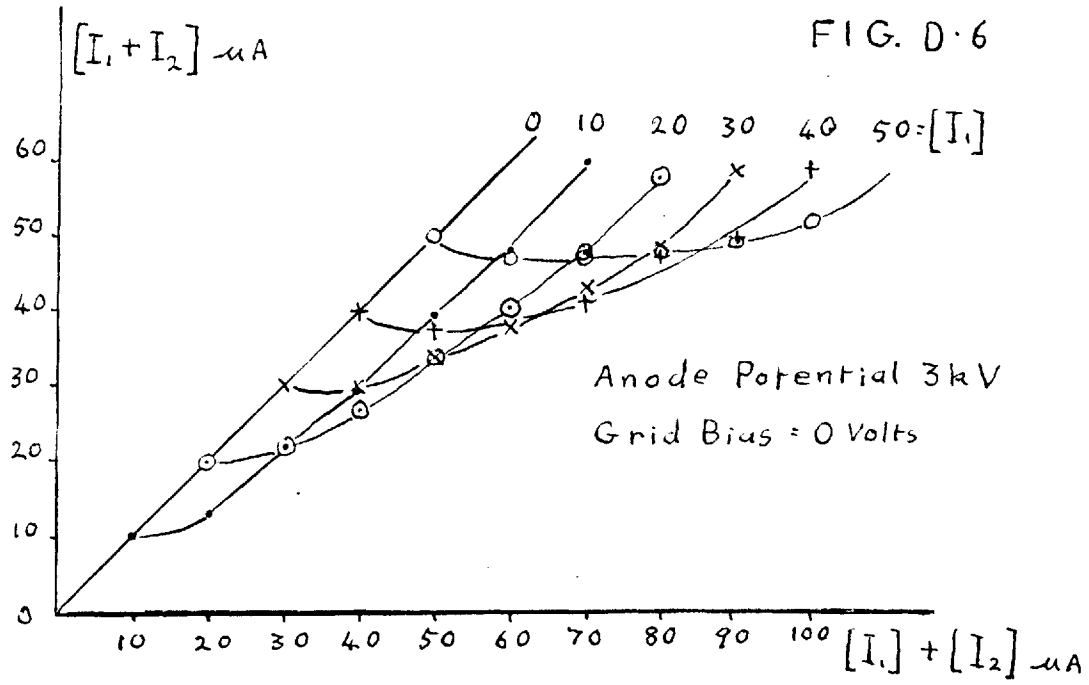

$[I_1 + I_2]$ μA
0 10 20 30 40 50 = $[I_1]$
60
50
40
30
20
10
0
10 20 30 40 50 60 70 80 90 100
$[I_1] + [I_2]$ μA
Anode Potential 3kV
Grid Bias = 0 Volts

FIG. D·6

changes in the magnetic and electrostatic fields around the filament legs.

7. The absolute potential of the cathode with respect to earth was varied.

8. The vacuum conditions were altered by performing an experiment in a system pumped by a mercury pump instead of the usual oil diffusion pump.

9. The size of the pepperpot holes was reduced to about 25 μ diameter. With holes of this size details 1/10 th. of the separation of the filament tips should be resolved.

10. Emission currents of up to 300 μA were drawn from each filament to ensure the maximum interaction of space charge.

Some effects were observed similar to those which were described by Dolder. These are plotted in fig. D.5.

The curve (1) shows black-out voltage for the total extinction of the images, as a function of anode voltage Va, curve (2) is the grid voltage for an ill-defined fusion of two images projected from two filaments. Graph (3) gives the grid voltage for apparent fusion due to superposition of two images from the same filament. Curve (4) gives the bias required for the disappearance of a third image. In each case the filaments were 1.5 grid aperture radii behind the grid.

Each line resembles the graph obtained by Dolder, showing that the phenomenon which he observed was probably connected with a sudden change caused by the focal length of the grid lens passing through a critical value, e.g. when the grid converged the emission from the filament tips on to the pepperpot diaphragm.

D2.2c Interaction of emission currents from twin hair-pin cathodes.

In order to see whether interaction of space charge from the two filaments used in section D2.2b had an important effect on the projected images, the following experiment was performed.

The two filament tips were placed 0.5 mm. apart, 2.5 mm. behind the grid aperture. First one filament was heated and the total emission from the filament $[I_1]$ was measured with a microammeter. This was repeated with only the second filament heated giving $[I_2]$, then both were heated and the total emission $[I_1 + I_2]$ was measured.

Fig. D.6 is a plot of $[I_1 + I_2]$ against $[I_1] + [I_2]$, with a constant value of $[I_1]$ as parameter for each curve.

The total emission $[I_1 + I_2]$ was always much less than the sum of the emission from each filament when heated separately. Sometimes the combined total emission was less than that from either filament separately.

Further investigations showed that these effects were partly due to the potential of the filament legs. The total emission from one filament was found to fall even when the current through the second filament was insufficient to cause thermionic emission, but it is doubtful whether this accounts completely for the reduction of total emission. No conclusions can be drawn from this type of experiment unless the filament legs are very carefully shielded to prevent their introducing stray fields at the filament tips.

D2.2d Straight Tungsten Filament - Seeman's Experiment.

Seeman (1932) reported that pinhole camera images formed by the electron emission from straight tungsten filaments, consisted of a series of separate spots or lines.

His experimental arrangement, which was reproduced here, consisted of a flat perforated anode placed in front of a straight tungsten filament so as to project an image on to a fluorescent screen.

Seeman believed that the projected image consisted of spots because of the rough, crystalline surface of the tungsten wire. On the other hand, Dolder and Klemperer (1956), tried to explain the multiple images by assuming standing waves in the electronic space charge along the surface of the filament. This view seemed to be supported by an experiment by Dolder (1954), in which he found that

multiple images were only visible when an additional electrode at cathode potential was placed behind the filament, thus increasing the density of the space charge.

The experiments performed by the author were in agreement with Seeman's explanation for the following reasons.

1. The presence of an additional electrode at cathode potential was not a necessary condition for spots to occur. Indeed, they were frequently observed more clearly when the additional electrode was at the potential of the anode. This potential appeared to affect only the electron optics of the system.
2. A new filament at first produced only uniform illumination on the screen. Only after remaining incandescent for about half-an-hour did the image break up into spots. The length of the image also increased by 400 per cent over a period of 3 hours. This corresponds to an increase of the transverse velocity component of the electrons.

Both effects were apparently associated with a change of the crystal structure of the tungsten. When the filament was examined optically after an experiment, it was much rougher than before being heated. This was also mentioned by Seeman, (1932).

3. The pattern of spots was stable with no critical dependence on temperature, anode potential, or geometry.

D2.2e Conclusions drawn from experiments with tungsten cathodes.

No observations were made of effects which required space charge oscillations as an explanation. The experiments with a straight filament emphasised the importance of surface irregularities. The experiments with twin hairpin cathodes showed that such systems must be considered from first principles and not treated as perfect, aberration free systems. So far no experimental evidence leads necessarily to the assumption of space charge oscillations.

D3 Oxide tipped hairpin cathodes.

D3.1 The theory of oxide tipped cathodes.

The hairpin filaments were made of 0.1 mm. platinum wire bent into as tight a loop as possible. Platinum has a relatively very high work function so that no substantial emission should be expected from it at the temperature employed. The tip of the hairpin was then dipped into a paste of 50% barium and strontium carbonates with a little water. This gave a small emitting layer of 0.1 mm. x 0.2 mm. and of about 10 μ thickness. After heating, the oxide formed a continuous glassy layer.

According to data published by Mahlman (1949), a resistive drop of about 1 volt across the oxide layer is to be expected when the temperature of the cathode is 1000°C, and when a current of 100 μ Amps is drawn. Such a voltage had no effect on the measurements carried out.

Since only a very small area on the front of the filament tip was coated, the space charge conditions are comparatively uniform over this patch. Thus the emission from the filament could be expected to follow the 3/2 power law when the anode potential was increased. This is different from the case of a tungsten filament, where the extreme tip may be temperature limited, while other parts may be shielded by the grid and rendered space charge limited.

D3.2a Multiple images.

It was noted that multiple images are formed by oxide tipped cathodes. Thus emission of electrons from the legs of hairpin filaments must be ruled out as the sole source of multiple images. The cause in this case is likely to be the irregular emission from the oxide coat already referred to in section C3.3c.

D3.2b Space charge limited emission.

An oxide tipped cathode was mounted in a simple electron gun with a circular grid aperture of radius 1 mm. and an open, cylindrical anode. Provision was made to measure the total emission from the cathode. Fig. D.7 shows the emission current I, plotted against anode voltage Va. The curves shown there refer to various cathode to grid spacings (c), expressed in terms of grid aperture radii (r_g), at zero grid bias (Vg = 0). Two different filament currents were used, which raised the temperature of the cathode to T_1 and T_2 respectively.

In order to give an indication of the conditions under which the emission occurs it was of interest to know the temperature limited currents. These were always measured under certain standard conditions given by a cathode to grid spacing c = o and with an anode voltage Va = 2kV. These currents under standard conditions Ist, are marked at each curve. In spite of the readings being taken in rapid succession, the specific emission from the oxide tip tended to vary.

The curves showed a region with space charge limitation in which the $^3/_2$ power law was obeyed. The latter was verified by plotting the emission current against $Va^{3/2}$ in fig. D.8. All but one of the curves in D.8 correspond

FIG. D·7

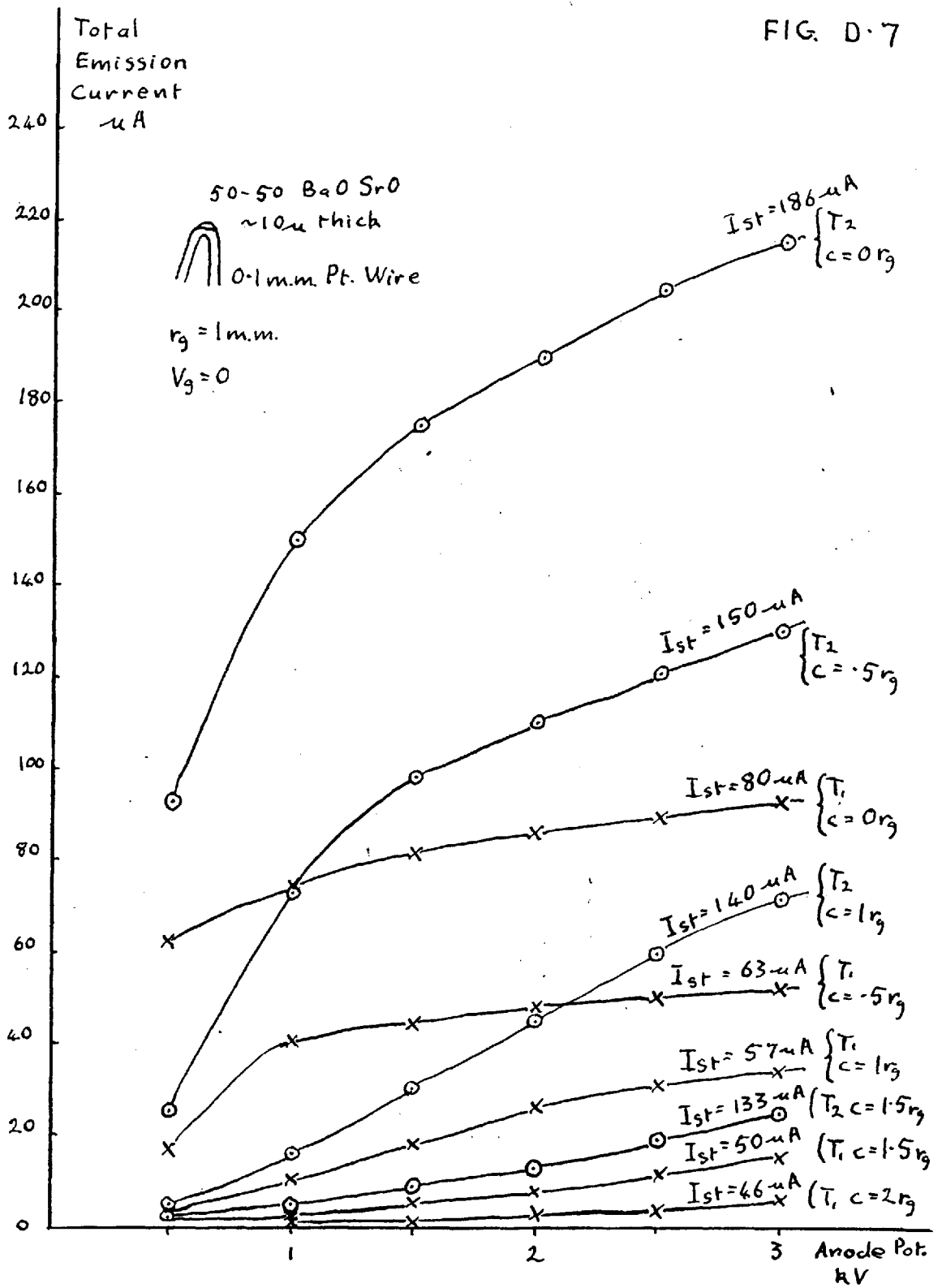

Total
Emission
Current
μA
240
220
200
180
160
140
120
100
80
60
40
20
0
50-50 BaO SrO
~10μ thick
0·1 m.m. Pt. Wire
r_g = 1 m.m.
V_g = 0
I_{st} = 186 μA
T2
c = 0 r_g
I_{st} = 150 μA
T2
c = ·5 r_g
I_{st} = 80 μA
T1
c = 0 r_g
I_{st} = 140 μA
T2
c = 1 r_g
I_{st} = 63 μA
T1
c = ·5 r_g
I_{st} = 57 μA
T1
c = 1 r_g
I_{st} = 133 μA
T2 c = 1·5 r_g
I_{st} = 50 μA
T1 c = 1·5 r_g
I_{st} = 46 μA
T1 c = 2 r_g
1
2
3
Anode Pot.
kV

FIG. D·8

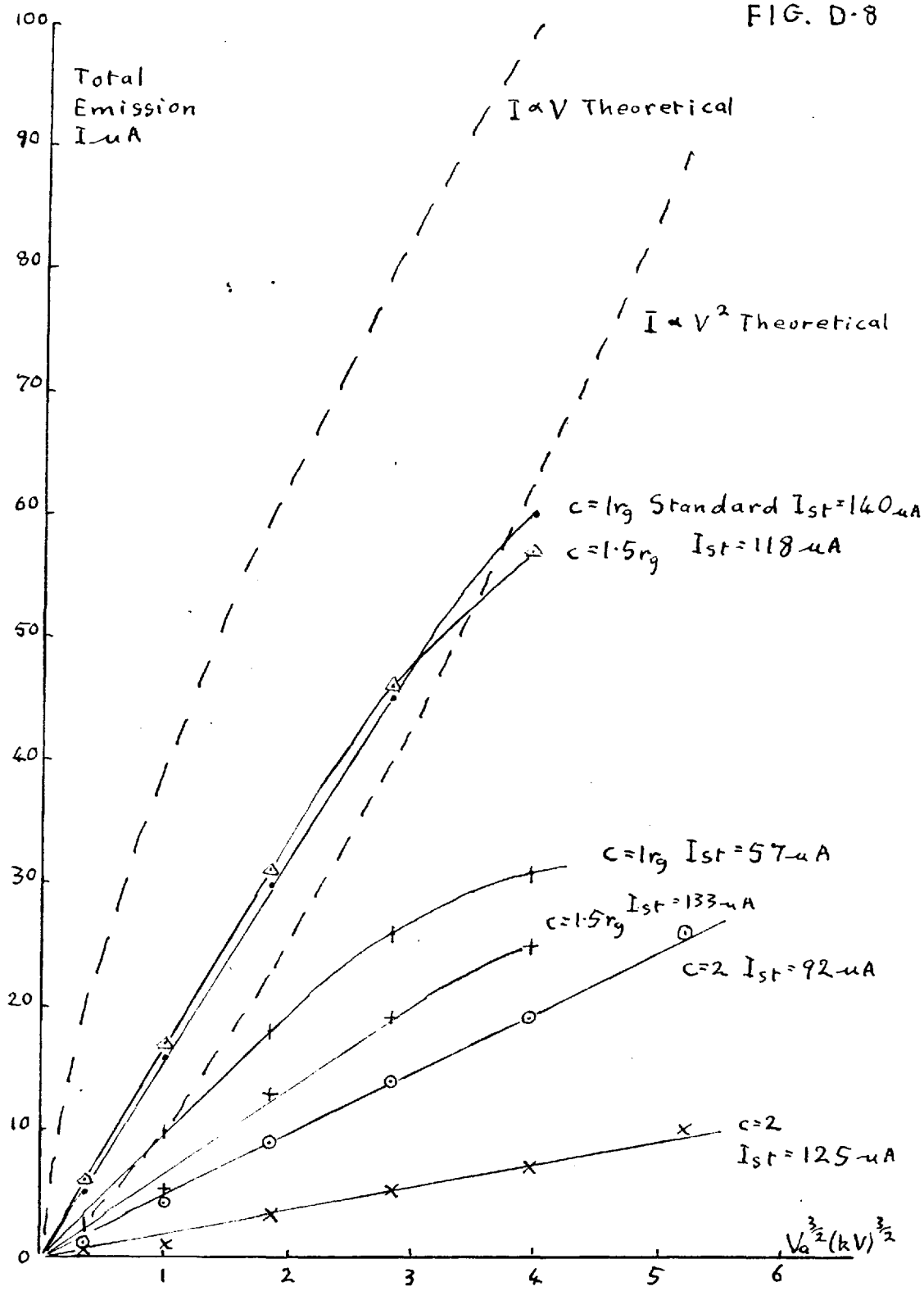
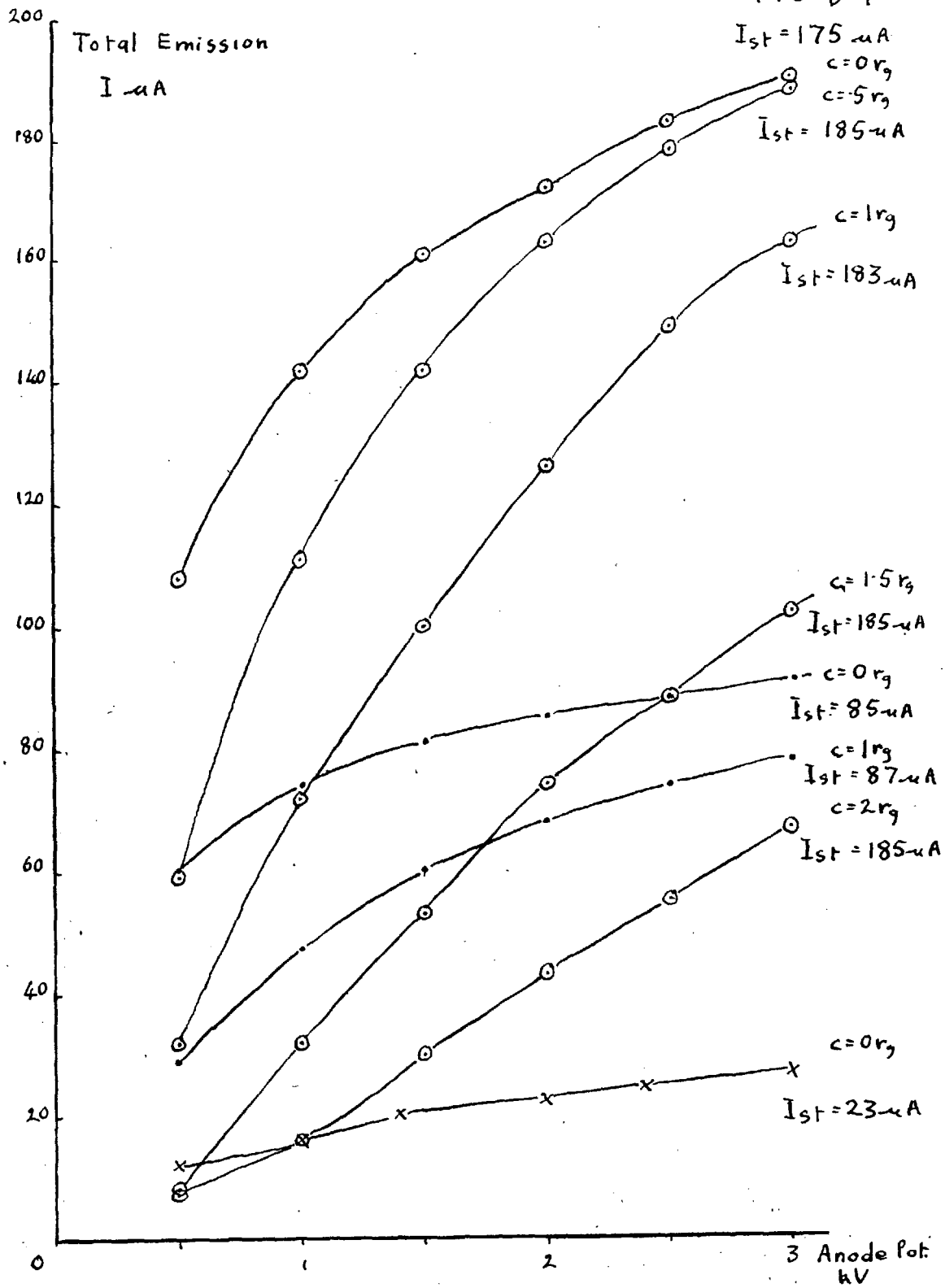

Total
Emission
I μA
I ∝ V Theoretical
I ∝ V² Theoretical
c = 1r_g Standard I_st = 140 μA
c = 1·5r_g I_st = 118 μA
c = 1r_g I_st = 57 μA
c = 1·5r_g I_st = 133 μA
c = 2 I_st = 92 μA
c = 2
I_st = 125 μA
V_a^{3/2} (kV)^{3/2}
0
10
20
30
40
50
60
70
80
90
100
1
2
3
4
5
6

FIG D·9


Total Emission
I μA
200
180
160
140
120
100
80
60
40
20
0
1
2
3 Anode Pot. kV
I_{st} = 175 μA
c = 0 r_g
c = ·5 r_g
I_{st} = 185 μA
c = 1 r_g
I_{st} = 183 μA
c = 1·5 r_g
I_{st} = 185 μA
c = 0 r_g
I_{st} = 85 μA
c = 1 r_g
I_{st} = 87 μA
c = 2 r_g
I_{st} = 185 μA
c = 0 r_g
I_{st} = 23 μA

to data in D.7. Plots of $I\alpha$ Va and α Va^2, are included for comparison.

Fig.D.9 shows I as a function of Va for a tungsten hairpin. The region of space charge limitation was less well marked and the $\frac{3}{2}$ power law was not obeyed.

When the tungsten filament was drawn back far behind the grid, far more current was emitted by the tungsten filament than by the oxide tipped platinum filament of the same Ist. This is due to the specific emission of the oxide cathode decreasing in the relatively poor vacuum when small currents were drawn.

Conclusions.

Multiple images can still be formed when the legs of a hairpin cathode are non-emitting.

The oxide tipped platinum hairpin cathodes were working under space charge conditions and approximated closely to a three-halves power law, as long as the emission was small in comparison with the saturation current. The emission from tungsten hairpin cathodes deviated substantially from the three-halves power law, probably because parts of the legs were always emitting under current saturation conditions.

Appendix 1:- Activation of the large concave oxide cathodes.

Since the cathode was used with a comparatively low anode voltage, it was not found necessary to highly activate the cathode. It was simply heated to about 1000°C., to decompose the carbonates in the coating, until the pressure in the vacuum vessel fell to 10^{-5} mm. Hg. The temperature was then reduced to the desired value and an anode voltage applied.

It was observed that the specific emission from the cathode at a given temperature was higher if, during the initial heating of the cathode, the temperature was raised to 1000°C. as quickly as possible.

The cathodes were of the type used in large Klystrons. They were obtained from E.M.I. Ltd., usually with oxide coated surface, but sometimes nickel bases were sprayed in the laboratory with a G.E.C. emissive coating using a pressure spray gun.

Whenever the cathode had to be exposed to air at atmospheric pressure it was, as recommended by Haas and Jensen (1957), heated to 100°C. during the admission of air in order to avoid condensation of moisture at the cathode surface.

Appendix 2:- Thermal expansion and measurement of the apparatus.

When transverse velocity distributions were determined as described in section C3.2, it was necessary to know the distance between the front of the Faraday Cage L, and the anode G (cf. Fig. C.1). This was done by measuring the distance between the brass end plates, when the vessel was under vacuum and subtracting the previously measured distances of the Faraday cage and the anode, from their respective baseplates.

The distortion of the baseplates under atmospheric pressure was calculated to be not more than 0.05 mm. at the centre of each baseplate.

Movement of the anode relative to the cathode due to thermal expansion was negligible. This was verified by attaching a small copper rule to the anode and observing the movement of a pointer on the Faraday cage. The separation of the two components appeared to decrease by 0.5 mm., but this was largely due to thermal expansion of the 50 mm. long rule which probably had a temperature of the order of 500°C. during the measurement.

Appendix 3:- Matching equipotentials at the cathode edge.

Ideally, the beam shaping shield of a gun designed according to Pierce's principle, should be part of the cathode. For practical reasons, however, it was necessary to separate these two electrodes by a small amount. This gap distorts the equipotentials at the cathode edge, producing anomalous transverse emission velocities and sometimes can enhance the thermionic emission from the edge of the cathode. These effects have been observed by Cutler and Saloom (1955), and have been treated theoretically by Lomax (1959).

A complete diagram of the equipotentials in the region of a beam designed by Pierce's principle, e.g. p.171 Pierce (1949) show that a cathode equipotential stretches back behind the cathode making an angle of 67.5° with the coated surface of the cathode. Cutler and Saloom (1955) recommend that the sides of the cathode should make this angle with the emitting surface. Fig. AP.1 shows the system used by the author. The side of the cathode was a cylinder making an angle of 70° with the front surface. The edge of the cathode was slightly rounded as shown, with a radius of curvature of about 0.5 mm. The arrangement has obvious limitations and was probably the cause of the anomalous current density distributions observed (see section C3.1).

FIG. AP·1

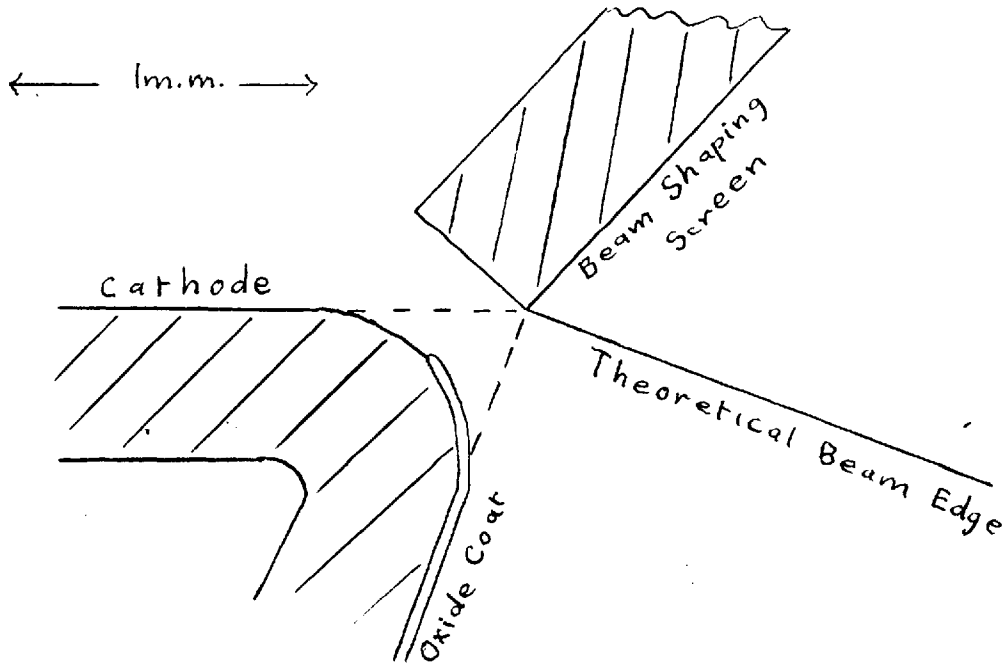
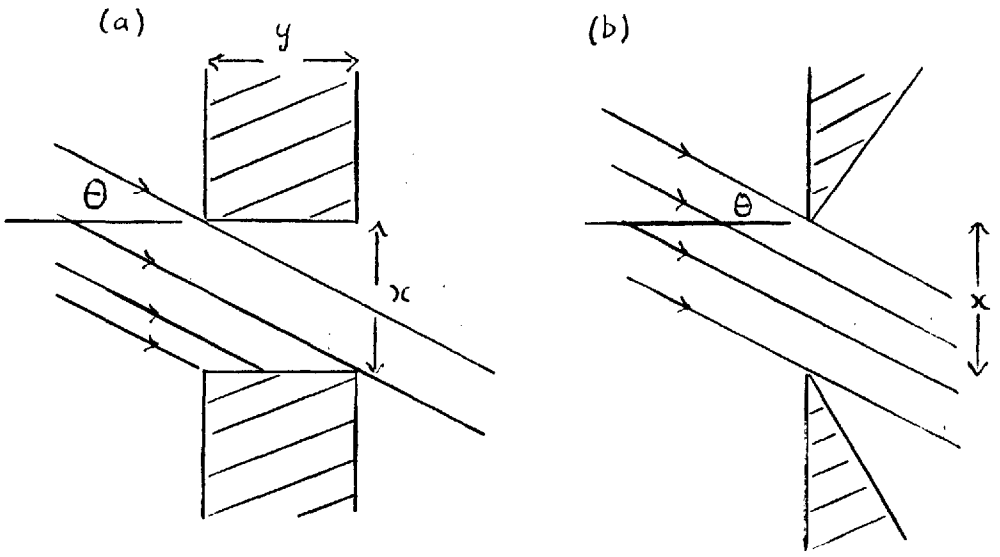


FIG. AP·2



Appendix 4:- Pinhole projection and resolving power.

Fig. AP. 2a shows a pinhole of diameter x, drilled in a diaphragm of thickness y. Of the four electrons initially entering the hole, only two pass through unimpeded. Fig. AP. 2b shows the type of pinholes used by the author, all four electrons entering the pinhole pass through unimpeded

Even when using the latter type of pinhole, the area of a parallel pencil which can pass through varies as cosine θ. Since the value of θ never exceeded about 20° in the experiments of section C, the cosine error was not greater than 6 per cent. It should be noted that measurements of current density distributions in the beam at the anode (sect. C3. 1), were not subject to cosine errors since the pinhole axis was always coincident with the axis of the projected pencil.

When electrons emerging from a pinhole fall on a fluorescent screen, the image sometimes shows small semi-circular notches at the edges. These are probably due to electrostatic charges on small particles of dirt near the pinhole. If such charges had occurred near the anode pinhole in sect. C3. 2, they would have produced anomalous results. The fact that the results were regular suggests that there were no such charges. This was probably because of the high temperature of the anode pinhole, which would render dirt particles electrically conducting. Thus electrostatic

charges would constantly leak away.

Fig.AP.3 illustrates in simplified form how the resolvin power in sections C3.3b and f, depended on the size of the pinholes employed. Angles are very much enlarged, and the distances, cathode to anode and anode to Faraday cage, are both equal to a. If θ is small $b = \theta(a + c)$

$$\theta = \frac{x}{c} = \frac{y}{d}$$

Hence $b = 2x + y$.

Thus the size of the anode pinhole is twice as important as the size of the Faraday cage aperture in limiting the resolving power of the system.

The values of x and y used in sect.C, were 150 μ and 100 μ respectively, except in section C3.3f, where both were reduced.

The value of b was thus 400 μ. In practice the electron trajectories between the cathode and anode are curved in such a way that electrons were accepted from a region of the cathode about 800 μ in diameter.

Appendix 5:- Pinhole position in measuring (1) Current density at the anode and (2) Transverse velocities in section C.

(1) It has been stated in the description of the experimental Pierce system (section C2.1), that the axis of the arm carrying the pinhole diaphragm, passed through the centre

FIG. AP. 3.

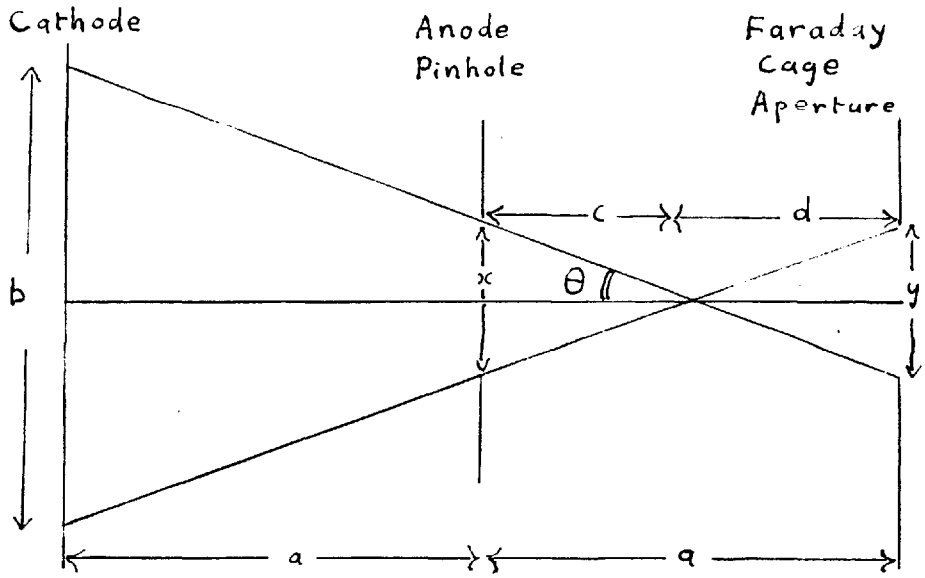
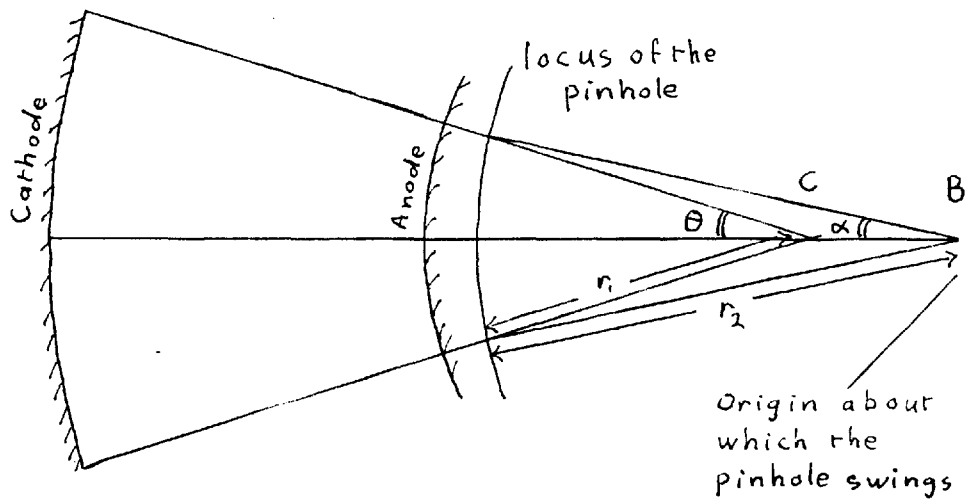


FIG. AP. 4



of curvature of the cathode. In fact, due to constructional errors this was only approximate. Fig.AP.4 shows how the pinhole moved just behind the front of the anode about centre B on a radius r_2. The path of the pinhole is distant r_1 from the centre of curvature of the cathode C. When the pinhole diaphragm was moved through angle α, the angular position of the pinhole in the beam changed by θ.

Since θ is almost equal to α

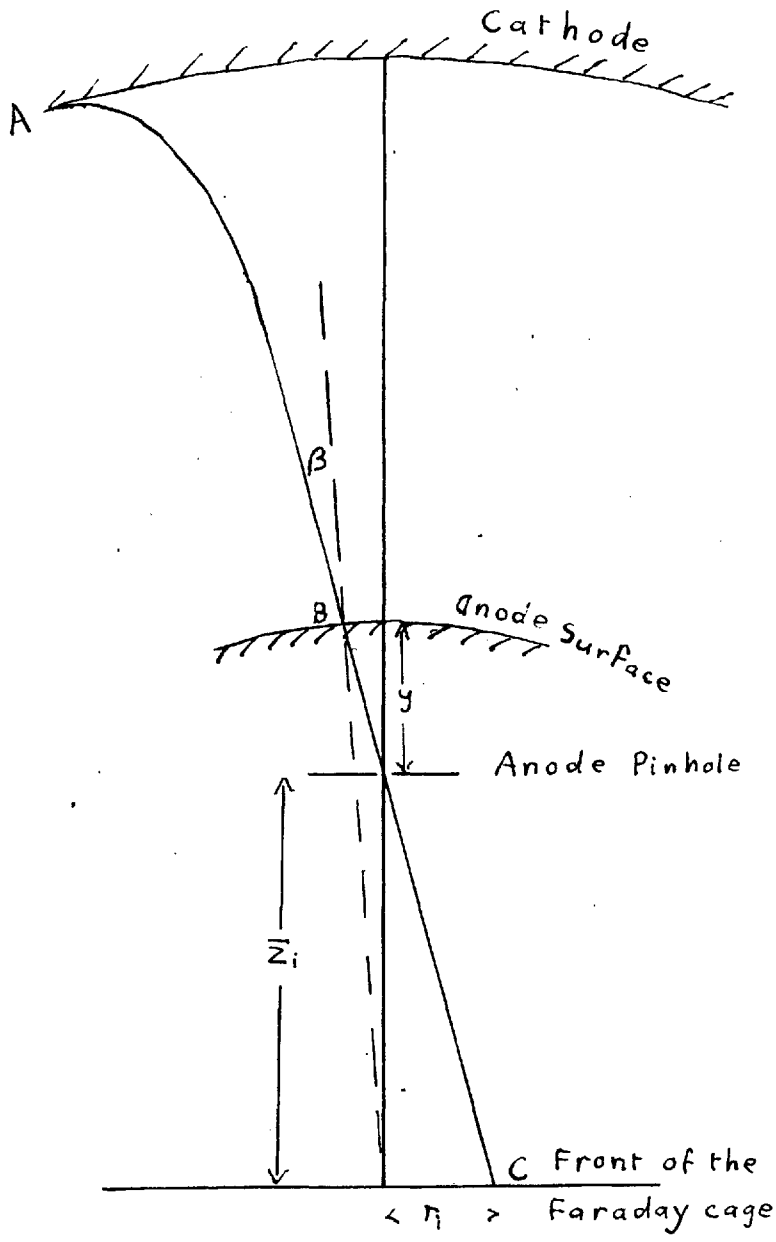
$$\theta r_1 \approx \alpha r_2$$

and $$\theta \approx \alpha r_2 / r_1$$

Both r_1 and r_2 were measured directly, angle α changed by 6° for each revolution of the rotating seal. The resultant change of θ was 6.6° per revolution of the seal.

(2) Fig.AP.5 shows the arrangement of the system used to measure transverse velocities. The anode pinhole is distant y, from the front of the anode. An electron leaving the cathode at A, with the appropriate thermal velocity, passes through the anode slot at B, to strike the Faraday cage at C, distant r_i from the axis. The distance from the anode pinhole to the Faraday cage is $\bar{z}_i$. For simplicity the front of the Faraday cage has been assumed to be coincident with the centre of curvature of the cathode.

FIG. AP. 5


Cathode
A
β
B
Anode Surface
y
Anode Pinhole
$\bar{z}_i$
C
Front of the
< r_i > Faraday cage

In order to measure transverse velocities the angle β, which the electron trajectory makes with the normal to the anode at B is required.

Under paraxial conditions, and neglecting the cosine error $\beta = \frac{r_i}{\bar{z}_i + y}$.

The value $\bar{z}_i + y$ was used as the equivalent distance between the pinhole and the Faraday cage in Sect. C3.2b.

Appendix 6:- Spurious focussing action on the pencil betwee anode and Faraday cage (1) by field penetration through the pinhole and (2) by space charge and positive ions.

(1) The anode pinhole can be treated as an aperture lens with zero electric field on one side. Using the Davisson and Calbick formula one obtains for the focal length

$$f = \frac{4\ Va}{E_a}$$ where Va is the voltage of the anode, and E_a is the field at the anode.

Using the notation of sect.B, the potential distribution between the cathode and anode may be written (cf. Langmuir and Compton (1931))

$$V = Va \left[\frac{-\alpha^2}{-\alpha_a^2}\right]^{2/3}$$ where $-\alpha$ is the Langmuir function for the appropriate spherical diode, and α_a is its value at the anode.

Differentiating with respect to axial position $\bar{z}$,

$$Ea = Va \frac{2}{3} \frac{1}{(-a_a^2)} \frac{d(a^2)}{d\bar{z}}$$

Putting in numerical values Ea = .95 Va/cm. and the focal length f = -4 cm.

The maximum deflection of a marginal ray is given by $\frac{r_p}{f}$, where r_p is the radius of the pinhole.

Since the radius of the anode pinhole was 0.075 mm., the maximum deflection suffered by an electron was 0.002^c.

The smallest half-radius encountered during measurements of transverse velocities at an anode potential of 640 volts, was 0.6 mm., corresponding to an angle of 0.02^c.

It must be noted that the transverse velocity of an electron is independent of the position at which it passes through the pinhole. Any given electron is equally likely to have its radial velocity increased or decreased. Thus in the above situation, the half width measured is likely to be increased by about 1 per cent, rather than 10 per cent, by the focussing action of the pinhole.

A further factor which reduces the importance of this focussing, is the fact that the pinhole is behind a 1 mm. wide slot which attenuates the electric field at the pinhole.

(2) The pencil of electrons projected by the anode aperture, travels in a field free region so the electronic space charge will be partly neutralized by positive ions. The greatest disturbance will occur if there is negligible neutralization by positive ions.

Consider the case of a parallel beam of electrons emerging from a pinhole 0.15 mm. in diameter and spreading under mutual repulsion over a trajectory of 3.0 cm. If the current in the pencil is I and its voltage is V.

$\int \frac{I}{V^{3/2}} = 7 \times 10^{-6} A^{\frac{1}{2}} V^{-3/4}$ invariant of voltage for all the measurements in sect.C made under space charge limited conditions. From the general equations for the beam spread, (see for instance Klemperer 1953 p.203) it follows that the pencil does not spread by more than 5 per cent of its diameter in travelling 3 cm. Thus, even under the most extreme conditions of no positive ion neutralization, space charge spreading is negligible.

Appendix 7:- Influence of positive ions on the beam between cathode and anode.

In the region between the cathode and anode of the Pierce system, the electrons ionized some of the residual gas molecules, partly neutralizing the electronic space charge. It is important to verify that the positive space charge density is nowhere great when expressed as a fraction of the electronic charge density.

In fig. AP. 6 this fraction is calculated for conditions where the residual gas pressure is 10^{-5} mm. of mercury and the anode potential is 640 v. With the latter value, the ionization is particularly great since the ionization reaches a maximum when the electron energy is about 200 eV.

In order to estimate the fraction of positive ions the beam was first divided into 5 slices of equal thickness, by drawing spherical surfaces about the centre of curvature of the cathode. The distance x, of each slice from the cathode surface as a fraction of the radius of curvature of the cathode $\bar{r}_c$, is shown in column 2 of table AP. 1. The potentials at the surface and half way through each slice respectively, were then obtained from a graph of potential against distance from the cathode. (See Samuel 1945). These values are shown in columns 3 and 4 of table AP. 1.

Column 5, shows the mean number of positive ions produced when an electron passed through a region of the beam at a velocity corresponding to the mean potential of the slice. The values for the number of ions per unit length of path, were taken from Cobine (1941).

The density of positive ions at a point is proportional to the rate of production of ions divided by their velocity, which is proportional to the root of the potential through which the ions have been accelerated. To obtain a quantity

TABLE AP·1

Slice No. S	Mean dist. x/r_c	Pot. V at slice Boundary	Mean Pot. V_s	Ions per slice per Electron $\times 10^{-5}$	Mean $\sqrt{V_s}$	$\frac{\text{Ions/slice} \times 10^{-5}}{\sqrt{(V_n - V_s)}}$ V_n = Mean Pot. of slice of origin					$\Sigma' \frac{\text{Ions}}{\sqrt{V_n - V_s}}$ $\times 10^{-5}$	$\sqrt{V_s} \times \Sigma'_1$ $\times 234$
						n=1	n=2	n=3	n=4	n=5		
						V_n=16v	72v	176v	304v	496v		
		0										
1	·05		16	0·1	4	·03	·40	·40	·24	·14	1·21	·011
		40										
2	·15		72	3	8·5		·48	·49	·26	·15	1·38	·027
		120										
3	·25		176	5	13·3			·67	·35	·17	1·19	·037
		232										
4	·35		304	4	17·4				·45	·22	·67	·027
		392										
5	·45		496	3	22·3					·27	·27	·014
		640										

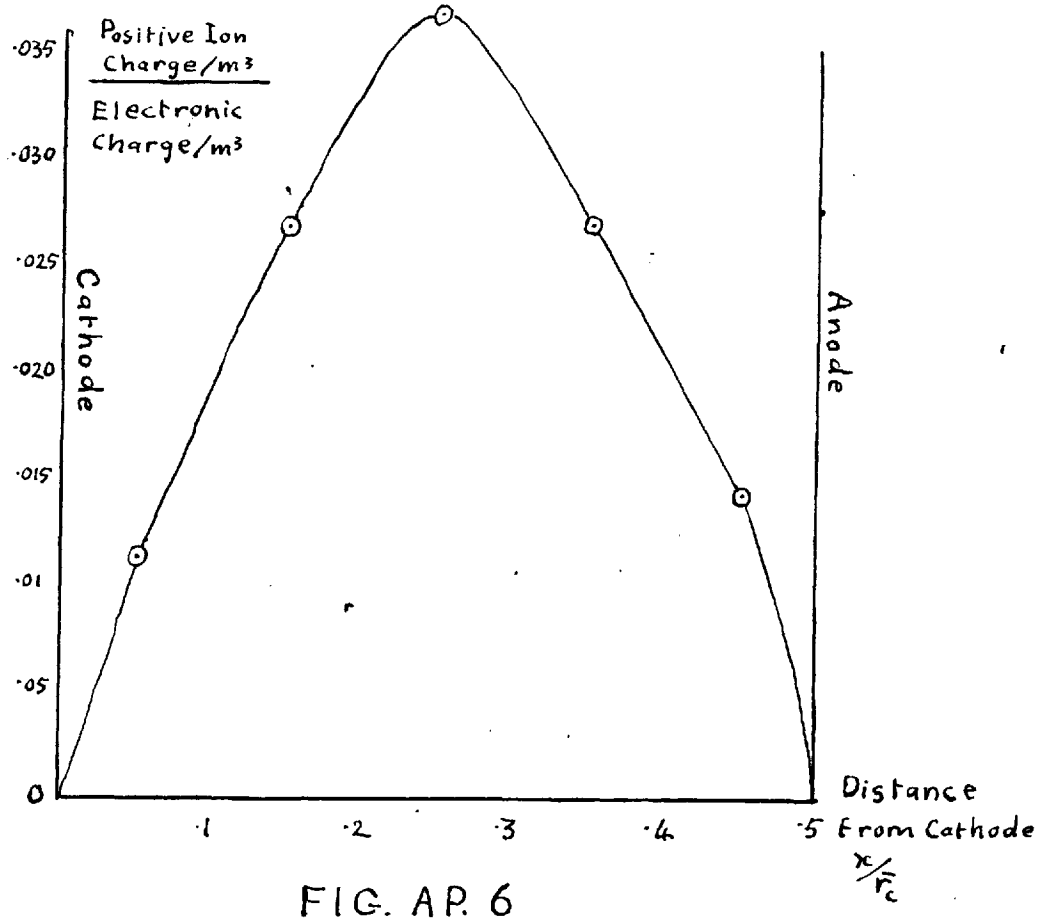


FIG. AP. 6

proportional to the number of positive ions in a given slice S the sum

$$\sum_{n=S}^{n=5} \frac{K(Vn)}{\sqrt{(Vn-V_S)}}$$ is taken, where K(Vn), is the number

of ions produced per electron in any slice number n, Vn is the mean potential of that slice, and V_S is the mean potential in slice S.

When n = S the value of $(Vn - V_S)$ was taken as half of the potential difference across this slice. Column 12 of the table shows the value of the above sum for each slice. In column 13 each value is multiplied by $\sqrt{V_S}$, which is inversely proportional to the electronic charge density, and by $\sqrt{\frac{ma}{me}}$, where ma/me is the ratio of the mass of an ionized air molecule to that of the electron. This takes into account the slower velocity of air molecules. The air molecules were considered to have a mass 30 times that of the proton.

The graph in fig. AP. 6 shows how the ratio of positive space charge to electronic space charge varies with position. The maximum volue is .037, the mean is .022.

In section C3.3a, it was shown that in the absence of space charge, the diameter of the beam at the anode was $\frac{1}{4}$ of the full space charge value. If it is assumed that this

diameter depends linearly on the space charge density in the beam, the positive ions can be expected to decrease the diameter of the beam at the anode by about 2 per cent in the case considered above.

Appendix 8:- Errors in the shapes of electrodes.

The beam shaping screen and the anode, used in section C, were spun from copper according to a template. The template was accurately made from data provided by Helm et al. (1947) (see fig.B.4). The electrodes nowhere deviated from the template by more than about 0.5 mm. The commercial cathodes had a radius of curvature which was accurate to above $\pm$ 2%.

Due to the inadequate facilities for centering the cathode with respect to the beam shaping screen, the cathode was sometimes up to 0.5 mm. off axis.

Appendix 9:- Elimination of stray electric and magnetic fields affecting measurements in section C.

The only insulators used in the construction of the electron gun described in section C, were the 3 ceramic rods, and these were well away from the electron beam. The inside of the glass vacuum vessel was lined with copper sheet, so it was impossible for large electrostatic charges to accumulate. Whenever the apparatus was dismantled, the electrodes were carefully cleaned with emery paper and

acetone to remove any resistive layers which might have been present.

The path length of the electrons in the apparatus was only about 5 cm., so that the effect of the earth's magnetic field was not very large even at anode potentials as low as 10 v.

The vertical component of the earth's magnetic field was compensated by a pair of rectangular coils. The horizontal component of the earth's magnetic field (0.2 gauss was parallel to the axis of the gun. Such a field does not change the electron orbits substantially, since it focuses a 10 v. electron helically in a distance of 3 metres.

The cathode heater was non-inductively wound with wires spaced $\sim$ 2 mm. apart and $\sim$ 5 mm. from the cathode surface. When it was switched off for a short time there was no change in the trajectories of the projected electrons.

The only ferromagnetic material used inside the vacuum vessel was the nickel cathode cap, which was above its Curie temperature.

Both the screws which secured the electrode structure and the gears mounted on the anode, were made of nonmagnetic stainless steel.

CAPTIONS TO FIGURES

B.1 A conical beam as part of the flow of electrons in a space charge limited spherical diode.

B.2 Determination of electrode shapes using the wedge trough.

B.3 Diagram showing the symbols used in the theory of the Pierce gun.

B.4 Electrode shapes for a Pierce gun of 20° semi-convergence angle.

B.5 Theoretical current density distributions in the author's version of Pierce's system.

C.1 Apparatus for investigation of a Pierce System.

C.2 Cathode assembly.

C.3 Circuit of the Pierce System.

C.4 Circuit for measuring current density.

C.5 Circuit for measuring transverse velocity distributions.

C.6 Current density distribution at 640 v. anode potential.

C.7 Current density distribution at 160 v. anode potential.

C.8 Current density distribution at 40 v. anode potential.

C.9 Current density distribution at 10 v. anode potential.

C.10 The effect of biasing the beam shaping screen at 640 v. anode potential.

C.11 The effect of biasing the beam shaping screen at 10 v. anode potential.

C.12 The transverse velocity distribution at 640 v. anode potential.

C.13 The transverse velocity distribution at 160 v. anode potential.

C.14 The transverse velocity distribution at 40 v. anode potential.

C.15 Halfwidth of transverse velocity distributions as a function of anode potential.

C.16 Transverse velocity distribution at the edge of the beam at 640 v. anode potential.

C.17 Transverse velocity distribution at the edge of the beam at 40 v. anode potential.

C.18 Current density distribution under temperature limited conditions.

C.19 Transverse velocity distribution under temperature limited conditions.

C.20)
C.21) Transverse velocity distributions under temperature
C.22) limited conditions.

C.23 Position of maxima in velocity distributions as a function of temperature.

C.24 Height of maxima in velocity distributions as a function of temperature.

C.25 Sketch of part of a cathode surface.

D.7 Total emission from an oxide tipped cathode as a function of anode potential.

D.8 Total emission from an oxide tipped cathode as a function of anode potential to the three-halves power.

D.9 Total emission from a tungsten hairpin cathode as a function of anode potential.

AP.1 Enlarged view of the edge of the cathode employed in section C.

AP.2 Transmission of a pencil through a pinhole.

AP.3 Resolving power of the transverse velocity analyser in section C.

AP.4 Angular motion of the anode pinhole used in section C for measurements of current density at the anode.

AP.5 Position of the anode pinhole used in section C for measurement of transverse velocity distributions.

AP.6 Calculation of the effect of positive ions between the anode and cathode of the Pierce system.

C.26 Frequency of surface irregularities.

C.27 Transverse velocity distributions with improved resolution.

C.28 Perveance of the Pierce system.

D.1 A surface irregularity on a heated tungsten filament.

D.2 The formation of a beam with two different electron temperatures.

D.3 An experimental arrangement with two hairpin filaments and a slotted grid.

D.4 Electron trajectories in a system with two hairpin filaments and a slotted grid.

D.5 Conditions required for fusion of images projected by a pinhole.

D.6 The interaction of emission currents from two closely spaced hairpin filaments.

REFERENCES:

Barber, M.R., and Sander, K.F. 1959 J.Electronics 7, 465.

Brewer, G.R. 1957 J.App.Phys. 28, 7.

Brewer, G.R., and T. Van Duzer 1959 J.App.Phys. 30, 291.

Coppola, P.P. 1960 Rev.Sci.Instr. 31, 137.

Clarke, W.W.H., and Jacob, L. 1953 Proc.Phys.Soc.66B, 284.

Clarke, W.W.H., and Jacob, L. 1955, Proc.Phys.Soc.68B, 805

Cobine, J.D. 1941 New York "Gaseous Conductors".

Cutler, C.C., and Hines, M.E. 1955 Proc.I.R.E. 43, 307

Cutler, C.C., and Saloom, J.A. 1955 Proc.I.R.E. 43, 299.

Danielson, W.E., Rosenfeld, J.L., and Saloom, J.A. 1956 Bell System Tech.Jour. 35, 375.

Dietrich, W. 1958 Z. Physik 152, 81 and 306.

Dolder, K.T. 1954 London Thesis.

Dolder, K.T., and Klemperer, O. 1956 J.Electronics 1, 601.

Dolder, K.T., and Klemperer, O. 1957 J.Electronics 3, 439.

Fack, H. 1955 Phys.Verhandl, 6, 6.

Field, L.M. 1946 Rev.Mod.Phys. 18, 353.

Haas, A., and Jensen, J.T. 1957 Rev.Sci.Instr.28, 1007.

Haine, M.E., and Einstein, P.A. 1952 Brit.J.App.Phys. 3, 40.

Harris, L.A., 1960 Proc.I.R.E. 48, 368.

Hechtel, R. 1956 Arch.El.Übertragung 10, 535.

Heil, O., and Ebers, J.J. 1950 proc.I.R.E. 38, 645.

Helm, R., Spangenberg, K., and Field, L.M. 1947 Elect. Comm. 24, 101.

Hillier, J., and Baker, R.F. 1945 J.App.Phys. 16, 469.

Johannson, H. 1933 Ann.Phys.Lpz. 18, 385.

Klemperer, O. 1947 Proc.Roy.Soc. A 190, 376.

Klemperer, O. 1951 Proc.Phys.Soc. B 64, 790.

Klemperer, O. 1953 Cambridge "Electron Optics".

Klemperer, O. 1959 London "Electron Physics".

Langmuir, I., and Compton, K.T. 1931 Rev.Mod.Phys. 3, 191.

Lomax, R.J. 1959 J.Electronics 6, 39.

Mahlman, G.W. 1949 J.App.Phys. 20, 197.

Masuda, T. Tronscope TRS-50D Electron Microscope.

Meltzer, B., and Holmes, P.L. 1958 Brit.J.App.Phys. 9, 139.

Müller, M. 1956 J.Brit.Inst.Rad.Eng. 16, 83.

Musson-Genon, R. 1947 Ann.Telecom. 2, 254, 298.

Nottingham, W.B. 1956 Encyclopedia of Physics 21.

Pierce, J.R. 1940 J.App.Phys. 11, 548.

Pierce, J.R. 1949 New York. "Theory and design of electron beams."

Sakaki Von Y., and Möllenstedt, G. 1956 Optik 13, 193.

Samuel, A.L. 1945 Proc.I.R.E. 33, 233

Sears, F.W. 1949 Cambridge, Mass. 'Optics'.

Seeman, H. 1932 Z.Phys. 79, 742.

Wittry, D.B. 1957 Rev.Sci.Instr. 28, 58.